Design of and Experimentation with an Insect Impact Simulator Setup

Mohammadamin Ghasemzadeh

A THESIS SUBMITTED TO
THE FACULTY OF GRADUATE STUDIES
IN PARTIAL FULFILLMENT OF THE REQUIREMENTS
FOR THE DEGREE OF
MASTER OF APPLIED SCIENCE

GRADUATE PROGRAM IN
MECHANICAL ENGINEERING
YORK UNIVERSITY
TORONTO, ONTARIO

AUGUST 2022

Abstract

Laminar flow aircrafts as a potential high speed and economical fuel saver airplanes are facing challenges by contaminations on the wings. These contaminations such as sand/dust, ice, and insect residual have been studied for a long time. Insect residual unlike the other two needs further investigation since it is more complicated. To study insect residue on aircraft airfoil, a new setup was conceptually designed. After reviewing setups from past studies, main objectives of the new setup were identified to be keeping insect intact before impact, presence of airflow, and reaching take-off speed of an aircraft. Also, secondary objectives of the new setup were defined to be maximizing the possibility of insect impact to leading edge of airfoil, simplifying the procedure of data collection, ability of modifying the speed during the test, and launching both insect and spherical objects. Then, the new insect impact simulator setup was manufactured; a motor rotated the airfoils to take-off speed of aircrafts and a particle launcher threw the insect toward the airfoils, then impact happened at the leading edge of airfoil. Three experiments were done to validate the new setup with past studies results, produce new results, and investigate controversary subjects. First, minimum rupture velocity of insect was clarified that instead of a threshold velocity number, it is a range which insect starts to rupture partially at 17.5 m/s until it fully ruptures at 30 m/s. Furthermore, presence of a coating on airfoil does not affect the minimum rupture velocity. Second, five commercially available coatings were tested at 60 m/s. It was observed that residue's area decreased by increasing the roughness. Also, residue's area decreased by decreasing the surface energy. Superhydrophobic coatings showed a promising ability to reduce the insect residue. Finally, it was observed that natural airflow which previously mentioned as a mitigation method does not change the residue's amount after coagulation.

Acknowledgements

For the guidance and support he provided me throughout my research, I would like to extend my sincerest appreciation and gratitude to Professor Alidad Amirfazli.

Table of Contents

Abstract ..... **ii**

Acknowledgements ..... **iii**

Table of Contents ..... **iv**

List of Tables ..... **vii**

List of Figures ..... **viii**

Chapter 1 Introduction **1**

1.1 laminar flow aircraft and challenges 1

1.2 Insect impact setups 7

1.2.1 Main characteristics of an insect impact setup 7

1.2.2 Main configurations of insect impact setups 12

1.3 Mitigation methods 24

1.3.1 Removal methods 24

1.3.2 Coatings and characteristics 25

1.4 Development of a new apparatus 28

1.4.1 Gaps of the past studies 28

1.4.2 Scope of the study 29

1.4.3 Objectives of study 30

Chapter 2 Methodology **32**

2.1 Design 32

2.1.1 Conceptual design 32

2.1.2 Rotation subsystem 33
2.1.3 Particle launching subsystem....38
2.1.4 Imaging and lightning....44
2.1.5 Computational and electrical subsystem 47
2.2 Sample preparation and experimental procedure....58
2.2.1 Insects and particles 59
2.2.2 Coating and material....60
2.2.3 Data collection 61
2.2.4 Impact test 62
2.3 Data processing....64
2.3.1 Area analysis 64
2.3.2 Coating characterization 64
Chapter 3 Results and discussion....66
3.1 Particles and coatings characteristics 66
3.2 Insect tests 67
3.2.1 Rupture velocity 67
3.2.2 Impact test at 60 m/s....69
3.2.3 Airflow removal 74
Chapter 4 Conclusion and future work....77
4.1 Conclusion....77
4.2 Future work....78

References 80

Appendices 87

Appendix A – Past coatings list from literature.....87

Appendix B – Arduino code 91

Appendix C – Mechanical drawings.....107

List of Tables

Table 1-1 Setups from past studies.....14

Table 2-1 Error descriptions of the components of insect impact 51

Table 2-2 Sample size and sample rate of the algorithm based on the initial estimated rpm 56

Table 2-3 Sample coding output 57

Table 3-1 Contact angle and roughness of the coatings.....67

Table 3-2 Results of Drosophila Melanogaster impact to uncoated aluminum for past studies..70

List of Figures

Figure 1-1 Transition of laminar flow to turbulent (from Ref. [7] with general permission from website) 2

Figure 1-2 Types of laminar flow control airfoils in comparison with conventional airfoils (adapted from Ref. [5], [15]) 3

Figure 1-3 Insect residue on airfoil and laminar flow transition caused by insect residue (top right Image credit to David C. Bowman from NASA Langley, top left from Ref. [16], and bottom from Ref. [17] with permission from Elsevier) 4

Figure 1-4 Insects population density in different altitudes (from Ref. [17] with permission from Elsevier)..... 5

Figure 1-5 Fruit fly residue components (from Ref. [22], reprinted by permission from author)... 6

Figure 1-6 Insects with different orientations and same impact angle..... 9

Figure 1-7 A car with a half cylinder installed on roof for attaching samples to it (from Ref. [46], publicly permitted to be used by NASA) 15

Figure 1-8 Pneumatic insect delivery device (from Ref. [33] with permission from Elsevier).....16

Figure 1-9 Stationary coupon impact test or SPIrIT (adapted from Ref. [26]) 17

Figure 1-10 BART wind tunnel (from Ref. [36], publicly permitted to be used by NASA) 19

Figure 1-11 Lab-scale wind tunnel with a custom-built pneumatic gun (from Ref. [36], publicly permitted to be used by NASA).....20

Figure 1-12 a) and b) NACA0038 in a wind tunnel (from Ref. [27] with permission from Elsevier) 21

Figure 1-13 Tilted flat plate used in a wind tunnel (from Ref. [49], reprinted by permission of the American Institute of Aeronautics and Astronautics, Inc.).....22

Figure 2-1 Schematic of conceptual design from top-view for the new apparatus 33

Figure 2-2 Power transmission subsystem 34
Figure 2-3 a) Cross-section of power transmission subsystem with frames and connectors and b) Full-view of power transmission subsystem placed on the bottom of the setup 35
Figure 2-4 NACA0012 airfoil sketch 37
Figure 2-5 Disintegrated airfoil 37
Figure 2-6 Aluminum cage, acrylic faces of the setup with metal meshes, and forced shut down sensor 38
Figure 2-7 a) CAD view, b) Cross-section, and c) a picture of particle dropper 39
Figure 2-8 a) Particle holder isometric view, b) Particle holder front view, c) Location of particle holder in the body of particle launcher, and d) Side view of particle holder in the body of the particle launcher 41
Figure 2-9 a) Particle launcher and b) Cross section of it 42
Figure 2-10 Picture of particle launcher 42
Figure 2-11 a) Starting position of particle launcher, b) Compressing the spring, c) Holding the compressed spring with solenoid, d) Releasing the thread, e) Releasing the spring by moving the solenoid, and f) Particle holder moves back to the starting position 43
Figure 2-12 Three-axis aligner 44
Figure 2-13 Position of cameras 45
Figure 2-14 Exact location of impact in the airfoils' path 46
Figure 2-15 Position of light sources 47
Figure 2-16 Location of insect residue accumulation on Jetstar C-140 with residue heights in inches (from Ref. [63], publicly permitted to be used by NASA) 52
Figure 2-17 Successful impact zone 53
Figure 2-18 Schematic of electrical circuit 58
Figure 2-19 Drosophila Hydei 60
Figure 3-1 Insects' measurements 66

Figure 3-2 Rupture velocity for aluminum and Polyurethane (PU) coated surface.....69
Figure 3-3 Residue areas of the coatings.....70
Figure 3-4 Top-view of insect impact 60 m/s.....71
Figure 3-5 Side-view of insect impact at 60 m/s.....71
Figure 3-6 Comparison of coatings with approximately similar surface energy values.....72
Figure 3-7 Comparison of coatings with different surface energy.....73
Figure 3-8 Probability of leaving residue after impact.....74
Figure 3-9 Airflow removal of residue after 10 min.....76

Chapter 1 Introduction

1.1 laminar flow aircraft and challenges

In fluid dynamics, laminar flow is considered as the smooth movement of fluid particles in parallel layers, which these layers do not mix with each other [1]. Pressure and velocity are stable and steady at each point. At low velocities or high viscosities, fluid particles tend to move in the layers and do not pass a layer to an adjacent one. In contrast, turbulent flow is considered as unsteadiness in pressure and velocity of the fluid at each point, fluid layers mix with adjacent layers and create eddies. Generally, inertia forces overcome the viscous force in turbulent flow and cause a chaotic movement of fluid. The distance from the leading edge of a plate where the transition from laminar regime to turbulent regime starts is denoted by X_{cr} (Figure 1-1) [2]; can be calculated by using the critical Reynolds number. For instance, the critical Reynolds number of a flat surface is about 3×10^5 to 3×10^6 [2]. After the laminar regime, during the transition regime, small instabilities such as Tollmien–Schlichting [3], [4] wave grow and make the flow chaotic and turbulent. Small disturbances on a surface can cause instabilities in the flow which lead to an earlier regime change. These instabilities are eliminable by active and passive methods [5], [6]. Suction as an active method absorbs the unstable part of the flow to a porous surface and avoids regime transition. Engineered surface shape as a passive method can delay the regime transition. Maintaining laminar regime methods have applications in aircraft.

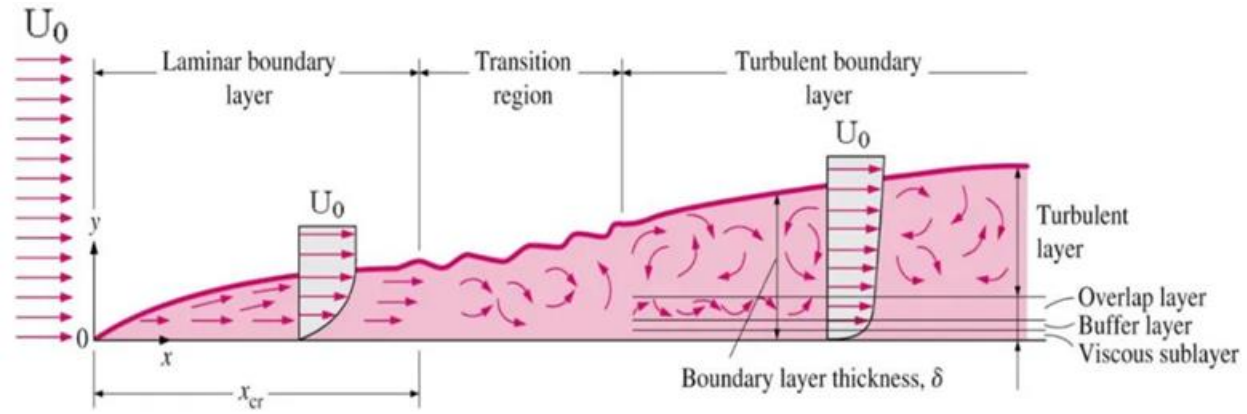

Figure 1-1 Transition of laminar flow to turbulent (from Ref. [7] *with general permission from website)*

The aviation industry plays a leading role in long-distance transportation. In 2019, about 38.9 million flights were performed by the airline industry, which consumed about 445 million cubic meters of fuel and emitted about 905 million metric tons of CO_2 [8]–[10]. Laminar flow aircraft as a concept in green aviation reduces pollution, flight duration, and fuel usage. By reducing the fuel consumption of aircraft, the airline industry saves money, and even flight transportation could be cheaper. A laminar flow aircraft could save up to 8.6% of fuel usage compared to a turbulent baseline aircraft [11]. The fuel usage reduction by laminar flow aircrafts avoids about 0.0001℃ of increase in global temperature yearly (the average increase per decade is 0.18℃) [12], [13].

A laminar flow aircraft has laminar flow over most of the airfoil's chord. Laminar flow aircrafts are divided into three main types: Natural Laminar Flow (NLF), Laminar Flow Control (LFC), and Hybrid Laminar Flow Control (HLFC) [5], [14]. NLF aircraft's airfoils are designed to maintain laminar flow only by airfoil's shape. NLF method is a passive method. LFC aircraft's airfoil uses suction over most of the airfoil's chord to preserve the laminar flow over the airfoils. HLFC aircraft use the suction method at the first part of the airfoil and then benefit from the airfoil's shape to maintain the laminar flow over the airfoils. LFC and HLFC are active methods. A graphical demonstration of these methods is provided in Figure 1-2.

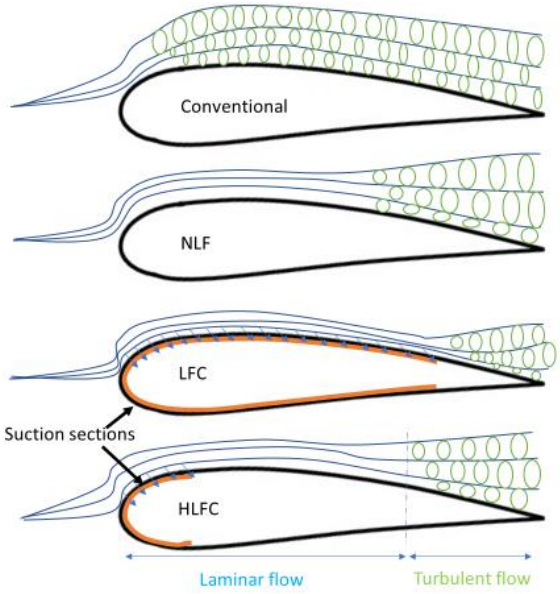

Figure 1-2 Types of laminar flow control airfoils in comparison with conventional airfoils (adapted from Ref. [5], [15]*)*

One of the challenges that hinder Laminar Flow Control aircraft from entering into service is that small contamination on the airfoil can disturb laminar flow for a considerable area of the airfoil (Figure 1-3). These contaminations are mainly sand and dust particles, water droplet icing, and ruptured insect residue. The focus of this work is on insect residue, as limited studies have been done on it.

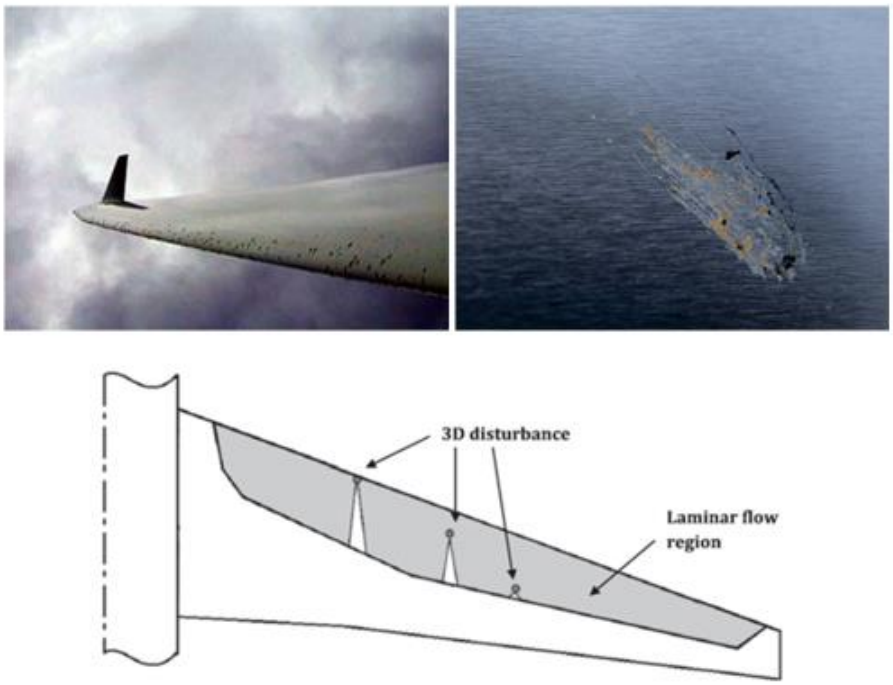

Figure 1-3 Insect residue on airfoil and laminar flow transition caused by insect residue (top right Image credit to David C. Bowman from NASA Langley, top left from Ref. [16]*, and bottom from Ref.* [17] *with permission from Elsevier)*

The number of insects in an area is a function of season, climate, food, temperature, humidity, etc. The accumulation of insects on aircraft is mostly related to the altitude (Figure 1-4). The accumulation mostly occurs near the ground during take-off, landing, and taxiing. Taxiing is the process in which an airplane moves on the ground before take-off or after landing. As Coleman [18] mentioned, around 54% of the insect accumulation on aircraft occurs during taxiing, 33% during the flight to 305 m (1000 ft), and the rest during the flight to 1524 m (5000 ft). Furthermore, it was observed that adhered insects to the aircraft were mostly 1 to 3 mm in length size [19], [20].

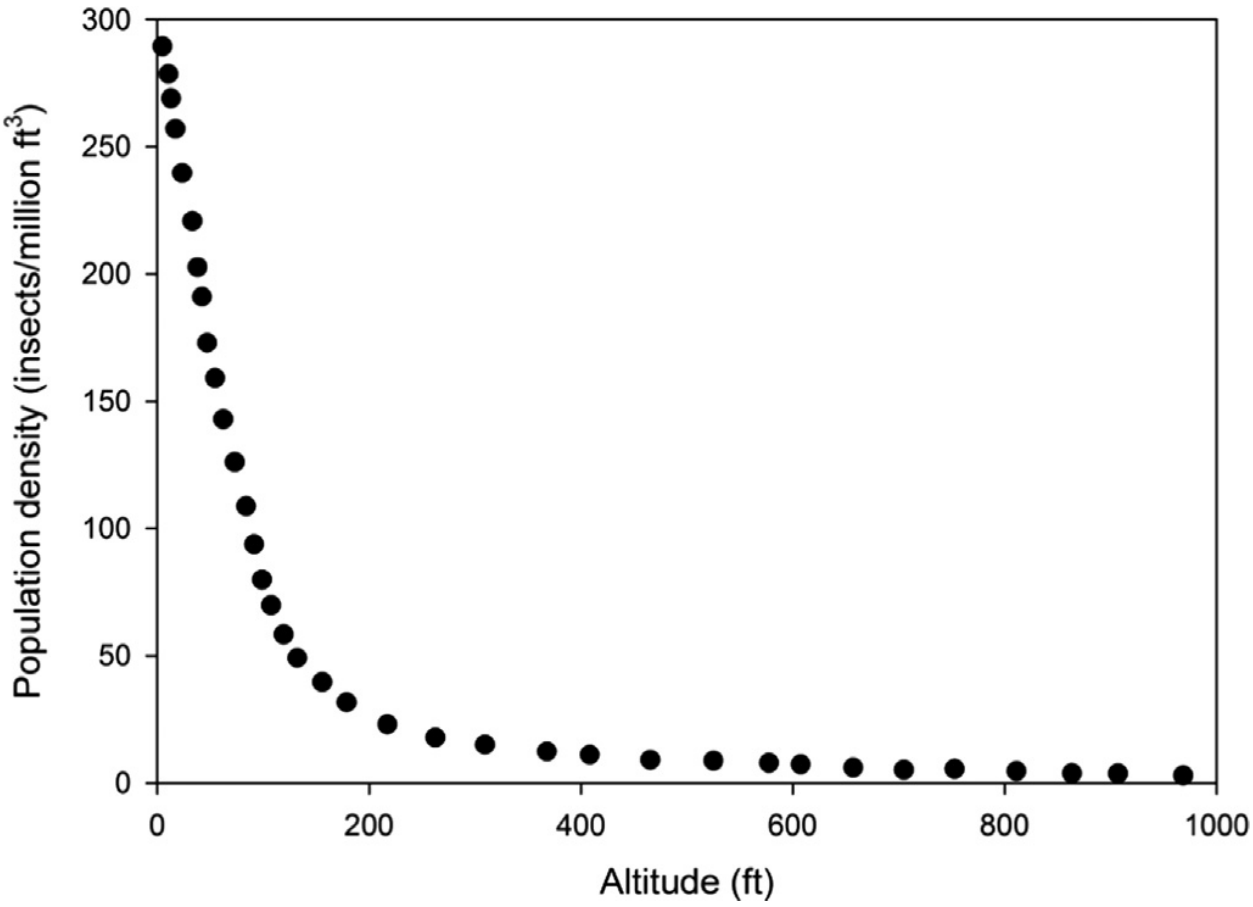

Figure 1-4 Insects population density in different altitudes (from Ref. [17] *with permission from Elsevier)*

When an insect hits an airfoil, it ruptures. Insect hemolymph coagulates in a short time[1] and acts like glue to adhere hard parts of the insect to the airfoil. These hard parts, e.g., foot or hard shell, disturb the laminar flow and cause the laminar regime to trip to turbulence. There are three main components of the residue [21]–[23] (Figure 1-5).

First, the exoskeleton which contains the leg, hard shell, and outer parts of the insect. Second, the yellow coagulated fluid which forms most of the hemolymph. Third, the red coagulated fluid

[1] Based on estimating the insect to water droplet and using https://calculator.academy/evaporation-rate-water-calculator, the evaporation time of a droplet in sizes of an insect is in order of magnitude about 10 seconds. However, besides the evaporation, there are enzymes in insect hemolymph that coagulate the blood in a shorter time (there is no data about the coagulation time considering both enzymes and evaporation).

which is less in comparison with yellow fluid. Red fluid belongs to the head and yellow fluid belongs to the abdominal part of the insect.

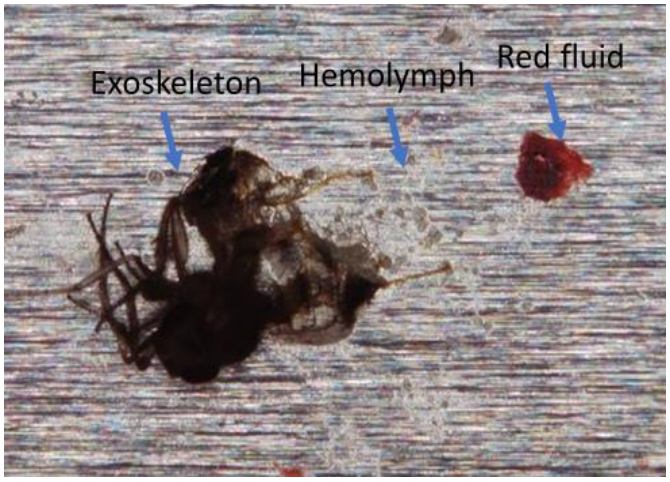

Figure 1-5 Fruit fly residue components (from Ref. [22]*, reprinted by permission from author)*

A deeper knowledge of the impact is required to tackle the insect residue issue. Also, a strategy for eliminating or avoiding insect residue is required to solve the problem of insect residue on the aircrafts. To get a better grasp of the issue, research groups examined the insect impact on an aircraft's airfoil. Experiments were done on aircraft in actual flight or setups in the lab. Different methods for mitigating insect residue have been suggested and investigated. The following sections summarizes the various setups and mitigating techniques. Finally, at Section 1.4, reasons for developing a new setup are discussed and objectives of the new setup are determined.

1.2 Insect impact setups

In the following section, the main characteristics of the setups used for experimenting with insect impact to the airfoil are discussed. Also, the most important findings from each setup are mentioned.

1.2.1 Main characteristics of an insect impact setup

To study insect impact to an airfoil, setups have to simulate the impact. An insect impact simulator consists of three main parts: (1) insect or a particle; (2) airfoil or a target plate; (3) an accelerator that either accelerates the particle or the target. Each part has some characteristics or outcomes that vary among setups. In the following, first, outcomes of insect impact are presented; then, their characteristics are introduced.

The measurable outcomes of an insect residue are the area and height of the residue. After the impact, the residue's height is one of the measurable variables since there is a critical height of the residue that disrupts the laminar flow; any height more than the critical height trips the flow to turbulent. The critical height is discussed in Section 1.3.1. Another measurable value after impact is the area of the residue that shows mostly the amount of adhered hemolymph.

Characteristics of an insect impact simulation setup are as below:

1. Insect or simulation particle:
    - Insect type, age, gender, mass: Different insects were used in the past studies: Cricket, Drosophila Melanogaster, and Drosophila Hydei were the most common insects in the studies [23]–[25]. Drosophila Melanogaster and Hydei were used more since their sizes (1 to 3 mm) represent the impacting insect to airfoil better than cricket [17], [18], [21]. It was reported that age, gender, and mass of insects affect their amount of hemolymph [26]. In most past studies, there was not any control on the age, gender, and mass of the insects.

- Orientation, rupture, and stickiness of each part: The orientation of an insect before impact is determined by what part of the insect hits the airfoil first, such as the abdomen or the head of the insect. Insect orientation before impact affects the insect rupture at certain velocities. These parts (e.g., abdomen, head, and legs) have different resistance to an impact to rupture [23], [26]. If soft parts like the abdomen impact the airfoil first, they rupture easily. However, if hard parts like the exoskeleton hit the airfoil, it needs a greater amount of energy to break. Besides the minimum rupture velocity for breaking each part, the stickiness of each part plays a role in leaving behind a residue on the airfoil. The abdomen (yellow fluid) has a better stickiness compared to the exoskeleton and red fluid [21]–[23], [27]. Although the insect's rupture and sticking of the insect's body parts depend on the orientation of the insect, after a threshold speed the dependency on orientation is removed. For instance, for Drosophila Melanogaster after speeds greater than 55 m/s, orientation has no effect on the rupture [26]. In summary, insect orientation plays a significant role in lower velocities, but in higher velocities (like the take-off that more than 33% of the insects' accumulation on airfoil occurs) orientation is not effective anymore. Also, there is no control on orientation by all the previous setups.

2. Airfoil or target plate:
    - Impact angle and patterns: Rupture pattern is a function of the impact angle. Figure 1-6 shows insects with different orientations and same impact angle. The perpendicular impact has the greatest amount of residue since all the impacting force applies to the insect. However, in lower impact angles, the exoskeleton does not break or stick to the airfoil. Kok et al. [26] investigated the effect of impact angle (15 to 90 degrees) on the area and height of the Drosophila Melanogaster's residue. Three zones were identified, 15 to 30 degrees, 30 to 70 degrees, and 70

to 90 degrees. The residue's height was decreased by decreasing the impact angle. However, by decreasing the impact angle from 90 degrees, the residue's area increased to the middle of the 70 to 30 degrees zone and then decreased to 15 degrees. Wohl et al. [28] study agreed with the results of the relation of the area and impact angle from Kok et al. [26] study using the same insect. However, in contradiction with Kok et al. study, the residue's height did not follow a particular pattern as the area or height of Kok et al. study. Impact at 70 degrees showed the largest residue's height. Reported errors for heights in Wohl et al. study were high and there were overlaps of residue's heights at different impact angles. This raises the issue that the result of this study might not be conclusive. Other studies [18], [22], [29], [30] reported that the largest residue height occurred at perpendicular impact. Kok et al. finding seems reasonable because as Krishnan [22] and others [18], [29], [30] showed the maximum amount of residue height is for exoskeleton and the highest amount of exoskeleton height remains at the leading edge of the airfoil during a perpendicular impact. There is no need for further investigation as most studies reported the same results and Wohl et al. opposing result is doubtful (as mentioned above because of overlapping high error values).

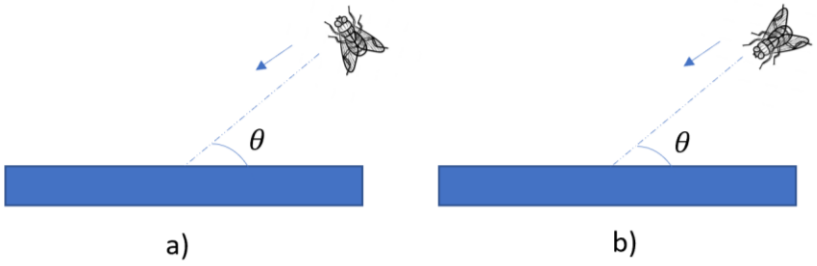

Figure 1-6 Insects with different orientations and same impact angle

3. Accelerator:
    - Airflow: Depending on the setup type, the natural airflow effect could be simulated or not. A past study [31] reported that airflow could remove up to half of the insects remaining on the airfoil. However, Peterson and Fisher [32] reported that during a flight test using a JetStar aircraft at 92 m/s insects' residues were not eroded. This contradiction might be related to the idea that most of the insect residue is eroded immediately after impact and the remaining residue is in a stable condition with airflow [32]. Also, right after the impact, before hemolymph coagulation, airflow can smear the residue [17], [33]. Results of two setups one with the presence of airflow and one without airflow [26], indicated that the presence of airflow caused higher residue area and lower residue height. To summarize, it was shown that the presence of airflow changes the amount of the residue height and area immediately after impact. However, contradictory results for the effect of the airflow on residue after a period of time needs further investigation to clarify whether airflow continuously removes the insect residue during flight or not.
    - Speed: Relative impact speed determines the breaking energy of the insect's body. Results of using Drosophila [26], [29] showed that at low velocities the insect does not rupture, or partially ruptures. At high velocities, the insect totally ruptures. Therefore, there is a transition range for insects from rupturing partially to a full rupture. For instance, consider the speed at which the exoskeleton hits the airfoil and breaks, but it is not enough for the insect to stick to the airfoil because there is no hemolymph to adhere the insect to the airfoil. Therefore, Insect rupture velocity starts from a range that few insects rupture and stick to a velocity that all insects completely rupture and stick [17], [26]. Kok et al. [26] showed that lower body parts like the abdomen of the fruit flies needed lower speed (24 m/s) to break in comparison with the exoskeleton (30 m/s). Other studies [23], [29], [34]–[37]

reported a threshold number instead of a range as the rupture velocity for the same insect (Drosophila Melanogaster). Coleman [18], [29] and Wohl [36] reported about 10 and 14 m/s, respectively. Krishnan [23] reported 21 m/s as the rupture velocity. Also, there are different regimes of impact velocity that show a higher velocity does not always mean higher insect residue for both area and height. Residue height is lower at higher velocity compared to lower velocity [26]. In contrast, the residue area is higher at high velocities. Kok et al. [26] varied the velocity from 20 to 100 m/s; it was concluded that by increasing the velocity, the residue's height decreases; however, the residue's area increases. In conclusion, the effect of velocity on height and area of residue was studied and there was no contradiction between different studies. However, further investigation is needed to study the rupture velocity since contradictory results were reported.

- Humidity, water, temperature: Ambient conditions may affect the amount of residue. Humidity, water, and temperature are conditions related to the whether the aircraft flies on a rainy day or not, whether it is in a tropical region or desert, or whether the flight is in winter or summer. Kok and Young [38] using a scrub testing method for removal of residue showed that changing humidity or soaking the residue in the water did not change the residue by a substantial amount. Using scrub over a soaked sample could be the simulation of the rain as a force (scrub) is applied to the residue in the presence of water like the force caused by impacting a water droplet on the residue during rain. On the other hand, testing was done for a formed residue. This brings up the issue that, whether formation of residue on a wet airfoil is resembled to a dry airfoil or not. In another study [39], by comparing the insect residues impacted to 20 ℃ and 70 ℃ (temperature of aircraft surface in summer in some desert regions) target plates, it was concluded that the effect of temperature was negligible. It was not mentioned whether the humidity was

controlled or not as the relative humidity changes with temperature. In summation, past studies showed that the temperature solely does not influence the residue size significantly. Also, mitigation of residue is not influenced by presence of water. However, effect of humidity and water on the formation of residue needs further investigation since reported results for effect of water were related to a previously formed residue on a dry surface.

1.2.2 Main configurations of insect impact setups

Most of the past insect impact simulator setups are divisible into three main groups: (1) Flight or road tests; (2) Insect shooters; (3) Wind tunnels.

1. In a flight test, an aircraft is used. During several hours of flying, insects impact the aircraft. In a flight test, a variety of insects rupture on the airfoils. For evaluation of coatings or other removal methods, coated Aluminum strip samples are attached to different places of the airfoil, especially the leading edge. To eliminate the weather condition, several flights are done on different days.

   A road test is the same as a flight test, but an airfoil or target plate is attached to a car while it drives on the road for several hours. Compared to the other setups, fewer conditions are in control in a flight or road test. However, a flight test is similar to real flight conditions. Also, a road test is similar to taxiing phase of flight.
2. Insect shooters are mostly pneumatic devices in the lab that accelerate insects in a tube till they reach the desired speed. Then, they are thrown toward an airfoil or an inclined plate. Insect shooters sometimes are combined with wind tunnels. It is necessary that there would be a mechanism for keeping insects intact during the shooting. Applying pressure to the insect for accelerating can cause tiny fractures on the body of the insect [40]. These fractures ultimately reduce the resistance of the insect body toward the

rupture. Also, if the insect speed after shooting and ambient airflow speed are not matched, shear stress could also deform the insect body [26], [39], [41]. Two main mechanisms were developed to overcome the mentioned issue. First, a soft foam-like coupon held the insect during the accelerating phase to keep it intact [40]. Second, the insect was accelerated to the ambient airflow speed and then released into the airstream toward the airfoil [25], [26], [39], [42]. The second mechanism was used in the wind tunnels.

3. Wind tunnels are used to simulate the airflow and flight conditions in the lab. Two main approaches were used to obtain an impact. First, insects are released into the air stream; using shear stress, they reach the velocity of the airstream after a certain distance [18], [26], [29], [43]. Finally, they impact an airfoil or an inclined plate. The first approach causes tiny fractures on the insect body during the accelerating phase [41]. These tiny fractures lower the insect body resistance to impact. The second approach uses insect shooters in the wind tunnel. The insect shooters have to be aerodynamically designed so they do not disrupt the airflow in the wind tunnel. Insects could either impact an airfoil or an inclined plate in the wind tunnel. There is no limitation for an airfoil in the wind tunnel except it is difficult to control the impact angle using an airfoil as it is challenging to control the trajectory of the insects in the wind tunnel. By using an inclined plate, impact angle could be controlled. However, there is a limitation for inclined plates in the wind tunnel. Due to the wind tunnel blockage, the inclined plate angle with the horizontal is limited to angles less than 30 degrees [25], [26], [39], [42]. A solid blockage occurs when the tunnel walls, during testing, restrict the flow field around an obstacle, increasing its drag [44], [45].

The description of setups from previous studies are presented and discussed in the Sections 1.2.2.1, 1.2.2.2, and 1.2.2.3. They are also summarized in Table 1-1.

Table 1-1 Setups from past studies

Setup name/Acronym from reference	Type	Speed (m/s)	Airflow	Impact angle (degree)
Jetstar aircraft[32]	Flight test	93	Yes	NA
Car[46]–[48]	Road test	24.7	Yes	NA
Bug gun[24]	Insect shooter	12.8	No	No
PIDD[33]	Insect shooter	34	Yes	Various
ASTIR[40]	Insect shooter	60-80	No	90
SPIrIT[40]	Insect shooter	100	No	Various
Wind tunnel[18], [29]	Wind tunnel	76	Yes	NA
BART[36]	Wind tunnel with insect shooter	56	Yes	NA
Wind tunnel with custom-built pneumatic gun[36]	Wind tunnel with insect shooter	67	Yes	Various
UVA wind tunnel[21], [23]	Wind tunnel with insect shooter	47	Yes	Various
Wind tunnel with custom-built pneumatic gun[49]	Wind tunnel with insect shooter	67	Yes	10 to 90
iCORE[26], [50]	Wind tunnel with insect shooter	100	Yes	10 to 30

1.2.2.1 Flight and road tests

Peterson and Fisher [32] used a Jetstar aircraft to detect flow transition on the leading edge. The aircraft was also equipped with hydrophobic coating and water spray systems to evaluate insect residue mitigation methods. The insect population is a function of location; therefore, aircraft flew over 15 airports in different locations of the US to collect insect residue on the airfoils [32]. The maximum speed during take-off was 93 m/s. Once the aircraft reached cruise conditions, it reached 11,600 m of altitude and 240 m/s of speed to investigate the effect of airflow on the accumulated insect residues. After landing, residue measurements like measuring residue height or the number of impacted insects were done. Wohl et al. [36] also conducted a study with flight tests to compare the results of flight tests and other methods. As an advantage of the flight tests, the natural airflow effect is observable. However, there is no control over the other conditions like impact speed or insect type. Also, flight tests due to the use of actual aircrafts are expensive and time consuming. Therefore, road tests were used to overcome this problem.

Yi et al. [46], [47] conducted research to study the effect of coating's characteristics on sticking of insect residue. Nyebar, Teflon, PMMA, and PSF, all coated on aluminum, were used as coating

samples. Samples were installed on a half-cylinder placed on top of a car (Figure 1-7). A car travelled a long distance to collect insect residues on the samples with an average speed of 24.7 m/s. After driving for 75 minutes, samples were dismounted and analyzed. Siochi et al. [48] used the same method to study the fundamentals of adhering insect residue to aircraft airfoils by conducting three days road test in the middle of summer with approximately same environmental conditions. Road tests were easier to conduct compared to flight tests. However, like flight tests, there is no control over the impact conditions. Further, the impact speed was about half the speed of the aircraft during take-off, which is when about 33% of insects are collected and since impact occurs at a low speed, sometimes insects do not rupture properly.

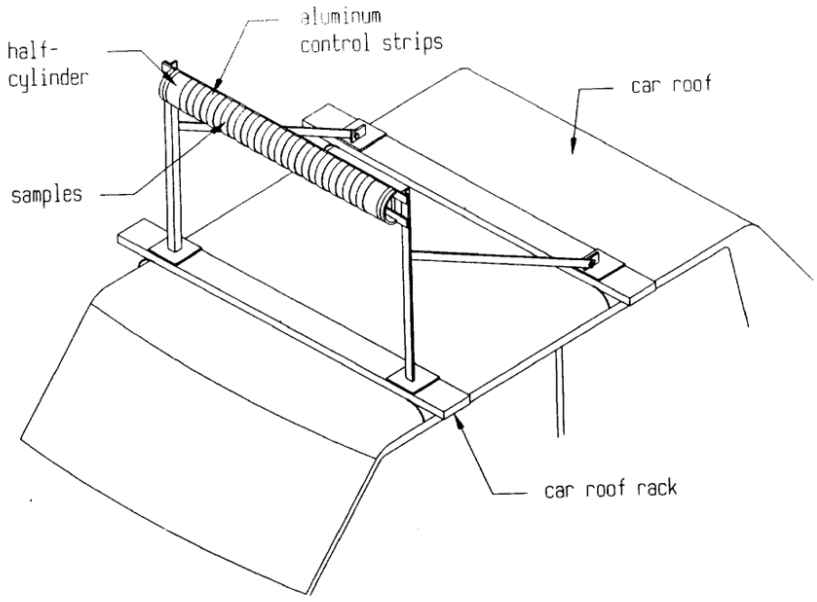

Figure 1-7 A car with a half cylinder installed on roof for attaching samples to it (from Ref. [46]*, publicly permitted to be used by NASA)*

1.2.2.2 Insect shooters

To conduct the experiment on the insect impact to airfoils in the lab, insect shooters were designed. As a preliminary study on coatings for residue mitigation [24], a simple bug gun was

constructed using plastic pipes and a 3,160 rpm fan to accelerate crickets toward a PVC pipe with coating samples installed on it. Insects' speed varied from 1.4 m/s to 12.8 m/s. By passing through the fan, cricket exoskeletons were partially damaged. Low speed of insect impact and partial fracture of insect body during acceleration were critical considerations of the upgraded bug gun for another study [33]. A pneumatic insect delivery device (PIDD) was manufactured (Figure 1-8) based on the previous bug gun; however, a vacuum pump accelerated the insect instead of the fan to avoid partial damages caused by the fan's blade. Crickets' speed was increased to 34 m/s. Additionally, after impact of cricket to sample, airflow was continued on the sample for 5 seconds to simulate the effect of natural airflow (it was not mentioned why 5 seconds was selected, but probably because residue was coagulated in less than 5 seconds). The upgraded insect shooter performed better than the past one for modelling insect impact to airfoils. However, the maximum speed of the setup was half of the take-off speed of an aircraft. Also, cricket is not a good representative of ruptured insects on aircraft airfoils since it is larger in size than 2 to 3 mm [18]–[20]. Therefore, it is preferred to use Drosophila instead.

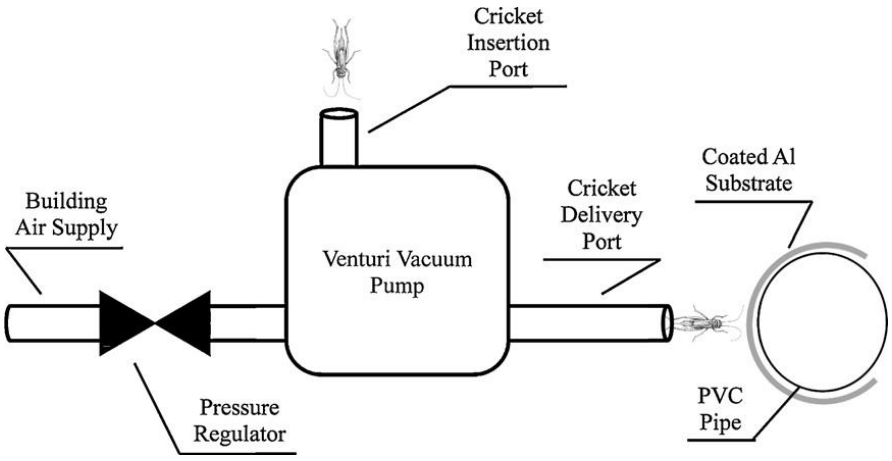

Figure 1-8 Pneumatic insect delivery device (from Ref. [33] *with permission from Elsevier)*

Young et al. [40] designed two insect shooters to test Drosophila instead of cricket. Additionally, the impact speed for both setups was between 60 to 80 m/s. The accelerated coupon impact test (ASTIR) consisted of a testing coupon, acceleration area, and deceleration area. Testing coupon

(coating surface) was accelerated to desired speed with high-pressure air. Then, it impacted insects, and pressure was released. Finally, it stopped at the deceleration part. However, at the stationary coupon impact test (SPIrIT), insects moved toward the coating surface. SPIrIT is shown in Figure 1-9. A cartridge made of compressible foam carried insects. The cartridge was accelerated by high-pressure air, but since it was from compressible foam, it kept the insects intact. Then a valve stopped the cartridge, and the insect left the cartridge and moved toward the coating surface. The impact angle was controllable by changing the angle of the coated surface. Both designs kept the insect intact, reached the take-off velocity of an aircraft, and were designed to use 2 to 3 mm insects. In addition, SPIrIT could control the impact angle too. However, the airflow effect was neglected in both designs. One solution to add airflow to the mentioned designs is to place them in a wind tunnel.

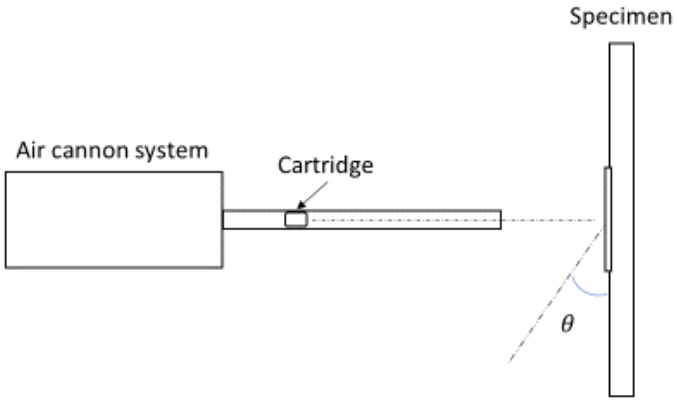

Figure 1-9 Stationary coupon impact test or SPIrIT (adapted from Ref. [26]*)*

1.2.2.3 Wind tunnels

Coleman [18], [29] determined the characteristics of the insect residue in a wind tunnel. Drosophila Melanogaster was the selected insect as it is a good representative of the impacting insects to aircraft airfoils. The maximum velocity of the wind tunnel was about 76 m/s. Insects were held in a closed tube. The position of the tube could be changed in two dimensions in order

to get insect rupture on different spots of the airfoil. The tube was opened when the air stream in the wind tunnel reached steady conditions. Then, insects were released into the airflow. Finally, insects reached the airflow speed after a while and impacted the airfoil. Coleman did not mention how the speed of the insect before impact was verified. Probably he assumed that the insect reached the speed of airflow after a short period of time. Although Coleman's setup characteristics like speed were similar to the real flight test, it had a significant issue. Accelerating the insects in the airstream causes tiny or considerable fractures on the body of the insects [41]. These fractures and velocity difference with airstream sometimes leads to early insect explosion in the air before reaching to the airfoil. Later Wortmann [43], [51] used the same method as Coleman to evaluate the effectiveness of the rubber coatings as a mitigation method for insect residue; however, wind tunnel speed varied from 11 m/s to 55 m/s. To solve the tiny fractures on insects caused by accelerating in wind tunnel setup issue, next setups used insect shooters to accelerate the insects to reach the airstream speed before releasing them to the airstream [21]–[23], [25]–[27], [36], [39], [49].

Basic Aerodynamic Research Tunnel (BART) consisted of a swept airfoil model (Figure 1-10) with 8 degrees angle of attack and an insect injector. Previously, BART [52], [53] was developed for studying the fundamentals of complex flows and verification of computational fluid dynamic (CFD) simulations. Wohl et al. [36] added an insect injector to BART to compare and verify the results of insect impact using three different setups: a flight test, BART, and a lab-scale wind tunnel (Figure 1-11). BART's wind tunnel speed was 56 m/s, and the chord length of the airfoil was 61 cm. Using a modified Vaccon HVP-300 Venturi pump, insects accelerated and injected into the airstream. About 15 to 25 insects were released each time. It was not mentioned whether the insects' residues overlapped each other or if there was a mechanism to hit the insects to different spots. A high-speed camera and insect injection system were triggered simultaneously. Venturi pumps use pressure differential to accelerate the particles. It was not mentioned how the insect injector prevents the insects from being partially fractured before impact due to the pressure

differential. Result of comparing three test setups showed that good performance of a coating in lab (e.g., BART) does not always mean a good performance in the flight condition like a flight test. In summary, the first setups used an aircraft or a car to collect insect residues over a plate. However, there was no control over most of the factors like insect type, impact angle, etc. Then, lab-scale insect shooters and wind tunnels were developed to control more factors in the lab (e.g., impact angle). Lack of presence of airflow in insect shooters and tiny fractures on insect body (caused by accelerating) in a wind tunnel were the main reasons for developing a new setup by combining insect shooters and wind tunnels.

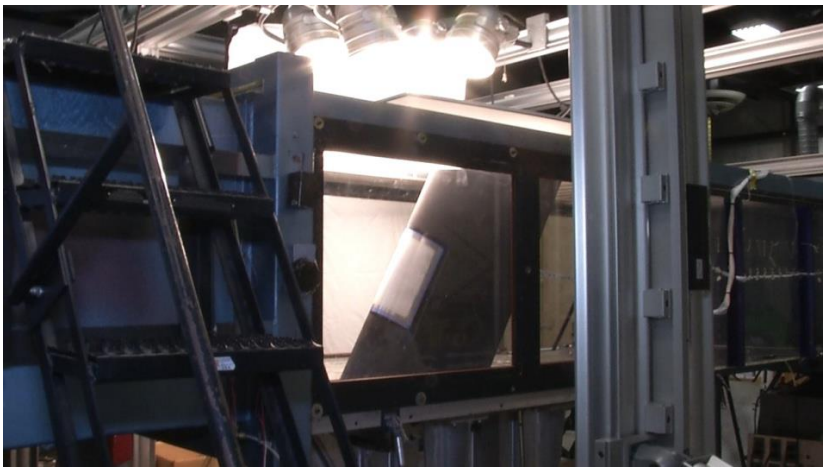

Figure 1-10 BART wind tunnel (from Ref. [36]*, publicly permitted to be used by NASA)*

Wohl et al. [36] also used a lab-scale wind tunnel with a custom-built pneumatic gun (Figure 1-11). The custom-built pneumatic gun was the modified version of the PIDD insect shooter (Figure 1-8) in Section 1.2.2.2. Insects were accelerated using a Venturi vacuum pump to 67 m/s airstream velocity. Coated aluminum samples were folded and installed on the airfoil model. In spite of the setup simulating natural airflow, take-off speed, and the use of Drosophila Melanogaster, no mention was made of how fractures on insect bodies could be prevented by a pressure differential (same issue as BART setup).

Figure 1-11 Lab-scale wind tunnel with a custom-built pneumatic gun (from Ref. [36]*, publicly permitted to be used by NASA)*

Krishnan [21]–[23], [27], [54] also used an insect shooter in the wind tunnel (Figure 1-12). A NACA0038 airfoil was placed in a wind tunnel. Using compressed air, insects were accelerated to the airstream speed before impact. From past studies [34], [35], Krishnan [23] assumed that rupture velocity was about 21 m/s. Therefore, the study was done at 47 m/s, so insects totally were ruptured after impact. For each experiment, 5 insects were released, until a total of 50 insects were released. The insect injection system was able to move upward and downward, so insects hit different spots on the airfoil. Same as the previous setup [24], [36], [49], there was no method to avoid insects from prior damage due to acceleration using high pressure. A mechanism for avoiding prior damage to insect before impact was the main issue that most of the past setups have faced.

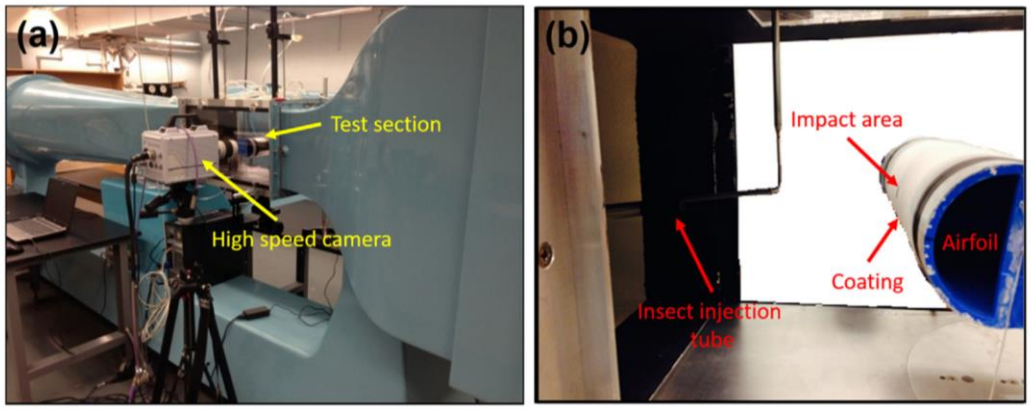

Figure 1-12 a) and b) NACA0038 in a wind tunnel (from Ref. [27] *with permission from Elsevier)*

Despite the fact that most of the wind tunnel setups did not include a method for preventing tiny fractures on insect bodies, they were able to simulate some aspects of insect impact like speed of impact and presence of airflow. Also, the impact angle was not controllable in most of the setups or impacts were done at a fixed angle (mostly perpendicular). For the airfoil in the wind tunnel setups, an estimation of impact angle could be calculated based on the location of the residue on the airfoil by assuming that the insect moves in a straight line; therefore, the angle between the trajectory line of the insect and tangent line of the surface at the impact point is a good estimation impact angle. In order to control the impact angle in wind tunnels, tilted surfaces were used instead of the airfoil.

Carter and Loth [49] used the lab-scale wind tunnel (Figure 1-13) which previously was designed by Wohl [36]. A tilted surface was installed on the airfoil model to change the impact angle. A flat plate bug launching system was developed. Same as Wohl's setup [36], the air stream speed was about 67 m/s. Three insects were released toward the tilted plate each time. Carter and Loth [49] experimented with impact angles ranging from 10 to 90 degrees, which raises the question of whether the wind tunnel blockage was considered (see Figure 1-13). Also, the same issue of tiny fractures on insect bodies was not considered.

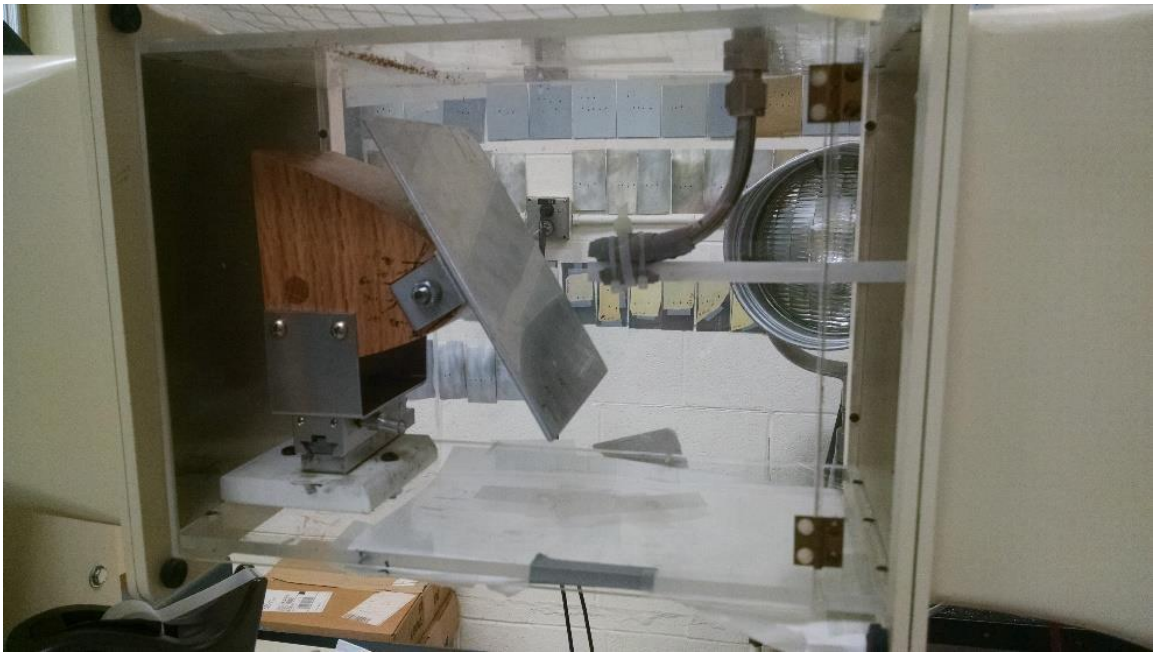

Figure 1-13 Tilted flat plate used in a wind tunnel (from Ref. [49]*, reprinted by permission of the American Institute of Aeronautics and Astronautics, Inc.)*

Icing and contamination research facility, iCORE, was modified by Kok et al. [26] to evaluate coatings for insect impact experiments. A tilted flat plate was placed in the test section of the wind tunnel. Impact angles varied between 10 to 30 degrees and air stream speed was about 100 m/s. Higher impact angles were not possible due to the wind tunnel blockage. Height and area of residue from this study were not useful to study the largest residue height or critical height of regime transition because low impact angles reduce the height of insect residue significantly. However, since the rupture happened completely at 100 m/s, the setup was adequate for evaluating the coatings. The shooting device was aerodynamically designed to disrupt minimum airflow. The delivery device used a housing chamber for insects to avoid direct contact of pressured air with insects and accelerated the insect to airstream speed. iCORE solved the problem of tiny fractures; however, a narrow range of impact angles was tested.

To summarize, it was understood from past setups that an insect impact simulator setup must keep insect intact before impact. Airflow should be presented during the test. Also, setup must be

able to produce impacts with take-off velocity of aircrafts. Impact angle is challenging to be controlled as it is not controlled by most of the setups, but it is valuable if it is controlled. Furthermore, other conditions like insect type and environmental factors are advised to be controlled or kept constant.

1.3 Mitigation methods

In this section, first, mitigation methods for insect residue on aircraft airfoils are introduced. Then, using coating as the main method of insect residue prevention in the latest studies is selected and its advantages are mentioned. Finally, characteristics of a coating that affect the residue size are introduced and the most important findings of past studies are mentioned.

1.3.1 Removal methods

To maintain laminar flow on the LFC aircraft, airfoils have to be either cleaned and smooth or the contamination height should be less than $100 - 400\ \mu m$ [17], [18], [21], [32], [55]–[57]. A removal method helps to either eliminate or mitigate the contamination on airfoils. These methods are either active or passive. Active methods mostly use a mechanical device to mitigate insect residue. A passive method uses the surface properties or environmental properties (e.g., airflow) to avoid or reduce the insect residue. Coleman [18] proposed a list of removal methods. The list is presented below and is divided into two groups of active and passive methods.

Active

- Mechanical scrapers: a mechanical device like a windshield's wiper, scraps insect excrescence from the airfoil.
- Deflectors: a deflector which either deflects insect paths or traps them.
- Removable covers: type of cover which would be torn during flight.
- Dissolvable covers: type of cover which would be dissolved by a certain fluid.
- Thermally removable covers: type of cover which would be removed by combustion or heat.
- Viscous fluid: a highly viscous fluid which traps insects in itself and would be removed by airflow shear.
- Fluid discharge: a continuous discharge of fluid to wash away the insect excrescence.

- Suction: suctioning the disrupted airflow, till all turbulent streams are suctioned and laminar flow is restored.

Passive

- Natural airflow: residues are eroded to a subcritical height by natural airflow.
- Coatings: avoid the adherence of contamination using surface properties.

1.3.2 Coatings and characteristics

Coatings are applied to the surface of an object in order to improve its surface properties e.g., reduce adhesion. Coatings are used for protection against corrosion, wetting purposes, dewetting, etc. In the latest studies of insect contamination reduction, coatings were developed and employed due to their premise to prevent insects from leaving a residue after rupture. In addition, coatings are passive methods which means there is no need to activate any mechanism during the flight; therefore, they are more convenient to use.

Modifying coatings characteristics affect the insect residue adhesion to the surface, e.g., lowering surface energy, reduces the residue's area. Since the insect body is filled mostly with water, it can be a good estimation that it behaves like a water droplet [38], [58], [59]. A summary of past coatings used is provided in the Appendix A.

Coatings characteristics are described below:

- Surface energy: In physics, free surface energy refers to the additional energy present at the surface of a material compared to its bulk. Surfaces with higher surface energy are more favourable to be wetted. Since most of the insect hemolymph is water, surface energy is one of the important factors that play a role in sticking the ruptured insect body to the surface. In almost all the studies, low surface energy coatings showed low residue area. However, it was reported that surface energy had no correlation with height of the residue [23]. Almost all studies suggested that lowering surface energy and increasing its

roughness, increases the coating residue mitigation strength. Superhydrophobic coatings with low surface energy and high roughness values showed the lowest amount of residue, and sometimes there was no residue (no special condition was reported for leaving no residue). For instance, Kok et al. [42] coated aluminum 2024 with an epoxy superhydrophobic polymer (SH Epoxy). After conducting tests on different coatings in iCORE facility (30° impact angle, 100 m/s impact speed), only on SH Epoxy coating no residue was left.

- Roughness: Surface roughness contains nano-scale and micro-scale valleys and peaks. Roughness affects the contact angle [60]. In lower contact angles, roughness decreases the contact angle, while in higher contact angles, roughness increases the contact angle. However, effect of roughness on residue is not related to its effect on contact angle. Past studies [25], [27] reported that the spreading mechanism of hemolymph was related to roughness. Peaks and valleys trap hemolymph or prevent hemolymph from spreading. Coatings with higher values of roughness showed lower residue area. The roughness was often created by sandblasting, which means small size particles were blasted onto the aluminum surface [25], [39], [50]. In contradiction with past studies, it can be hypothesized that, increasing roughness should increase the residue area as roughness causes mechanical locking of the insect on the surface during the impact which leaves more residue behind. Therefore, further investigation is needed to examine the effect of roughness on insect residue.
- Surface chemistry: In addition to water, hemolymph contains proteins, lipids, etc. The chemistry or composition of a surface can avoid or attract special substances. For instance, an oleophobic surface resists lipids adhering. Kok et al. [42] compared two similar superhydrophobic coatings with similar surface properties, but one was epoxy based (surface energy and surface chemistry are not independent of one another so to examine effect of surface chemistry, surface should be kept constant in a test). It was

concluded that the change in amount of insect residue was caused by surface chemistry. Only few studies mentioned the effect of surface chemistry. They compared two coatings and used the surface chemistry as the reason of the difference between the residue reduction ability of two coatings with almost similar surface energy and roughness values. Therefore, further studies are needed to do an in-depth analysis of the surface chemistry.

- Elasticity: The elasticity for a coating can be thought of as behaving like a spring. The insect's impact energy is partly stored in the surface elastic mechanism instead of being spent on rupturing. As a result, some residue bounces off the surface instead of adhering. Wortmann [43], [51] coated the leading edge of an aircraft with rubber coatings. Comparing the residue's amount for 1 to 3 mm thickness rubber, it was concluded that 3 mm thickness rubber decreased the residue's amount better than thinner coatings because of its elastic properties and higher compression range. However, a comparison with an uncoated surface was not done to elaborate the effect of elasticity. Further investigation could be done to study the effect of adding elasticity to coatings.
- Durability and erosion: A surface must maintain its desired property over an extended period of time to be practical. Coatings are eroded during flight due to impacting sand, dust, ice particles, and insects. Few studies [38], [61] used different methods to evaluate the resistance of their coatings to erosion by e.g., scrubbing. However, a general method has not been developed yet to evaluate the coatings resistance to erosion for the purpose of insect residue reduction.

1.4 Development of a new apparatus

In this section, first, a summary of deficiencies of past setups is mentioned, and gaps of past studies are identified. Then, scope of this study is determined. Finally, objectives for development of a new apparatus are determined.

1.4.1 Gaps of the past studies

Flight tests or road tests did not have control over most of the conditions of the experiment. In addition, they were time-consuming. Then, insect shooters were developed to overcome the problems of the flight and road tests. Velocity, insect type, and impact angle were controllable; however, the effect of the natural airflow was neglected mostly. Moreover, wind tunnel setups were developed to overcome shortcomings of flight tests and simulate the natural airflow. First wind tunnel setups released the insects in the airflow to accelerate and reach the speed of the wind tunnel; however, the speed difference between insect and airflow caused tiny fractures on the insect's body. Insect shooters were placed in the wind tunnel to accelerate the insect to the speed of airflow before it was released into the air stream; however, in most of them, it was not mentioned how the insects were kept intact during the delivery.

As it is mentioned in Subsection 1.3.2, effect of surface chemistry, roughness, elasticity, and erosion need further investigations. Limited study was done on surface chemistry and due to dependency of surface chemistry to surface energy, more study is required to clarify the effect of surface chemistry. Roughness also needs further investigation due to a contradiction between past studies and intuition. Furthermore, only one study was done on surface elasticity which no comparison was done between the coated and uncoated surfaces. Therefore, elasticity of surface requires more research. Lastly, a general method for evaluating the coatings' erosion resistance for the purpose of minimizing insect residues needs to be developed.

1.4.2 Scope of the study

In this study, a new approach was taken to control most of the conditions and simulate the insect impact to airfoils. In the past setups, except for flight and road tests, the insect was thrown toward the airfoil, which in most of the setups caused tiny fractures on the body of the insects [18], [21], [23], [27], [29], [33], [36], [43], [49], [51]. However, in a real flight condition, the airfoil moves toward the insect, and the insect has only a minimum speed to not deflect from the airfoil path. In this study, it was aimed to develop a setup in which the airfoil moves toward the insect. Therefore, insects would be kept intact before impact.

In addition, as it is mentioned in Subsection 1.2.1, effect of airflow needs further investigations since results from limited studies which were done on airflow were contradictory. Therefore, presence of airflow was a main goal of designing the new setup to study the airflow effect on insect's residue.

Furthermore, it was aimed that the new setup would be able to reach the take-off velocity of the aircraft. In addition, velocity change would be possible to simulate the acceleration of aircraft. Fundamentally, accelerating airfoil causes that a greater force applies to the insect during impact in comparison with a constant speed airfoil. Also, as it is mentioned in Subsection 1.2.1, rupture velocity of the insects needs further investigation since different numbers were reported for the rupture velocity of insects. Another investigation was aimed to be done to clarify the numbers for rupture velocity.

Studying other conditions like temperature, orientation and impact angle was not the scope of this study. However, it was aimed to keep few of them constant or control them in some extent. For instance, one insect type was used. However, there was no control on the age, gender, and mass of insects. Also, to simplify the experiment, tests were done in the room condition. In addition, since it was not possible to control the orientation of the insect before impact, like in past studies, more tests were done to minimize the effect of the insect orientation. Furthermore, the impact

angle was not controlled. However, the insects impacted different spots of the airfoils. Therefore, a range of impact angles was tested.

As it is mentioned in Subsection 1.3.2, surface chemistry, roughness, elasticity, and erosion require more study. Since the focus of the current study was manufacturing a new setup and verification of it, only effect of roughness was investigated. Effects of surface energy and superhydrophobicity were tested for setup validation purposes.

1.4.3 Objectives of study

There are two groups of objectives in this setup, design (objectives 1 and 2) and experimentation (objectives 3, 4, and 5). However, the main goal of this study is designing a new setup that overcome the deficiencies of past setups (objectives 1 and 2). Other objectives are the minor goal of this project.

Main objectives of designing the new setup are listed below.

1.1 Keeping insect intact before impact

1.2 Presence of airflow

1.3 Reaching take-off speed of an aircraft.

To improve and design a standard setup, a group of secondary objectives were determined and are mentioned below.

2.1 Maximizing the possibility of insect impact to leading edge of airfoil

2.2 Simplifying the procedure of data collection

2.3 Ability of modifying the speed during the test

2.4 Launching both insect and spherical objects

After designing the setup with the above-mentioned objectives, the new setup needed to be verified with past setup results and produce new outcomes. Three experiments were designed with below mentioned objectives.

3 Verification of the setup

3.1 Clarifying the magnitude of the rupture velocity for fruit fly

3.2 Comparison of insect residue size values on aluminum with other studies

3.3 Effect of surface energy on residue area

3.4 Effect of superhydrophobicity on residue area

4 Producing new outcomes

4.1 Effect of using a coating on rupture velocity number

4.2 Evaluating available commercial coatings

5 Further investigation on controversial topics

5.1 Clarifying the rupture velocity number

5.2 Studying effect of natural airflow removal

5.3 Studying effect of surface roughness

Chapter 2 Methodology

This chapter is divided into three sections. In the first section, the design and manufacturing methods of the new apparatus are presented. In the next section, sample preparation and experiment procedures are explained. Finally, methods for analyzing the results are presented in the last section.

2.1 Design

In this section, all the methods for designing and manufacturing the setup are explained. First, an overall design of the setup is presented in the conceptual design subsection. Setup includes three main subsystems: rotation subsystem, particle launching subsystem, and computational subsystem. In the rotation subsystem, power transmission and related subjects are discussed. The particle launching subsystem includes the design of apparatus for launching the insect toward the airfoil. In the computational and electrical subsystem, the design of electrical circuits and the time synchronization of insect and airfoil for impact are explained. Finally, methods for imaging the impact and increasing the magnification and brightness of the images are discussed.

2.1.1 Conceptual design

An overall design of the setup with its objectives is required for designing a detailed setup. A schematic of the conceptual design of insect impact to the airfoils is shown in Figure 2-1. A particle dropper presents one particle at a time to the particle launcher. The particle launcher directs the particle toward the moving airfoils, aiming for the airfoil's leading edge. Airfoil moves with a rotary system.

Besides the main objectives of the setup, the present system was designed with four secondary objectives in mind. The initial objective was to maximize the likelihood of successful impact. A

successful impact is defined in the Section 2.1.5.2. The second objective was to simplify the procedure of collecting samples to develop a standardized setup for rapid testing. The third objective was to eliminate previous studies' velocity constraints and to modify velocity during testing. The final objective was to lunch both spherical particles and insects.

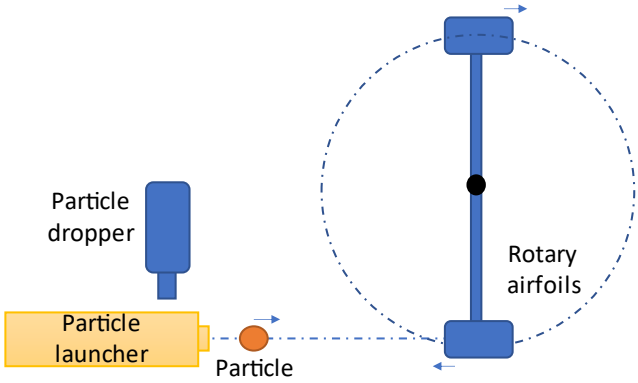

Figure 2-1 Schematic of conceptual design from top-view for the new apparatus

2.1.2 Rotation subsystem

In this section, the design of a power transmission system for rotary airfoils is discussed. Since the rotary airfoils move with high velocities the vibration of the system, disintegration of the airfoils due to high air pressure, and safety are the concern.

The rotation subsystem was previously designed and manufactured by another student. However, the rotation subsystem needed modifications since setup vibrated with large amplitude, airfoils disintegrated, and safety of setup was poor. The modifications are discussed in the following sections.

2.1.2.1 Power transmission

A power transmission system has to be designed and manufactured to move the airfoil. The rotary airfoils need to reach the take-off velocity of an aircraft (67 to 80 m/s for typical jetliners [62]), a brushless 25V MayTech DC motor with a peak speed of 1700 rpm was used to rotate the airfoils. As it is shown in Figure 2-2, two arms of 25 cm long with diameters of 1 cm made with aluminum rods were used to connect the airfoils. The radius of impact was 33 cm from the centre, due to the fact that the bug hit the front edge 8 cm from the inner side of the airfoil. Motor speed and radius of impact were selected based on the reaching the take-off velocity of an aircraft (about 60 m/s) and compactness of setup. An aluminum hub connected the aluminum rod and motor shaft expansion (Figure 2-2). Two ball bearings secured the aluminum motor shaft expansion vertically. A flexible shaft coupling was installed between the motor and the shaft expansion to adjust for minor misalignments between the motor shaft and the airfoil structure. A functional power transmission system at high velocities was designed and manufactured. Power transmission subsystem was placed in the setup using metal connectors. A cross-section and full picture of the setup with steel frames and connectors is shown in Figure 2-3. Mechanical drawings of the parts are provided in Appendix C.

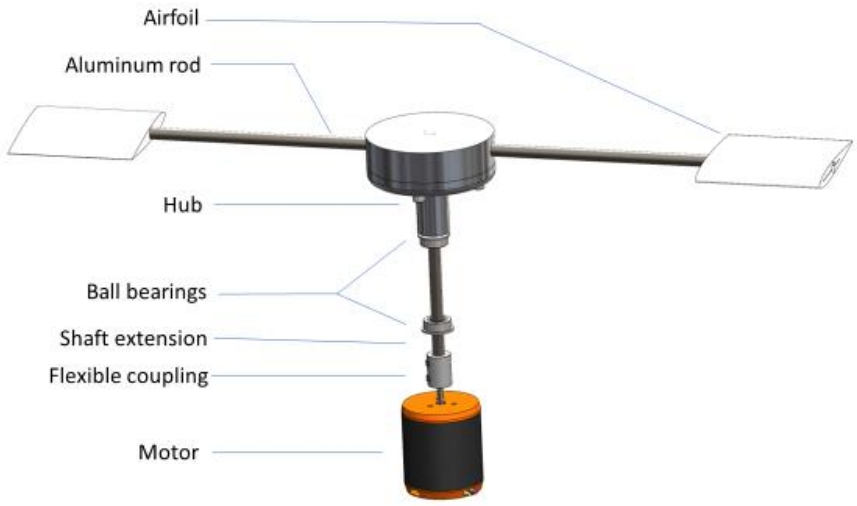

Figure 2-2 Power transmission subsystem

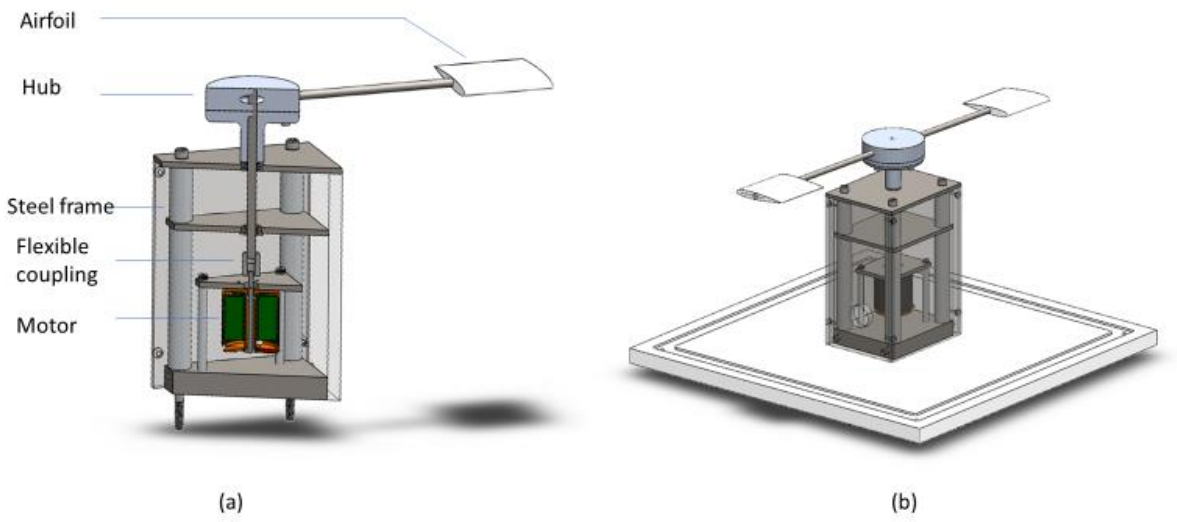

Figure 2-3 a) Cross-section of power transmission subsystem with frames and connectors and b) Full-view of power transmission subsystem placed on the bottom of the setup

2.1.2.2 Vibration

At high speeds, a minor imbalanced mass on the airfoils causes significant vibration across the whole structure. Generally, vibration in a setup affects the precision of the setup and damages the setup in the long term. Therefore, solutions to vibration are required to reduce the vibration amplitude. Vibrations were minimized in a series of steps; these steps were carried out either by mass reduction, symmetrical design, shortening the radius of rotation, or vibration absorption materials. All power transmission components were designed symmetrically about the rotation axis, balanced, and levelled. For instance, two airfoils were used symmetrically about the motor's rotation axis in order to balance the rotational system. However, if one airfoil was used, it could cause high vibration amplitude due to the imbalance of mass. Airfoils and other rotational parts were levelled to the horizontal surface using a manual levelling tool. Furthermore, the vibration

was reduced by mass reduction. The mass reduction was addressed by using aluminum parts and hollow plastic airfoils. Finally, Super-Cushioning Abrasion-Resistant Polyurethane Rubber, a vibration-absorbing polymer was put beside all of the setup's fasteners. In brief, system vibration was reduced to a negligible low amplitude vibration compared to the setup’s vibration before implementing these techniques.

2.1.2.3 Airfoil design

Another issue that has to be considered about the high speed and very light airfoil is the high shear stress of airfoil with air can eventually damage the airfoil. Also, since the leading edge of the airfoil is the stagnation point, it is the highest pressure point on the airfoil which could propagate damage from this point. Therefore, the airfoil has to be designed and selected from materials that are resistant to shear stress and pressure. Polylactic acid or PLA was used to create two symmetrical NACA0012 airfoils with a chord length of 10 cm (Figure 2-4). NACA0012 is a standard airfoil for modeling and since it is a symmetrical airfoil it does not experience lift force (there is no need to model lift force for insect impact to airfoil). A chord length of 10 cm is an optimized length that is large enough to neglect the effect of insect’s length in comparison with airfoil’s length (like an aircraft) and it is small enough to reduce the weight of the airfoil. PLA is a thermoplastic with low density and good impact strength that is normally used in 3D printing. The inner body of airfoil was porously filled by 3D printer to reduce the weight of airfoil. However, the outer body was fully filled to increase the strength of the airfoil (2 mm thickness of outer shell). In early trials, the leading edge or the stagnation point operated as the most concentrated point of stress and pressure, eventually resulting in airfoil disintegration (Figure 2-5). Therefore, the leading edge of the airfoil was increased in thickness to 5 mm to solve the disintegration issue. Also, a layer of high resistant tensile tape was added to the airfoil’s outer body to increase the strength of the airfoil. Airfoils were designed light, resistant to shear and pressure, and symmetrical.

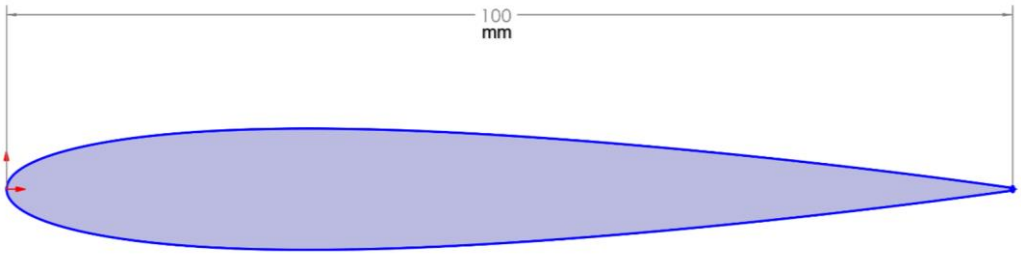

Figure 2-4 NACA0012 airfoil sketch

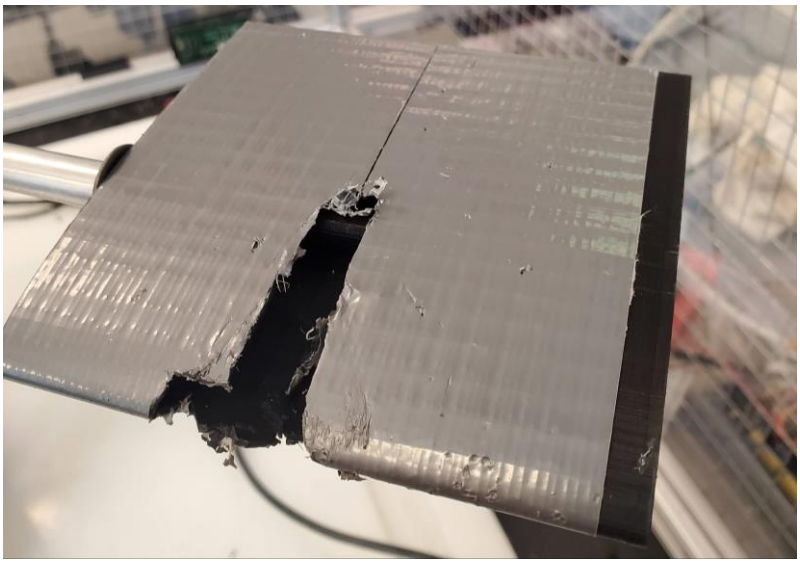

Figure 2-5 Disintegrated airfoil

2.1.2.4 Safety

A final consideration that has to be taken into action is that if any of rotary parts disintegrate, it can cause serious damage to people near the apparatus. Therefore, a safety system has to be developed and installed for the apparatus. The whole system was enclosed in an aluminum cage with acrylic faces. Additionally, four metal meshes were added to the cage's side faces for increased protection. To prevent an unexpected injury, a forced shutdown sensor was used to

turn off the whole system, if the cage's door opened. Setup was safely designed by adding the mentioned methods. A picture of safety mechanisms of the apparatus is shown in Figure 2-6.

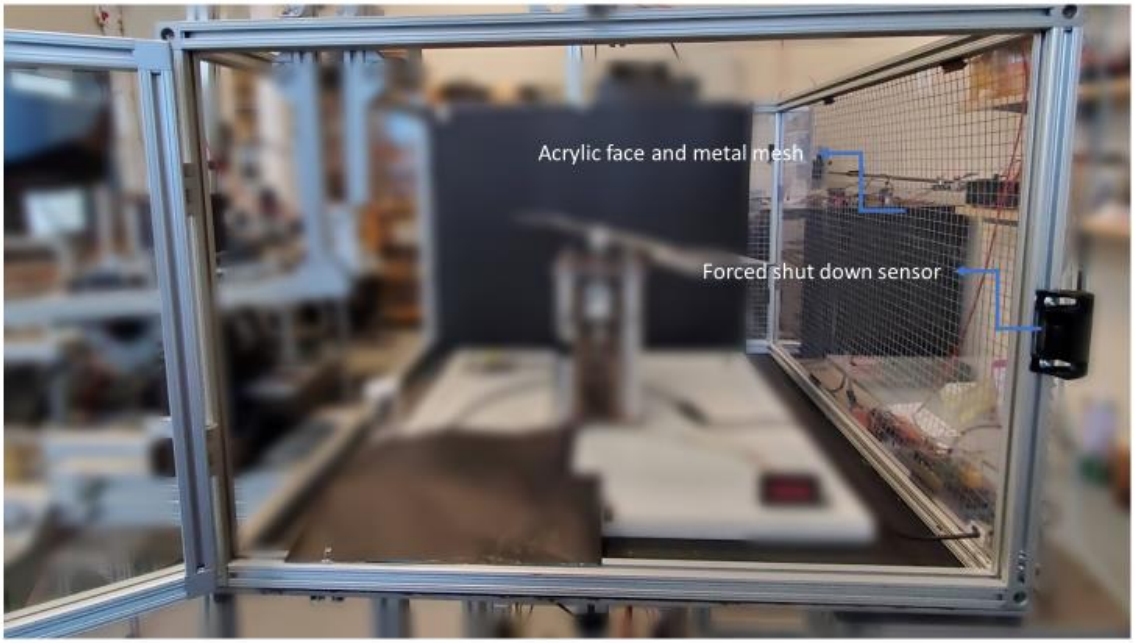

Figure 2-6 Aluminum cage, acrylic faces of the setup with metal meshes, and forced shut down sensor

2.1.3 Particle launching subsystem

The particle launching subsystem includes a particle dropper, a particle launcher, and an aligner. The particle dropper provides the particle for the launcher. The particle launcher throws the insect toward the airfoil. The aligner corrects the insect's path toward the airfoil (before launching).

2.1.3.1 Particle dropper

Before the particle launcher activates, it has to be provided with particles. Since one of the objectives of the setup is to facilitate the process of data collection, therefore by storing and getting ready several insects in the setup, the filling time of setup with insects would be reduced. However, the setup needs to be able to pick an insect, among the stored insects, at a time for

shooting because if several insects are launched toward the airfoil together, their residue could cover each other which later makes the residue analysis difficult. The particle dropper resembled a segment of a revolver gun (Figure 2-7). The apparatus was composed of two concentric horizontal discs, one is able to rotate and the other one was fixed. The top disc included ten holes, whereas the lower disc contained just one hole. Fruit flies or any particles of the same size were inserted into the holes on the top disc. Particles were dropped into a tube when holes on the top and bottom discs line up. An Arduino controlled the Mercury Motor 12V stepper motor with 200 steps on the particle dropper. The tube connected the particle dropper to the particle launcher. Particles moved through the tube to be placed in the particle launcher.

Also, the particles have to be kept intact during the delivery process (Section 1.4). Processes of top disk rotation and dropping particles via tube were designed to avoid insect injury by reducing the speed of rotation and filleting the sharp edges. Therefore, the setup kept insects undamaged during the delivery.

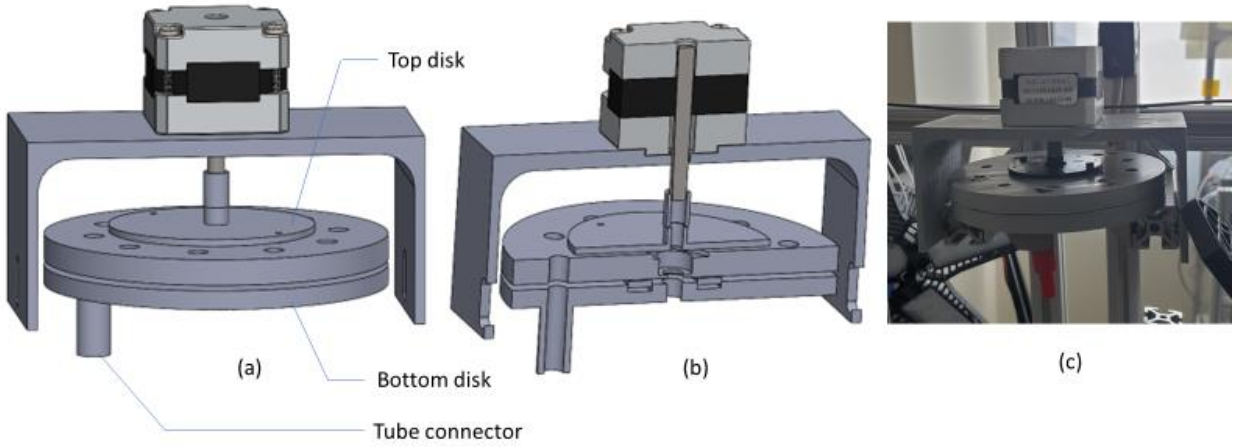

Figure 2-7 a) CAD view, b) Cross-section, and c) a picture of particle dropper

2.1.3.2 Particle launcher

To simulate the insect impact to an airfoil, insects either are thrown toward a fixed airfoil, airfoils are moved toward the insects or a combination of both. The last option in which both move, is more similar to the actual insect impact phenomenon which also simulates the presence of natural airflow and smearing effect. A particle launcher is needed to be able to throw insects having complex geometrical shapes, and also such particles may not be placed on the particle launcher with the same orientation every time.

The particle launcher's basic components were a body, a spring, a particle holder, a 24V trigger solenoid with 1cm movement, and a combination of a stepper motor (14V, 1A, and 1.8 degree/steps) with a slider and a thread. First, a conceptual explanation of particle launcher is provided. Using the stepper motor, the particle holder moves in the body to compress a spring (Figure 2-9). Then, the compressed spring is locked by the solenoid and released to launch a particle. In the following, each part is explained in detail. The particle holder was designed so that any particle would sit roughly in the middle of the container (Figure 2-8 a and b). Two extensions were added to the particle holder to limit the particle holder to move only in one direction (Figure 2-8 c and d). A schematic of whole shooting parts assembled together is shown in Figure 2-9, a picture is available in Figure 2-10, and stages of launching particle is shown in Figure 2-11. A thin coating of oil was put between the particle holder and the body to decrease friction and work smoothly. A spring was used to store the compression in the body, which was placed between the particle holder and the body. The particle launcher at its starting position is shown in Figure 2-11 part a. An 8.5 cm one-axis slider transformed the stepper motor's rotating movement into linear movement. By attaching a thread to the slider and particle holder extension, the stepper motor compressed the spring for 1.8 cm (Figure 2-11 part b). The calculation for the length of spring compression is explained in the next paragraph. The solenoid then held the compressed spring (Figure 2-11 part c). After that, the motor returned the slider to its starting position (Figure

2-11 part d). Due to the fact that the thread could compress but not push, it will not restrict the spring's motion when it is released. Finally, the solenoid worked as a trigger, allowing the spring to be released (Figure 2-11 part e). Once the spring was restored to its original position (Figure 2-11 part f), the particle launcher fired the particles. Resin curing 3D printing was used to create the particle launcher's parts. An Arduino controlled the stepper motor and solenoid. Arduino is fully explained in Section 2.1.5.3.

Another factor which affects the speed of the insect during throwing is that airflow (from air circulation in the setup caused by rotary airfoils) should draw the insect away from its straight path with the lowest possible deflection. Spring compression length was obtained by trial and error for an insect speed of about 2.3 m/s which kept the insect undamaged, and it was deflected a very small amount from the straight line by airflow (see Section 2.1.5.1). Therefore, the particle launcher was able to throw insects in a straight line with low deflection while keeping the insect intact.

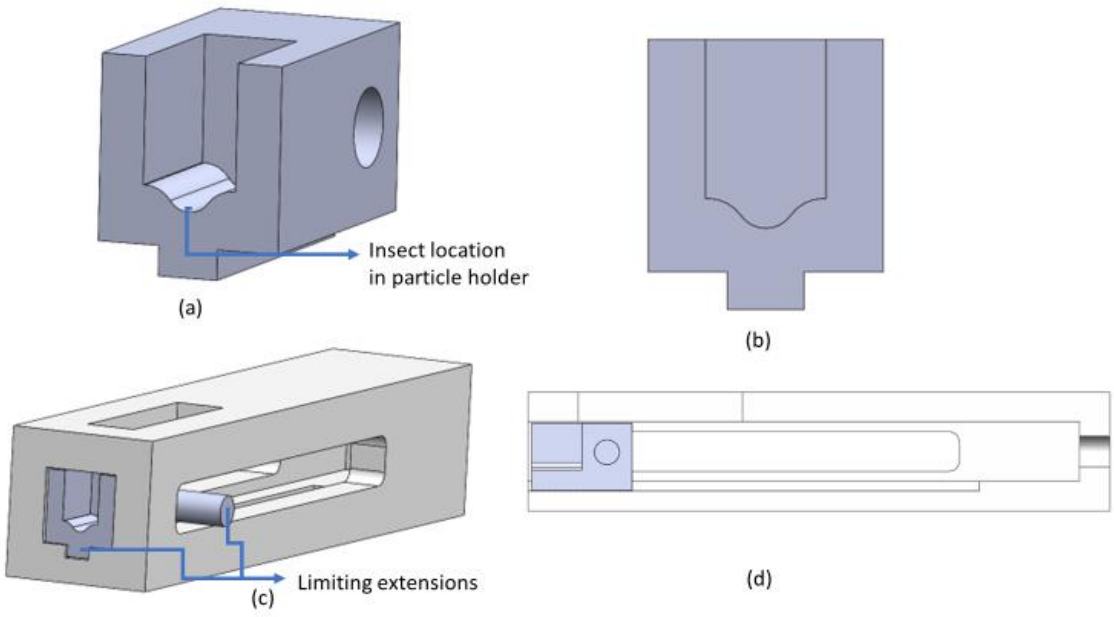

Figure 2-8 a) Particle holder isometric view, b) Particle holder front view, c) Location of particle holder in the body of particle launcher, and d) Side view of particle holder in the body of the particle launcher

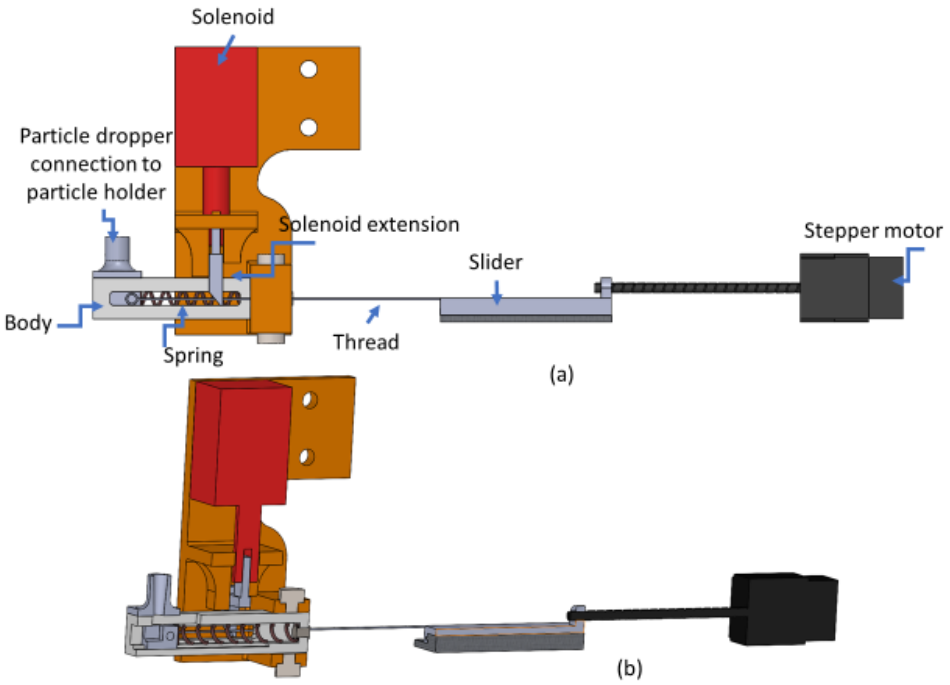

Figure 2-9 a) Particle launcher and b) Cross section of it

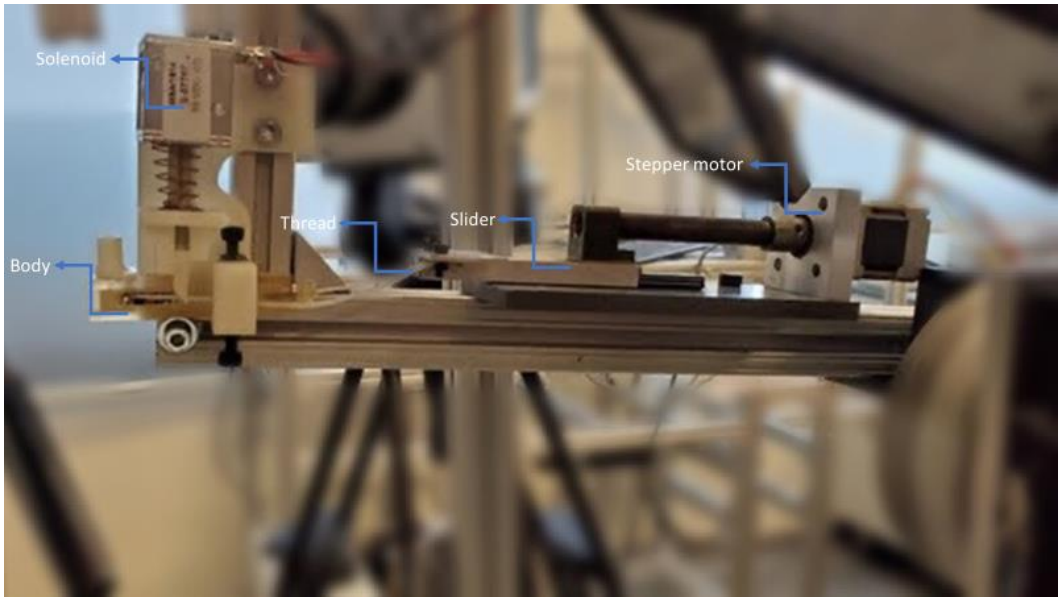

Figure 2-10 Picture of particle launcher

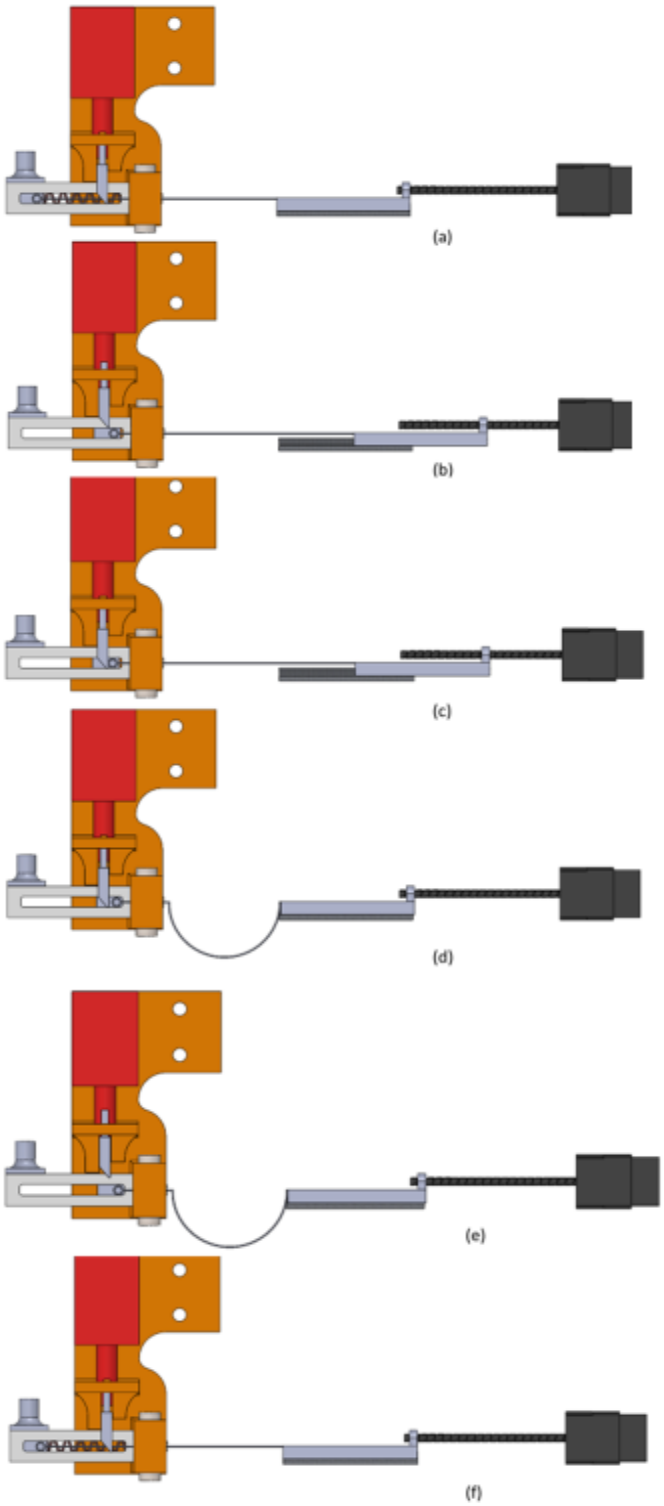

Figure 2-11 a) Starting position of particle launcher, b) Compressing the spring, c) Holding the compressed spring with solenoid, d) Releasing the thread, e) Releasing the spring by moving the solenoid, and f) Particle holder moves back to the starting position

2.1.3.3 Aligner

While the insect launcher throws the insect in a straight line, it may not hit the airfoil because of misalignment. Also, sometimes because of path deflection caused by airflow, the moving path of the insect needs to be redirected toward the airfoil. By calibrating the position of the particle launcher, the above issue can be avoided. The whole particle launcher mechanism was mounted on a HARVARD APPARATUS CANADA three-axis aligner (Figure 2-12). The aligner could easily calibrate the insect's path after shooting it if the insect did not hit the front edge of the airfoil. The calibration procedure was done by observing the location of insect impact. Then, by trial and error, particle launcher was moved until insect impacted the leading edge of airfoil.

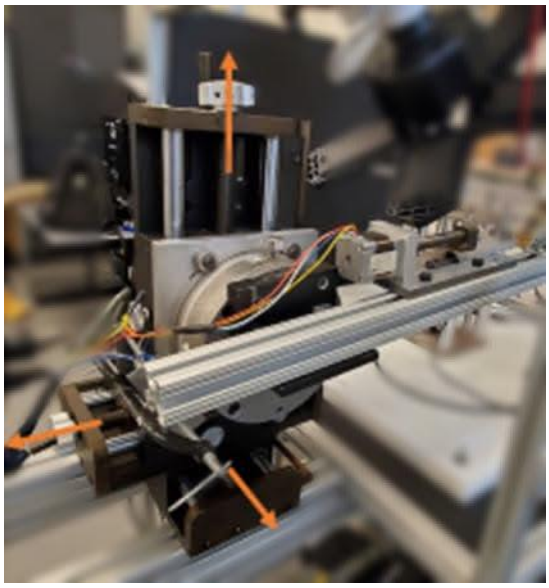

Figure 2-12 Three-axis aligner

2.1.4 Imaging and lightning

In this section, first, it is discussed why high-speed cameras are necessary to record the impact. Then, higher magnifications for obtaining detailed images and how to obtain them are explained.

Finally, methods for increasing the brightness of the picture are introduced and a method is selected.

2.1.4.1 High-speed camera

For analysis of the insect rupture, it is essential that the rupture be recorded during the impact. A detailed image or video of the impact shows which part of the insect hits the airfoil first, what is the orientation during the impact, and how each part of the insect body ruptures. Since airfoils move with high velocities, high-speed cameras are necessary to record the impact. A Phantom Miro M310 and a Phantom v1611 recorded the impact accordingly from the top and side views with 25k frames per second rates. While the top-view camera is for observing impact patterns, the side-view camera is for recording and later determining if the impact occurred at the leading edge of the airfoil. The locations of the cameras are shown in Figure 2-13. 25k fps was selected by trial since it could record insect impact in details at the highest speed of airfoils.

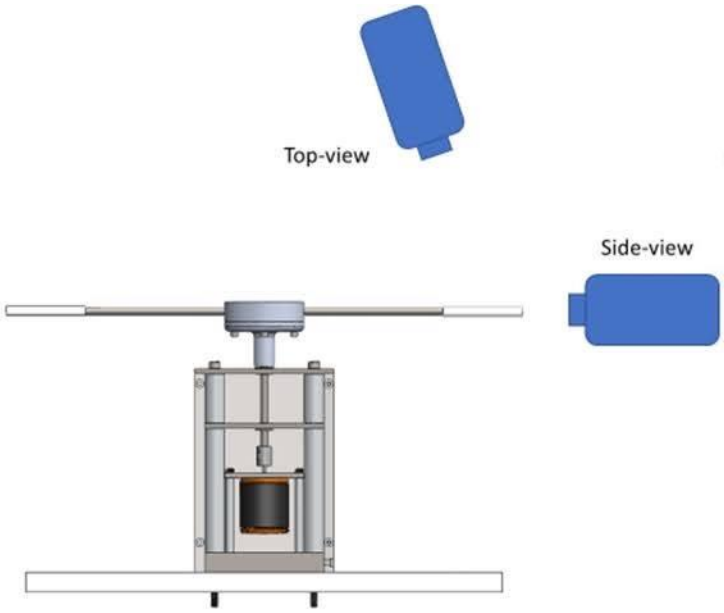

Figure 2-13 Position of cameras

2.1.4.2 Magnification

The impact is required to be observed under high magnification for detailed images to be captured. By increasing the magnification, the area of imaging decreases. Since cameras capture only a small area with high zoom, the impact location is needed to be fixed on the circular path of the rotary airfoils. Some strategies were implemented in the Arduino algorithm part (see Section 2.1.5.2) that made this possible. The impact point was set at 18 degrees from the point of the IR diodes on the circular path of rotary airfoils (Figure 2-14). Detailed images of insect impact were captured by determining the location of impact and increasing the magnification.

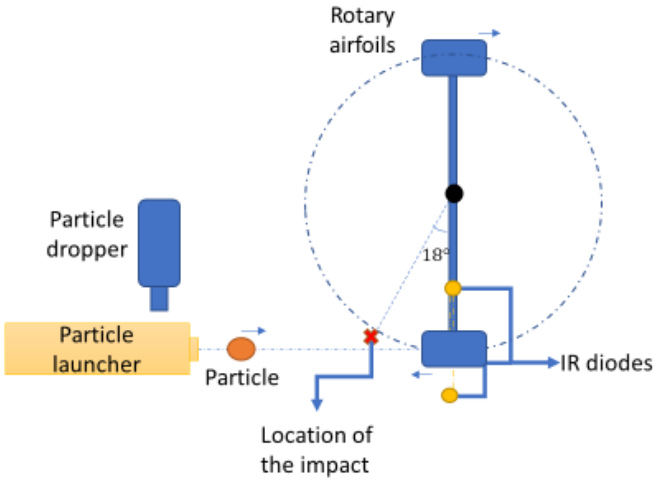

Figure 2-14 Exact location of impact in the airfoils' path

2.1.4.3 Lightning

By increasing the frame rate of videos, there is less time available for the camera's sensors to absorb light during the imaging. Therefore, the images are darker. To overcome this issue, there are two options: increasing the brightness by software or adding external lights. The second method is preferred since it does not lower the quality of the images. Since the video was recorded at a high frame per second rate, great illumination was required to display the impact in great detail. Light sources were required to provide illumination from different orientations to prevent

from dimming image details because of shadow of insect residue. Therefore, six 150 watts of garage lights were used to illuminate the impact scene from various angles (Figure 2-15). Images in high speed of motion were captured without lowering the quality.

Figure 2-15 Position of light sources

2.1.5 Computational and electrical subsystem

In this section, all the duties of the computational and electrical systems are explained. Generally, they are divided into four subsections: speed, timing, coding, and electrical circuits. In the first subsection, methods for calculation and validation of speed of impact are presented, followed by the synchronization, and an equation for timing of the impact is introduced. Then the type of error of each component is identified and analyzed. Finally, calibration methods for each component to reduce the error are discussed. In the third subsection, a brief explanation of the coding of the Arduino is presented and algorithms like coding of self-calibration are explained. In the final subsection, a schematic of the electrical circuit with a brief explanation is presented.

2.1.5.1 Speed

Impact speed is important due to the fact that at different speeds, different rupture patterns occur. For instance, at low speeds, the insect does not rupture; however, after a threshold speed (Section 1.2.1), the insect starts to rupture occasionally, and after another threshold, the insect definitely ruptures. The impact speed is determined by the insect's relative velocity to the airfoil. Due to the fact that both the insect and the airfoil are travelling toward each other, both measured values are necessary. A method is required to be developed to calculate the impact speed. Also, the developed method needs to be verified independently.

The airfoil's speed was computed by multiplying the angular velocity by the distance between the collision point and the center of rotation. The angular velocity was determined by Arduino using the data collected by the IR diodes. Additionally, an external rpm meter was utilized to verify the Arduino computation. The impact location was set to 33 ± 1 cm from the center of rotation. Finally, a number of calculated velocities were compared by measuring the velocity using a camera to verify the method.

The speed of an insect without airfoil rotation was determined through five experimentations by dividing the travelling length by the travelling duration, and the average was reported. A high-speed camera was used to capture the movement of insects. The insect's travelling distance and duration were determined using a ruler and the camera's time. The insect flew at a speed of 2.3 ± 0.2 m/s. As the airfoils rotated at maximum speed, which means there was maximum airflow to deflect the insect, insect speed was measured using the same method. The impact of airflow on insect speed was determined to be around a 0.2 m/s decrease at maximum speed, which was insignificant. As a result, it was assumed that insects moved at a constant speed of 2.3 m/s.

Given that both the airfoil and the insect travelled toward each other, the following formula was used to determine relative speed:

$$V = 2.3 + \omega \times 0.33\ (\frac{m}{s}) \qquad 2\text{-}1$$

where ω was the angular velocity calculated by Arduino. Some calculated values of speed were verified by other methods to validate the formula (e.g., using camera's time and a predetermined distance in camera's image).

2.1.5.2 Timing, error analysis, and tolerable error

Both the insect and the airfoil move towards each other, so launching of insect must be synchronized with position of airfoil to cause the impact. For synchronization, exact travelling times and positions of both airfoil and insect are needed. Then, a relation between mentioned parameters is required to be identified. In the next paragraphs, methods for indicating rotation time and position of airfoils are explained. Then, the relation between the parameters for synchronization of insect and airfoil is identified.

At the top and bottom of the cage, IR emitter and receiver diodes were vertically aligned. When they were able to view each other, the Arduino received a low value from diodes but a high value when the line was blocked. A half rotation was defined as the time interval between two high values or, in other words, the time interval between the passage of two airfoils.

After determining the half rotation time, Arduino detected the line to be interrupted again to determine the airfoils' position. The particle was released when a calculated waiting time by Arduino had passed. The waiting time for particle release from the particle launcher and the number of half revolutions (n) were computed using the formula below using the half rotation time, data from IR diodes, and particle travel time:

$$t_{wait} + t_{shoot} = nT + \frac{\alpha}{180}T, n \in N \qquad 2\text{-}2$$

where t_{wait} was the waiting time of Arduino, t_{shoot} was the travelling time of particle from the launcher to the airfoil, T was the half rotation time, n was the least natural number that the t_{wait}

was positive, and α was the azimuthal angle of the impact point from the point of the IR diodes on the circular path of rotation which was 18 degrees. The angle was determined on the setup base on the closest position of the airfoil to the particle launcher while airfoil is on the path of insect during launching. (the 18 degrees angle between path of insect and airfoil do not change the normal impact to an angled impact since the speed and mass of insect are significantly less than the airfoil which it can be assumed that insect is in a stationary position relative to the airfoil).

After waiting for t_{wait},the launcher and the cameras were triggered simultaneously using a 12V relay controlled by Arduino.

Impact occurred at the calculated time and predetermined location (18 degrees azimuthal from the point of the IR diodes on the circular path of rotation) by synchronizing the airfoils and the insect. Cameras started to record simultaneously with launching the insect.

The theoretical equation for synchronization of the impact is identified in the last paragraphs. However, all of the parameters have errors. Ignoring the errors results in the failure of impact. Therefore, it is necessary to conduct an error analysis on each of the parameters of the synchronization equation. Errors are either random or systematic. Systematic errors can be eliminated by calibration. However, random errors are not addressed by calibration. They are either reduced or tolerated.

Error descriptions, magnitudes, and their types are summarized in Table 2-1.

Table 2-1 Error descriptions of the components of insect impact

Error	Description	Type	Magnitude
launcher and travelling time of insect	Due to air friction, there is a time delay in the measured launching time as velocity rises. It may also result in deflection from the insect's straight path at greater speeds.	Random	Both are negligible (see Section 2.1.5.1)
RPM fluctuation	There is fluctuation in the rpm of the motor. RPMs reported by Arduino are the instantaneous velocity of the last rotation, whereas actual rpm can vary when particles impact at the next rotation.	Random	±10 rpm (twice of the maximum standard deviation of 100 rpm samples for different speeds)
IR diode sampling time	This is the time interval between two outputs of diodes. While a shorter sample period generally enhances accuracy, the Arduino imposes a limit to this effect. The sample time must be less than the time spent executing the code.	Systematic	1500 - 120 µs (see Table 2-2)
Code running time	The interval between the collection of two samples (outputs of diodes) is defined by the time gap between the collection of the samples and the execution of the sampling code. While code execution may seem insignificant, it becomes significant when 400 samples are collected. By neglecting it, one gets an erroneous error for rpm.	Systematic	110 - 120 µs (see Section 2.1.5.3)

An error analysis was done on the parameters of the time synchronization equation (Equation 2-2). Types and magnitude of each error were identified. Systematic errors are calibrated in coding section (see Section 2.1.5.3). Random errors are tolerated as explained in the next paragraphs.

As discussed above, random errors are either reduced or needed to be tolerated. Motor rpm fluctuation and insect travelling deflection are not avoidable. Therefore, random errors were needed to be tolerated. The maximum amount for accumulation of errors which need to be tolerated was calculated based on an acceptable area of impact for the insect on the airfoil. The calculation is explained below.

A successful impact was defined as one that occurred at the leading edge of the airfoil. The front edge was formerly thought to be a place where insects often rupture, especially the first 15 to 20% of the airfoil from the leading edge [18], [30], [34]. Location of insect residues on airfoil is shown in Figure 2-16.

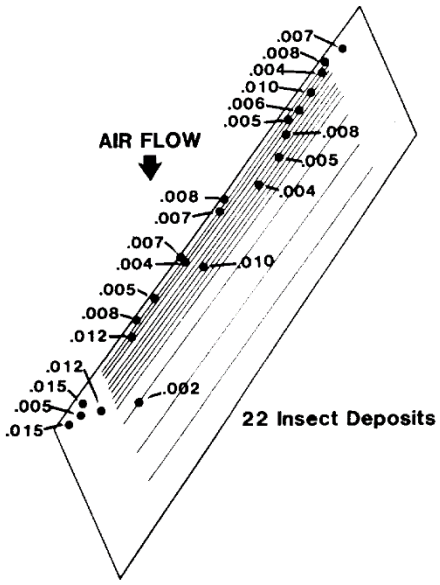

Figure 2-16 Location of insect residue accumulation on Jetstar C-140 with residue heights in inches (from Ref. [63]*, publicly permitted to be used by NASA)*

The first 15% of chord length from the stagnation point was identified as a high-impact zone. As a result, the successful impact zone was defined as $\pm$0.5 cm from the leading edge's midline (Figure 2-17).

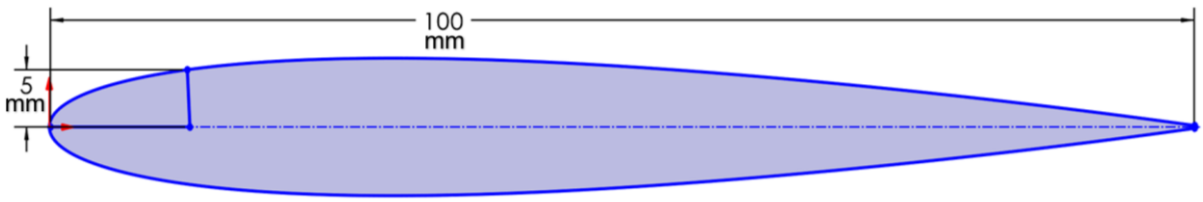

Figure 2-17 Successful impact zone

Using the equation 2-3, and assuming the launcher was horizontal, and the particle travelled 51 ms before colliding with the airfoil, the particle's vertical displacement would be as follows:

$$h = \frac{1}{2}gt^2 = 0.5 \times 9.81 \times 0.051^2 \simeq 0.013\ m = 1.3\ cm \qquad 2\text{-}3$$

Assuming the launcher's alignment was such that the impacting point was precisely vertically in the middle of the front edge (stagnation line). Due to the acceptance threshold for collision (successful zone which is ±0.5 cm from stagnation line), particles may have a vertical displacement of 1.3 ± 0.5 cm, and the time at the upper and lower thresholds are determined using the calculation below:

$$t = \sqrt{\frac{2h}{g}} \Rightarrow t_1 = \sqrt{\frac{2\times0.008}{9.81}} = 0.040\ s = 40\ ms, t_2 = \sqrt{\frac{2\times0.018}{9.81}} = 0.060\ s = 60\ ms \qquad 2\text{-}4$$

The above indicates that some time-related errors may be allowed:

$$\Delta t = \frac{t_2 - t_1}{2} = \frac{60-40}{2} = 10\ ms \qquad 2\text{-}5$$

So, ±10 ms was the tolerable error of particle travelling time; ±10 ms was the accepted random errors accumulation due to the fact that collision at the first 15% of the airfoil is acceptable.

2.1.5.3 Coding and calibration

An Arduino controls the electrical components (e.g., diodes, relay triggers, stepper motor, etc.) using an algorithm. The algorithm is responsible for computing values, controlling the time, and

commanding electrical components. Also, systematic errors could be corrected by a time calibration variable in the coding of the algorithm. In the next paragraphs, the algorithm is explained. First, constant variables were assigned and the threshold value of IR diodes for detection of airfoils was calculated. Then particle dropper provided a particle for the particle launcher. Next, the algorithm computed the velocity and position of airfoils. To obtain a more accurate value, time calibration was done during the velocity computation. Finally, the insect was launched at the right moment.

A sample output of the algorithm is provided in Table 2-3. First, constant variables were assigned appropriate values such as travelling time (measured using the camera in Section 2.1.5.1). IR diodes were used to determine the airfoil speed. Reporting a high value (5V) by IR diodes means that the line of sight between them is interrupted, and a low value (1.5V) means it is not. Using 1000 data points with a 300 μs time interval, the maximum and the lowest values of the IR sensors were determined, and the average was used as the cut-off value for determining whether an IR sensor's output would be high or low (Table 2-3 a). The two values of 1000 data points and 300 μs time interval were picked based on the detection of an airfoil with a speed range between 100 to 4000 rpm which covered all the rpm that setup needed to run.

After doing initial setups, the algorithm requested from the person who is operating the system that whether a particle be prepared for shooting or shoot the prepared particle (Table 2-3 b).

Preparing particle: The algorithm commanded the particle dropper to provide a particle to the particle launcher. The top disc of the particle dropper revolved and dropped the particle into the tube. A five second delay was executed by the algorithm to allow the particle to pass the tube and enter the particle launcher. The stepper motor then compressed the spring, preparing the trigger for shooting (Table 2-3 c).

Shooting the prepared particle: Equation 2-2 was used to obtain the Arduino wait time by calculating the half rotation time and the number of half rotations required. The initial stage was to estimate the rpm using 1000 samples at 300 μs intervals. For better precision, another sample rate (time interval between obtaining two samples) and sample size were required to be selected based on the estimated rpm. Table 2-2 was used to establish the sample size and sample rate (Table 2-3 e and f) based on an accuracy that is required to obtain sample for each 0.4 cm movement of the airfoil (successful impact zone). However, the sample rate cannot be smaller than the time required to execute the code, which was around 120 μs. Therefore, for higher speeds (as it is shown in Table 2-2) which needs lower sample rate than 120 μs, the accuracy was decreased to obtain a sample of 0.8 cm movement of the airfoil. Additionally, in Table 2-2, 400 and 200 were selected as number of samples since 400 and 200 samples were adequate for detection of both airfoils and computing rpm.

Table 2-2 Sample size and sample rate of the algorithm based on the initial estimated rpm

rpm	Rotation time (ms)	Velocity (m/s)	Phases of aircraft [62], [64]	Sample rate (μs) for 400 samples (0.4 cm accuracy)	Sample rate (μs) for 200 samples (0.8 cm accuracy)
100	600	5.7	Taxiing	1500	NA
200	300	9.2	Taxiing	750	NA
300	200	12.6	Taxiing	500	NA
400	150	16.1	Taxiing	375	NA
500	120	19.5	Take-off	300	NA
600	100	23.0	Take-off	250	NA
700	85	26.5	Take-off	214	NA
800	75	29.9	Take-off	187	NA
900	67	33.4	Take-off	166	NA
1000	60	36.8	Take-off	150	NA
1100	54	40.3	Take-off	136	NA
1200	50	43.7	Take-off	125	NA
1300	46	47.2	Take-off	NA	230
1400	42	50.6	Take-off	NA	214
1500	40	54.1	Take-off	NA	200
1600	37	57.6	Take-off	NA	187
1700	35	61	Take-off	NA	176

After that, the exact time of code execution was determined through error and trial, which ranged between 125 and 110 μs (Table 2-3 g and h). Following that, the exact half rotation time was measured. Then, n was calculated based on the fact that it was the least natural number that the waiting time of the launcher would be positive (Table 2-3 i). Next, when the airfoil cut the IR line sight again, the calculated wait time was executed by algorithm. Finally, the cameras and launcher were triggered simultaneously.

Table 2-3 Sample coding output

Description	Output
a) High and low values of IR diodes are found.	524 155
b) Allows you to choose whether to load the launcher with a particle or to launch the particle.	1) Shoot 2) Fill
c) loading the particle launcher with a particle is chosen. A particle is dropped into the tube by the particle dropper. It waits five seconds to ensure the particle is properly positioned on the particle holder. The spring is then compressed, the solenoid holds the spring, and the stepper motor returns to its starting position after compressing the spring. Everything is in place for the shooting.	Fill 5 4 3 2 1 preparing 0/2 preparing 1/2 preparing 2/2 Go!
d) Shooting is selected.	Shoot
e) The initial amount of rpm is estimated.	Calibration 2: 304488 --> 300000 Calibration 2: 304020 --> 300000 Calibration 2: 304052 --> 300000 Calibration 2: 304056 --> 300000 Calibration 2: 304052 --> 300000 Calibration 2: 297324 --> 300000
f) Based on the estimated rpm, number of samples is computed.	0.4 cm! 400 Samples!
g) A calibration process is done to consider the exact time of code execution.	Calibration 1: 115276 --> 112800 Calibration 1: 115252 --> 112800 Calibration 1: 115228 --> 112800 Calibration 1: 115068 --> 112800 Calibration 1: 115068 --> 112800 Calibration 1: 115076 --> 112800 Calibration 1: 115116 --> 112800 Calibration 1: 112052 --> 112800
h) Accuracy of calibration is reported.	Accuracy = 99.34 %
i) Precise values for rpm and rotation time are calculated. Based on the rotation time, the number of half rotations is computed (n).	RPM: 535.47 Rotation time: 112052 # of half rotations: 1

2.1.5.4 Electrical circuits

To control multiple components (e.g., diodes, solenoid, etc.) of the system seamlessly, an electrical system is required to control the components. As it was discussed, the Arduino was selected as the main processing unit of the electrical circuit. Wiring of the electrical circuit is shown in Figure 2-18. An Arduino Mega controlled the circuit. IR diodes were responsible for locating the airfoils. The camera and solenoid were triggered by relays, while the solenoid controlled the

compressed spring. Drivers supplied higher power for stepper motors since Arduino's output was not adequate for them. An electrical circuit was developed that controlled the particle launcher, particle dropper, and cameras in parallel. It also identified the position of the airfoil and measured the rotation time of the airfoil.

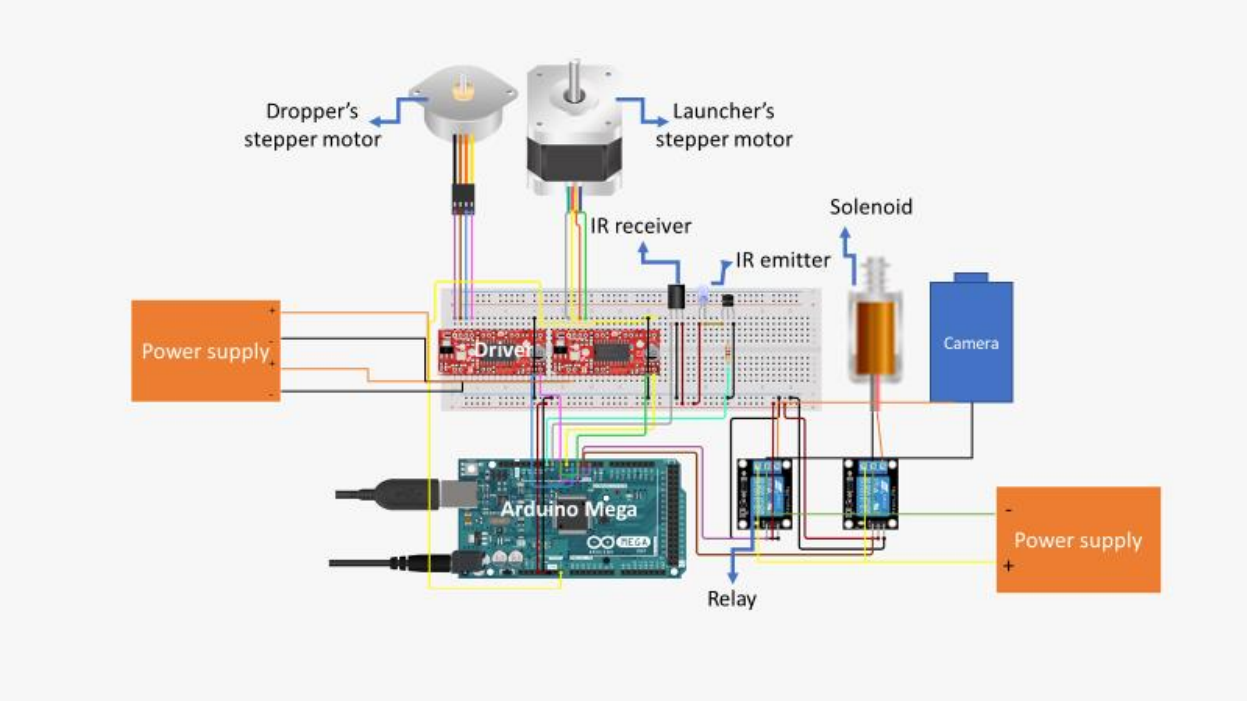

Figure 2-18 Schematic of electrical circuit

2.2 Sample preparation and experimental procedure

In this section, insect and coating preparation are discussed. Then, the designed tests are explained. In the insect and particle subsection, reasons for selecting a specific insect and treating method are presented. Then, a group of coatings are introduced and methods for applying them are presented. Next, the results and the methods used for collecting them are explained. Finally,

three designed tests are presented that will be used to either verify the setup functioning or produce new results to address some of the gaps identified in the first chapter.

2.2.1 Insects and particles

For experimenting in a laboratory, a type of insect should be selected that the result from this study could be compared to other studies. The most important criterion for selecting the insects is that it is needed to be a practical representative of most of the insects which hit the aircraft's airfoil. The Drosophila (Figure 2-19) or, in common terms, fruit flies, as mentioned in Coleman's study and other studies of aircraft airfoil impacting insects represented the most frequent impacting insects during a flight due to their size (2 to 3 mm) and insect species. Two common types of Drosophilas are Melanogaster and Hydei. Hydei is about 3 mm which is 1 mm larger than the Melanogaster. Past experiments were mostly done with Melanogaster; However, experimenting with both is valid and comparable [25]. Since Drosophila Hydei has more hemolymph and body fluids, it is more likely to adhere to the airfoil after rupture. As a result, the wingless Drosophila Hydei was selected as the impacting insect. Purchasing, storing, feeding, duration of use, measurements, and disposal of Drosophila are explained below.

- Purchase: Fruit flies are a common food source for reptiles, so they were purchased from an online reptile food supplier.
- Store: Delivered items from online websites had some breathing holes for drosophila. To prevent drosophila from escaping the container, these holes were sealed with a filter. Additionally, the package included peanut butter as drosophila nourishment.
- Treatment: Before using them, they were put to sleep by CO_2. Then, they were loaded into the particle launcher and were shot toward the airfoils. CO_2 was provided from online bike tools suppliers as 16 g CO_2 capsules.
- Duration: Insects were used for three weeks period.

- Measurements: A Satorius TE214S scale with a precision of 0.1 mg was used to weigh eleven Drosophila Hydei, and the average was calculated. Three of them were measured in length using ImageJ with a ruler held near to the bug, and the average was reported as Hydei's length.
- Disposal: It was unfortunate that we had to dispose of insect's remains after use. Flies that had already been immobilized were immediately thrown into soapy water, mineral oil, or ethanol till they were drowned.

For calibration purposes, there is no need to use insects, instead 2mm spherical glass beads were used. The consistency of spherical glass beads compared with insects is beneficial for calibration purposes. The particle launcher worked with both insects and spherical particles.

Figure 2-19 Drosophila Hydei

2.2.2 Coating and material

To mitigate the insect residue on an aircraft's airfoil, studies on coatings and their efficiency have been done. Aluminum was the baseline substrate in all studies. Aluminum has a low density, shows good strength, and is resistant to corrosion; as a result, it is widely used in the aerial

industry as the main material for the body of aircraft. Therefore, coatings were applied to the aluminum. Coatings with different contact angles and roughness show different behaviours to insect residue. The contact angle is an angle that a liquid-vapor interface makes on a solid. Therefore, several coatings are needed to be studied to indicate the effects of contact angle and roughness. Aluminum 1100 was chosen as the baseline substrate because of its application in aircraft bodies. Before applying the coatings, all metal samples were cleaned with ethanol and acetone. Polyurethane (PU) and acrylic were chosen because these compounds are often used to cover aeroplanes. PU was acquired from BEHR as a quick-drying water-based matte Polyurethane that needed at least two applications with a one-hour break between them. Varathane offered acrylic as a water-based premium diamond wood finish. Polyurethane and acrylic were coated using the dip-coating technique. Polyurethane and acrylic were selected to study the effectiveness of the common coatings in the industry for reducing insect residue.

According to previous studies [25], [42], the most effective coatings are superhydrophobic. A pair of commercial superhydrophobic coatings, UltraEverDry and NeverWet, were chosen. NeverWet was bought as a liquid repellent solution in two-part sprays from the Rust-Oleum corporation. The first spray created a rough surface as a foundation layer by spraying tiny particles. The second spray imparted superhydrophobicity to the surface. UltraEverDry was sprayed in two sections, the top-coat and the bottom-coat.

Coated aluminum samples formed on the airfoil by folding them over the airfoil and were held in place by taping. After each experiment, the impact region was cut out after unfolding the aluminum foil and attached to a microscope slide for later analysis.

2.2.3 Data collection

For further analysis of insect residue and rupture, data of impact is required to be collected. These data are either videos of impact or insect residue. During the experiment, top and side videos of

impact and impacting speed were recorded. After that, the aluminum sample was dismounted from the airfoil and unfolded. Finally, the residue-covered area was cut and adhered to the microscope slide. Data from the impact were collected in the two forms of impact videos or residue-covered samples.

2.2.4 Impact test

First, the developed apparatus has to be verified with past setups. Three experiments were designed to either verify the newly developed apparatus by comparing it to the findings of prior investigations or to test and provide novel information. All tests were done at room temperature by the same methods explained earlier. Designed tests were rupture velocity, coatings evaluation, and airflow removal. At rupture velocity, the minimum speed for rupturing an insect was investigated. During coating evaluation, coatings and their insect residue mitigation ability at the take-off speed of an aircraft were studied. Finally, natural airflow removal was investigated since it was mentioned in the literature as a means to reduce insect residue; however, limited studies were done to elaborate on the effect of airflow.

2.2.4.1 Rupture velocity

To fully understand the insect rupture phenomenon, it is necessary to investigate at which speed rupture starts. Is it a threshold speed that all insects rupture or is there a transition range? Also, is the rupture velocity related to the coating or not? Insects were thrown to the airfoil at intervals of 5 m/s from low to high speeds. Three samples were taken at each speed. When the number of ruptured insects increased, the gap between velocity measurements decreased to 2.5 m/s. Aluminum and PU were examined as coating materials. Hence previous investigations documented aluminum's rupture velocity, aluminum was utilized to validate the newly developed apparatus. PU was chosen as a new data point to investigate what happens to rupture velocity

when a different coating is used in place of aluminum. An experiment was designed to investigate the rupture velocity and indicate whether the coating type affects the rupture velocity or not.

2.2.4.2 Coatings evaluation at 60 m/s

Effectiveness of a coating is required to be evaluated during the most accumulating time of insects on aircraft. Aircraft accumulates insects mostly during taxiing, take-off, and landing. Other studies have reported that the maximum speed of a commercial airplane during these phases is take-off speed which is around 67 m/s to 80 m/s; 60 m/s was chosen for the present investigation because it was commonly used in the literature. Also, insect fully ruptures at 60 m/s, which is sufficient for coating evaluation. Ten tests were done at 60 m/s for all coatings. Aluminum was done for apparatus validation and other coatings were done to observe the effect of roughness and contact angle.

2.2.4.3 Natural airflow removal

During the flight, airflow removal was observed to be a natural technique for removing insect leftovers. Also, past studies [18], [31] mentioned that airflow removal is a mitigation method; however, limited studies were done. The effect of airflow at 60 m/s on the residue of all coatings was investigated by monitoring the residue at multiple time intervals. Area of residue was the parameter to be monitored. An experiment was designed to elaborate the effect of natural airflow removal.

2.3 Data processing

2.3.1 Area analysis

To evaluate coatings, some parameters of the insect residue are required to be measured. Area of insect residue was selected since it was used in all of the past studies. Residue area shows amount of the spread hemolymph which binds the other parts of insect like excrescence to the surface. For measuring the area of residues, images of the samples were taken with a smartphone. ImageJ was used to select the edges of the residue to measure the area of the samples manually. Measured area was used for evaluation of coatings.

2.3.2 Coating characterization

A coating's main characteristics are roughness, surface energy, elasticity, and surface chemistry. In the past studies, mostly roughness and surface energy were measured since they were the most influential parameters on insect residue. To determine the effect of the roughness and surface energy on insect residue, they are required to be measured.

The degree of roughness of each coating was determined using a BRUKER ContourGT-K non-contact surface measuring profilometer and Vision64 software. For each coating, the arithmetic mean surface roughness (Ra) was determined at three separate points on the sample, and the average value was reported as the coating's roughness.

The contact angle of each coating was determined by using a KRUSS drop shape analyzer. Before measuring, all samples were cleaned with acetone and ethanol. Using the sessile drop method [65] and Young-Laplace fitting method [66] in the KRUSS ADVANCE application, the coating's contact angles for deionized water on three separate points of the sample were

recorded, and the average was used as the contact angle of the coating. All measurements were done at room temperature.

Chapter 3 Results and discussion

In the following sections, first, measurements of the insect and coatings features are presented. Then, rupture velocity, coatings evaluation at 60 m/s, and airflow removal results are reported and discussed.

3.1 Particles and coatings characteristics

Average weight for eleven Drosophila Hydei was 1.6 $\pm$ 0.1 mg. Average length for three Drosophila Hydei (Figure 3-1) was 3.05 $\pm$ 0.11 mm.

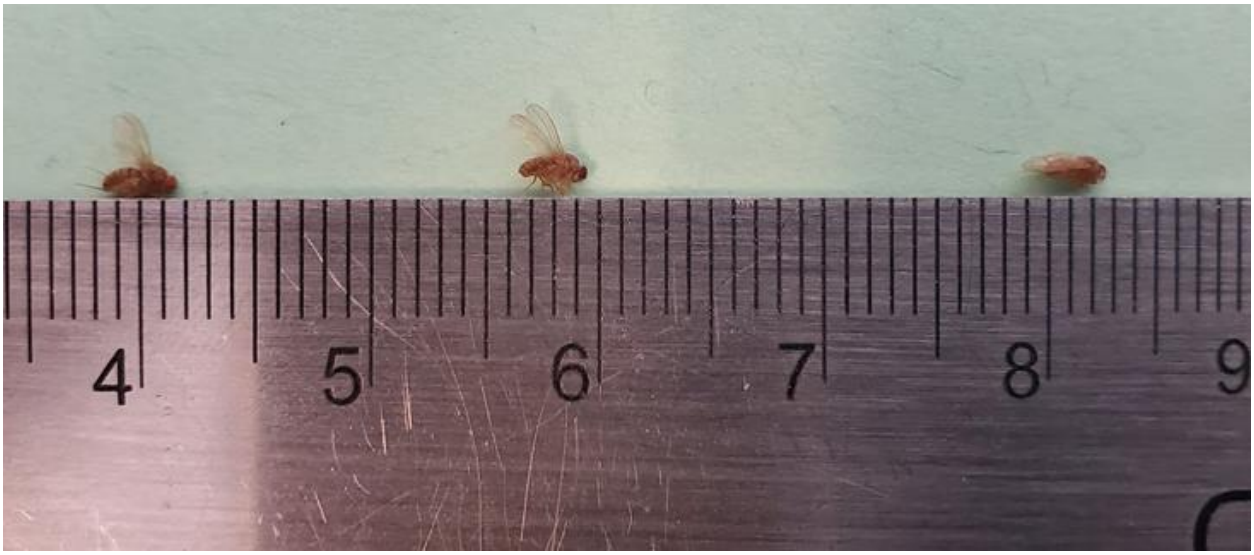

Figure 3-1 Insects' measurements

The contact angle and roughness of each coating were measured three times at different points. Results are given in Table 3-1.

Table 3-1 Contact angle and roughness of the coatings

	CA1 (Contact angle - degree)	CA2	CA3	Average	Error $(\frac{max-min}{2})$	Ra1 (Roughness - µm)	Ra2	Ra3	Average	Error $(\frac{max-min}{2})$
Aluminum SonicCleaned	69.8	70.6	70.5	70.3	0.4	NA	NA	NA	NA	NA
Aluminum Uncleaned	100.0	96.2	92.0	96.1	4.0	583.37	648.99	553.88	595.42	47.56
Acrylic	88.0	94.1	90.9	91.0	3.0	1068.68	835.41	804.37	902.82	132.16
PU	79.2	72.2	83.8	78.4	5.8	752.50	799.14	745.54	765.72	26.80
NeverWet	151.8	151.3	150.9	151.3	0.5	1650.60	1868.95	1697.19	1738.91	109.17
UltraEverDry	166.2	167.1	163.7	165.7	1.7	857.55	933.57	1091.69	960.94	117.07

After measuring the contact angle of uncleaned aluminum, it was discovered that it was greater than what was anticipated for a metal (a high energy surface). Typically, metal suppliers leave a coating, film, or particles on the metal sheet throughout the raw metal manufacturing process. Typically, debris on metal alters the material's contact angle. As a result, the metal was cleaned with Sonic for ten minutes to see whether there was any debris on it. A lower contact angle from cleaned aluminum was obtained.

3.2 Insect tests

3.2.1 Rupture velocity

Rupture probability was defined as the number of successful ruptures over the total number of trials (three). As it is shown in Figure 3-2, the rupture was seen occasionally at about 17.5 m/s

and at about 30 m/s rupture was always occurred. Comparing the results from aluminum and PU, it was concluded that rupture velocity was not a function of the coating characteristics, but only it was related to impact velocity. PU was selected among other coatings since it was not superhydrophobic and traces of rupture could be observed. In the case of superhydrophobic, based on the past studies, it was possible that rupture happens, but the insect does not adhere to the airfoils due to the low wettability of superhydrophobics. Also, it was understood that rupture velocity is a phenomenon that is better defined as a range of velocities rather than reported as a solid number. Young's study [26] reported rupture velocity as a range of velocities between 24.5 ± 2.1 m/s to 30 ± 1.9 m/s which at the beginning of the range only soft parts like the lower body of insect ruptured while at the end of the range harder parts like exoskeleton were ruptured. Krishnan [23] reported 21 m/s as the start of fruit flies rupturing. Results from these two studies were in good correspondence with the current study which validated the current setup. However, Coleman [18] and Wohl [36] reported lower values between 10 to 15 m/s for rupture velocity. Since none of the four studies mentioned how the rupture velocity experiment was done, the difference in final values could not be explained. As a possible explanation, the insect delivery method in Coleman's study seemed to cause small fractures on the insect body since insects were released in a wind tunnel to accelerate until they reached the speed of airflow and then impacted the airfoil in the wind tunnel. As it is discussed in the Section 1.2.2, small fractures on the insect body lower the body's resistance to impact and it ruptures easier. There was no rupture velocity test in Wohl's study, and the reported number was from other studies. However, the insect delivery method was not clear, if it kept the insect intact during acceleration or not. Wohl's insect delivery method accelerated the insect using a pneumatic gun in a wind tunnel and released the insect toward the airfoil when it reached the velocity of the airflow in the wind tunnel. It was not clearly mentioned what method for avoiding the small fractures caused by the high pressure of the gun was used.

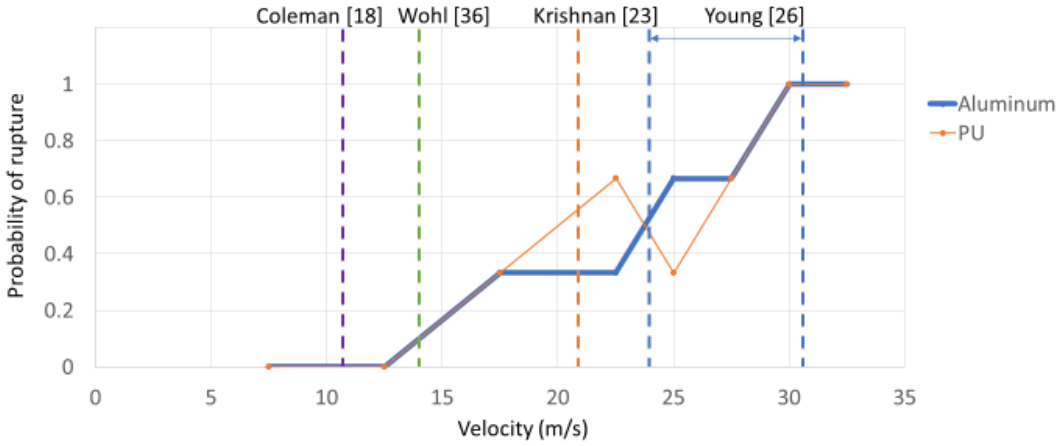

Figure 3-2 Rupture velocity for aluminum and Polyurethane (PU) coated surface

3.2.2 Impact test at 60 m/s

Data of insect impact at 60 m/s (see Section 2.2.4.2) are shown by boxplots in Figure 3-3. A boxplot shows half of the data which is interquartile interval in a box [67]. Lower and upper quartile of data are shown by whiskers in both sides of the box excluding outliers which are statistically distant values from other values. Results from past studies were presented by averaging all data for a coating. Averaging could not be suitable here as the impacts were located on the impact zone, which means a range of impact angles. Having a range of impact angles, residue area and heights varies. Therefore, reporting a range for area or height results is a more suitable way for data interpretation. Top and side views of insect impact for aluminum at 60 m/s are shown in Figure 3-4 and Figure 3-5, respectively.

Results for aluminum in other studies are shown in Table 3-2. Current study results for aluminum ranged from 2 to 47.6 mm^2, but mostly from 15 to 45 mm^2. Results from this study is comparable with past studies, as both velocity and impact angle affect the area. Other studies with higher velocities and lower impact angles resemble to a lower velocity with a perpendicular impact angle.

As this study reported a range of area values with different impact angles, results can be compared to perpendicular impact with a range of velocities lower than 60 m/s. Comparing reported values for the area, it can be said that current study values had good correspondence with Young and Krishnan's studies. Wohl's value was significantly different from all studies. This correspondence evidently means that the setup is validated by past studies.

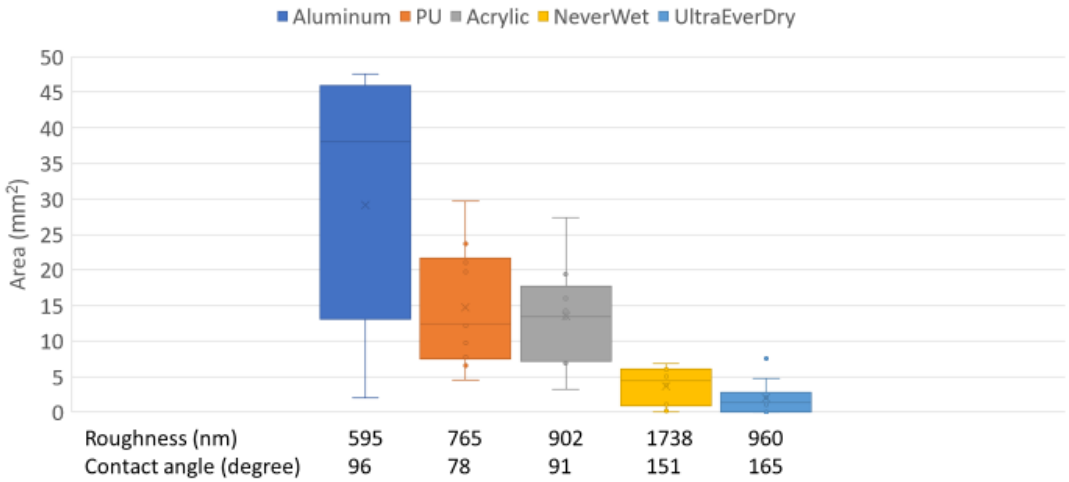

Figure 3-3 Residue areas of the coatings

Table 3-2 Results of Drosophila Melanogaster impact to uncoated aluminum for past studies

	Young [25]	Wohl [28]	Krishnan [27]
Area (mm^2)	18.34	2.1	42
Height (nm)	34.3	235	700
Contact angle or surface energy	37.18 mJ/m^2	84 degrees	78 degrees
Roughness (nm)	200	310	470
Description	90 m/s - 30 degree - Al2024	66 m/s - 60 degree - Al2024	47 m/s - 90 degree - Al2024

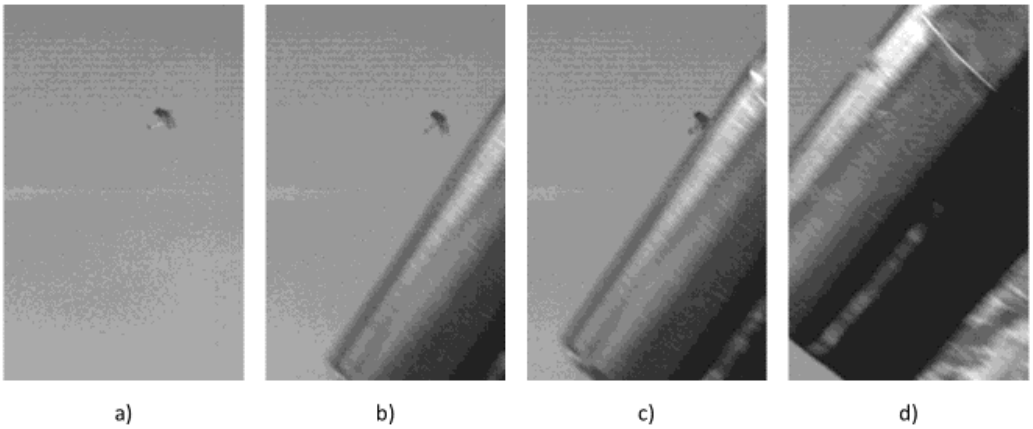

Figure 3-4 Top-view of insect impact 60 m/s

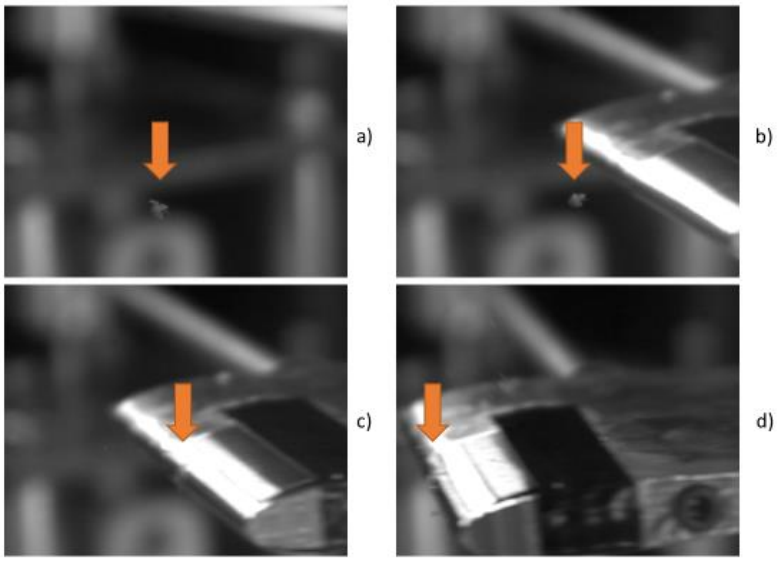

Figure 3-5 Side-view of insect impact at 60 m/s

3.2.2.1 Area of residue and roughness

Aluminum, PU, and Acrylic had almost similar contact angle values, and all were not showing intense hydrophobicity and neither hydrophilicity behaviours. Also, they were quite different in

terms of roughness values. Therefore, they were compared to each other to investigate the effect of roughness on insect residue as the contact angle was kept approximately constant. From Figure 3-6, based on the difference in averages of the boxplots (residue's area for each coating) and comparison of the boxplots, it can be said that as the roughness increased, conversely residue's area decreased. This statement was reported by past studies too [42]. The reason can be that the valleys and tops of the surface tried to prevent the insect's hemolymph to expand further and stuck in the microscopic valleys of the surface [17], [25], [50], [58].

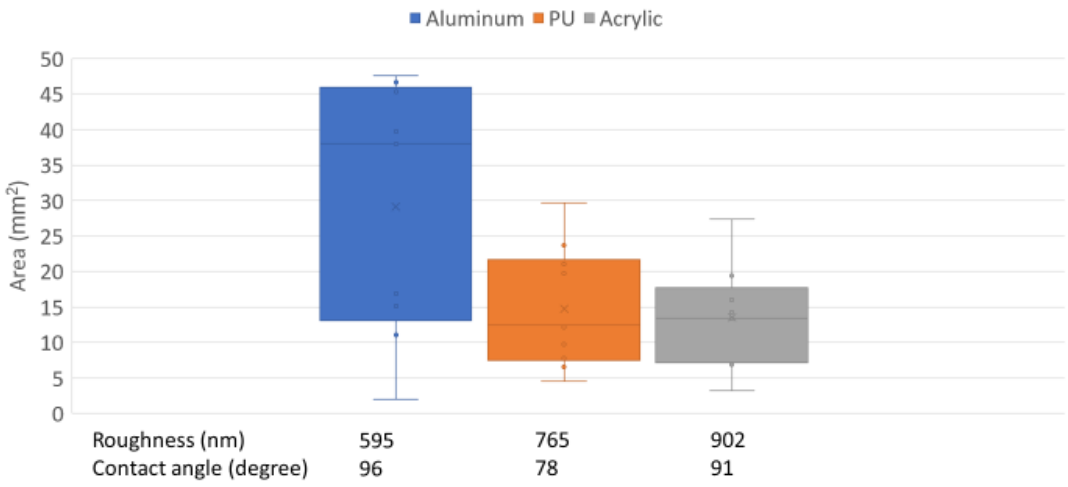

Figure 3-6 Comparison of coatings with approximately similar surface energy values

3.2.2.2 Area of residue and contact angle

PU was selected from the group of aluminum, PU, and Acrylic as representative of a coating with moderate hydrophobicity or hydrophilicity to be compared by a superhydrophobic coating (i.e., UltraEverDry coating as representative). Based on Figure 3-7, by increasing the contact angle, the residue's area was significantly decreased. This conclusion was tested by a paired sample T-test. Since P-value was less than 0.001, it was concluded that the values of PU and UltraEverDry were significantly different. Results from past studies concur this conclusion [23], [26], [39], [42].

High contact angle means that the wetting area is small. Therefore, insect hemolymph before coagulation wets a smaller area on superhydrophobic compared to a moderate hydrophobic or hydrophilic and in some cases no residue remains on a superhydrophobic coating. After coagulation which happens fast, a small area of residue (or sometimes no residue) remains on the superhydrophobic coating.

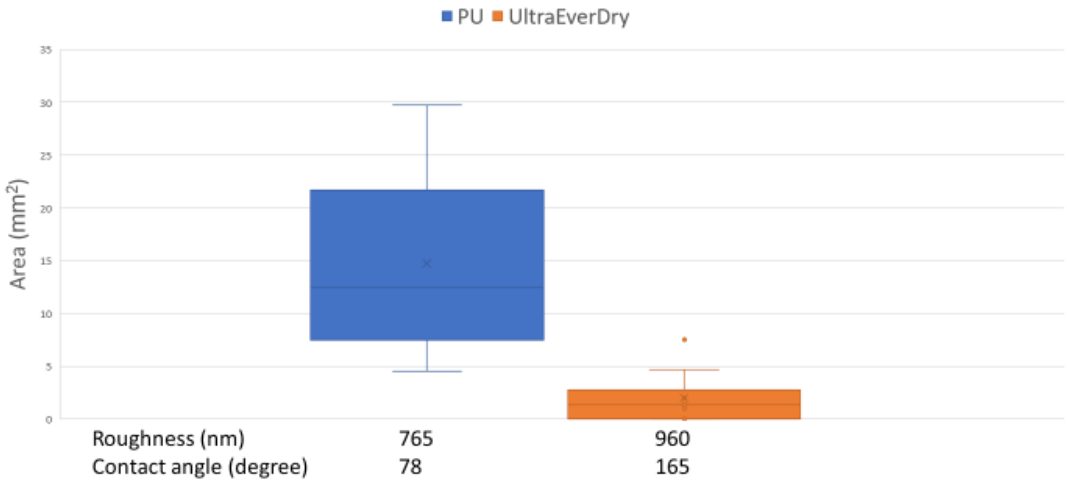

Figure 3-7 Comparison of coatings with different surface energy

3.2.2.3 Superhydrophobicity

In some cases, the insect impact to airfoil did not leave a residue on superhydrophobic coatings. In Figure 3-8, the probability of leaving residue on all coatings was plotted. Both superhydrophobic coatings did not leave a residue in some of the tests. UltraEverDry performed better than NeverWet. It seemed that the reason was the higher contact angle of the UltraEverDry caused fewer residue remained on the surface since higher surface energy means a smaller wetting area. Superhydrophobic coatings regardless of the ability to leave no residue, showed lower residue area when there was one. Other studies [25], [27], [36], [42] mostly reported superhydrophobic

coatings as the solution for insect residue mitigation on airplane wings. The residue's area mostly consists of the insect's body fluids [21], [23]. Lowering the residue's area essentially decreases the chance of adhering hard large parts like the exoskeleton to the surface since there are lower body fluids to adhere these parts to the airfoil. Using superhydrophobic seems to be promising.

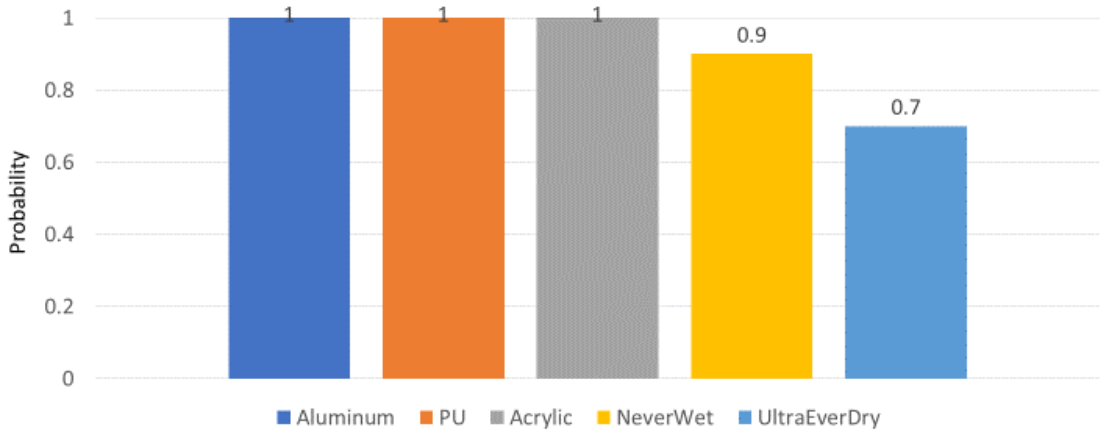

Figure 3-8 Probability of leaving residue after impact

3.2.3 Airflow removal

Pictures of residues of 60 m/s insect impact on all five coatings are shown in Figure 3-9. Pictures were taken in a short time after impact (less than 20 seconds as turning off the system takes few seconds), and after 10 minutes exposure to airflow. Based on the observation, there was not any qualitative height or area change in residues after exposure to airflow. The reason can be that after coagulation, all residues are in steady conditions with airflow since before coagulation removing residues is easier and every residue that is supposed to be removed by airflow is totally removed before coagulation happens (see Footnote 1 in page 5 for coagulation time). However, other studies claimed that natural airflow removal was effective in insect residue mitigation without explaining how the airflow removal was tested [17], [18], [30]. There were only few experiments

related to airflow removal [31], [32]. One study [31] stated that airflow could remove about half of insect residue. However, Peterson and Fisher [32] showed that airflow has no effect on residue size after coagulation. Other studies only assumed that airflow removal is convincing and might be significant. In conclusion, effect of natural airflow on insect residue is negligible after coagulation.

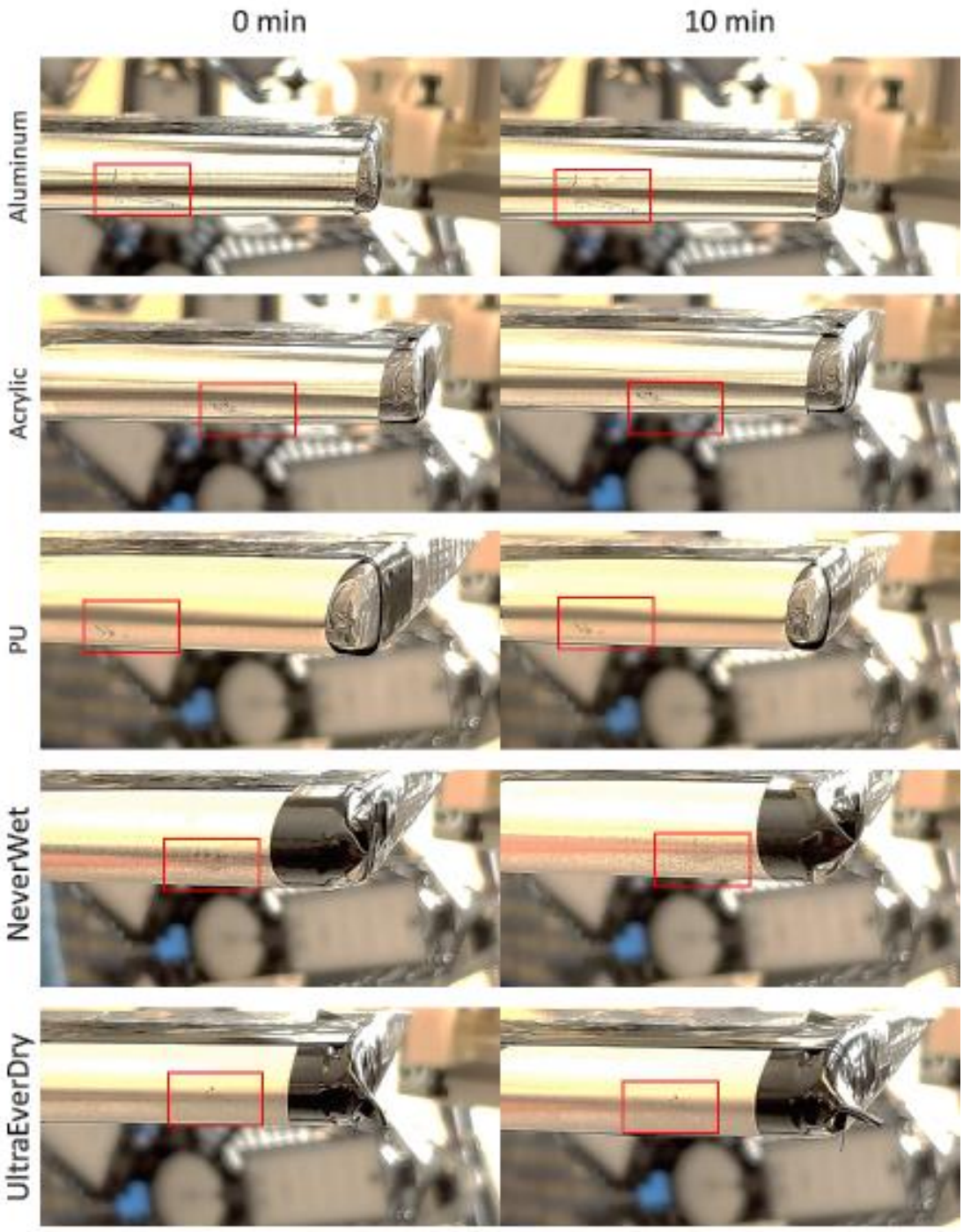

Figure 3-9 Airflow removal of residue after 10 min

Chapter 4 Conclusion and future work

4.1 Conclusion

In conclusion, a new setup for testing insect impact to an airfoil was designed and tested. To overcome deficiencies of past studies' setups, three primary objectives for new setup were set and reached: 1.1) insect kept intact during the launching toward the airfoil by accelerating the airfoil instead of insect, 1.2) airflow was present during the impact because of air circulation caused by rotary airfoils and, 1.3) setup reached to 60 m/s near the take-off velocity of aircrafts. Also, four secondary objectives for setup were determined to enhance the process of simulating insect impact: 2.1) possibility of successful impact was increased by calibration methods, 2.2) tests were done in a short period of time as most of the procedure was automated, 2.3) velocity change was possible during the test, and 2.4) particle launcher was able to launch both insect and spherical glass bids for calibration purposes.

Three experiments were done to validate the setup (objective 3), produce new results (objective 4), and investigate controversial topics (objective 5).

In the rupture velocity experiment, fruit flies started to partially rupture from 17.5 m/s and completely rupture at 30 m/s. It was noticed that it is better to report rupture velocity as a range instead of a threshold number. Therefore, rupture velocity number was clarified (objective 5.1) since different numbers for rupture velocity were reported by past studies. Also, the newly developed setup was validated by two studies with rupture velocities in the same range (objective 3.1). In addition, from comparison of insect rupture velocity of different coatings, it was concluded that rupture velocity is not related to the coating but only impact velocity (objective 4.1).

In the insect impact at take-off velocity of aircraft experiment, five commercially available coatings were tested, and insect residue values were reported (objective 4.2). From comparison of insect residue size on aluminum with past studies results, setup was validated because of good correspondence with past studies (objective 3.2). Also, setup was verified by past studies by showing that by decreasing the surface energy, residue's area decreases (objective 3.3). In addition, superhydrophobic coatings showed a good ability to mitigate insect residue as in some cases no residue was left on them after impact (objective 3.4). Effect of roughness on residue's area was previously studied; however, result was not intuitively logical. Therefore, it was tested again and results from past studies were verified (objective 5.3).

In the final experiment, effect of natural airflow removal was tested as contradictory results were reported from past studies. By observing residues a short time after impact and ten minutes after impact, it was concluded that airflow do not change the insect residue after coagulation (objective 5.2).

4.2 Future work

As it is mentioned in Section 1.4.2, effect of surface chemistry and surface elasticity need further investigation. New coatings with elasticity properties or different surface chemistry can be examined to clarify the effect of elasticity and surface chemistry.

A practical coating has to be resistant to impact with sand and ice particles for a long period of time. A standard experiment can be developed to measure the coatings durability and examine the resistance of the coatings to erosion.

As it is mentioned in Section 1.2.1, effect of environmental factors needs further investigation. In addition, formation of insect residue under water needs to be studied as in the past only effect of

water on residue after residue formation was examined and reported as negligible. However, water (e.g., rain) can influence the residue formation. Also, effect of flying through the clouds can be added to the setup using a humidifier.

For future works, it is possible that rpm of motor could be controlled more precisely since rpm fluctuates. Therefore, by lowering the rpm fluctuation, possibility of successful impact would increase. Besides, a speed control system could be added to the Arduino to automate the speed change and simulate the acceleration during take-off.

Furthermore, an insect residue's height measurement could be added to the experiment. Several methods were tested (e.g., SEM, confocal microscope scanning, stylus profile reader, etc.), however, none showed a precise result or convenient measuring time. An optical micrometer seems promising as it measures with precision of 1 μm and it is a portable handheld tool.

References

[1] "Laminar and Turbulent Flow." https://web.archive.org/web/20101021003853/http://www.efm.leeds.ac.uk/CIVE/CIVE1400/Section4/laminar_turbulent.htm (accessed Jun. 26, 2022).

[2] K. J. Rawson and E. C. Tupper, "Powering of ships: general principles," *Basic Ship Theory*, pp. 365–410, 2001, doi: 10.1016/B978-075065398-5/50013-3.

[3] I. B. D. Paula, W. Würz, V. I. Borodulin, and Y. S. Kachanov, "Weakly-nonlinear Interactions of Modulated T-S Waves in the Boundary Layer of an Airfoil," *Procedia IUTAM*, vol. 14, pp. 433–437, Jan. 2015, doi: 10.1016/J.PIUTAM.2015.03.071.

[4] "Tollmien–Schlichting wave - Wikipedia." https://en.wikipedia.org/wiki/Tollmien%E2%80%93Schlichting_wave (accessed Jun. 26, 2022).

[5] K. S. G. Krishnan, O. Bertram, and O. Seibel, "Review of hybrid laminar flow control systems," *Progress in Aerospace Sciences*, vol. 93, pp. 24–52, Aug. 2017, doi: 10.1016/J.PAEROSCI.2017.05.005.

[6] S. L. Chernyshev, A. P. Kiselev, and A. P. Kuryachii, "Laminar flow control research at TsAGI: Past and present," *Progress in Aerospace Sciences*, vol. 47, no. 3, pp. 169–185, Apr. 2011, doi: 10.1016/J.PAEROSCI.2010.11.001.

[7] "Boundary Layer | Definition & Characteristics | nuclear-power.com." https://www.nuclear-power.com/nuclear-engineering/fluid-dynamics/boundary-layer/ (accessed Jul. 16, 2022).

[8] "CO2 emissions of airlines worldwide 2004-2022 | Statista." https://www.statista.com/statistics/1186820/co2-emissions-commercial-aviation-worldwide/ (accessed Jun. 26, 2022).

[9] “Commercial airlines: worldwide fuel consumption 2005-2022 | Statista.” https://www.statista.com/statistics/655057/fuel-consumption-of-airlines-worldwide/ (accessed Jun. 26, 2022).

[10] “Airline industry worldwide - number of flights 2004-2022 | Statista.” https://www.statista.com/statistics/564769/airline-industry-number-of-flights/ (accessed Jun. 26, 2022).

[11] T. M. Young and J. P. Fielding, “Potential fuel savings due to hybrid laminar flow control under operational conditions,” *The Aeronautical Journal*, vol. 105, no. 1052, pp. 581–588, 2001.

[12] “A new study puts temperature increases caused by CO2 emissions on the map.” https://phys.org/news/2016-01-temperature-co2-emissions.html (accessed Jul. 18, 2022).

[13] “Climate Change: Global Temperature | NOAA Climate.gov.” https://www.climate.gov/news-features/understanding-climate/climate-change-global-temperature (accessed Jul. 18, 2022).

[14] R. J.-A. R. of F. M. 1998 and undefined 1998, “Aircraft laminar flow control,” *ntrs.nasa.gov*, vol. 30, pp. 1–29, 1998, Accessed: Jun. 26, 2022. [Online]. Available: https://ntrs.nasa.gov/citations/20040110294

[15] T. Pe and F. Thielecke, “Methodik zur Leistungsabschätzung von HLFC-Absaugsystemen im Flugzeugvorentwurf,” *Proceedings of the Deutscher Luft-und Raumfahrtkongress (DLRK), Hamburg, Germany*, vol. 31, 2010.

[16] “Aircraft.” https://weceramiccoating.com/aircraft (accessed Jul. 16, 2022).

[17] M. Kok, J. G. Smith Jr, C. J. Wohl, E. J. Siochi, and T. M. Young, “Critical considerations in the mitigation of insect residue contamination on aircraft surfaces–A review,” *Progress in Aerospace Sciences*, vol. 75, pp. 1–14, 2015.

[18] W. S. Coleman, “Roughness due to insects,” *Boundary Layer and Flow Control*, pp. 682–747, Jan. 1961, doi: 10.1016/B978-1-4832-1323-1.50006-3.

[19] C. G. Johnson and H. L. Penman, “Relationship of aphid density to altitude,” *Nature*, vol. 168, no. 4269, pp. 337–338, 1951.

[20] A. C. Hardy and P. S. Milne, “Studies in the distribution of insects by aerial currents,” *J Anim Ecol*, pp. 199–229, 1938.

[21] K. G. H. Krishnan, A. Milionis, M. Starr, and E. Loth, “Fruit fly impact outcomes and residue components on an aerodynamic surface,” in *53rd AIAA Aerospace Sciences Meeting*, 2015, p. 1279.

[22] K. G. H. Krishnan *et al.*, “Characterization of insect residue on an aerodynamic leading edge,” in *8th AIAA Atmospheric and Space Environments Conference*, 2016, p. 3445.

[23] K. G. Krishnan, A. Milionis, F. Tetteh, and E. Loth, “Fruit fly impact on an aerodynamic surface: Types of outcomes and residue components,” *Aerosp Sci Technol*, vol. 69, pp. 181–192, 2017.

[24] T. M. Lorenzi, C. J. Wohl, R. K. Penner, J. G. Smith, and E. J. Siochi, “Insect residue contamination on wing leading edge surfaces: a materials investigation for mitigation,” in *242nd American Chemical Society National Meeting and Exposition*, 2011, no. NF1676L-12548.

[25] M. Kok, T. Mertens, D. Raps, and T. M. Young, “Influence of surface characteristics on insect residue adhesion to aircraft leading edge surfaces,” *Prog Org Coat*, vol. 76, no. 11, pp. 1567–1575, 2013.

[26] M. Kok, E. F. Tobin, P. Zikmund, D. Raps, and T. M. Young, “Laboratory testing of insect contamination with application to laminar flow technologies, Part I: Variables affecting insect impact dynamics,” *Aerosp Sci Technol*, vol. 39, pp. 605–613, 2014.

[27] K. G. Krishnan, A. Milionis, E. Loth, T. E. Farrell, J. D. Crouch, and D. H. Berry, “Influence of hydrophobic and superhydrophobic surfaces on reducing aerodynamic insect residues,” *Appl Surf Sci*, vol. 392, pp. 723–731, 2017.

[28] C. J. Wohl *et al.*, “Influence of surface properties and impact conditions on adhesion of insect residues,” in *38th annual meeting of the Adhesion Society, Savannah*, 2015, pp. 20–25.

[29] W. S. Coleman, “The characteristics of roughness from insects as observed for two-dimensional, incompressible flow past airfoils,” *Journal of the Aerospace Sciences*, vol. 26, no. 5, pp. 264–280, 1959.

[30] J. G. Smith, R. Robison, and E. Loth, “An overview of insect residue accretion and mitigation strategies on aerodynamic surfaces,” *Contamination Mitigating Polymeric Coatings for Extreme Environments*, pp. 217–233, 2018.

[31] I. G. C. Lachmann, “Aspects of insect contamination in relation to laminar flow aircraft,” 1960.

[32] J. B. Peterson Jr and D. F. Fisher, “Flight investigation of insect contamination and its alleviation,” *CTOL Transport Technol., 1978*, 1978.

[33] C. J. Wohl, J. G. Smith Jr, R. K. Penner, T. M. Lorenzi, C. S. Lovell, and E. J. Siochi, “Evaluation of commercially available materials to mitigate insect residue adhesion on wing leading edge surfaces,” *Prog Org Coat*, vol. 76, no. 1, pp. 42–50, 2013.

[34] J. Maresh and M. Bragg, “The role of airfoil geometry in minimizing the effect of insect contamination of laminar flow sections,” in *2nd Applied Aerodynamics Conference*, 1984, p. 2170.

[35] C. C. Croom and B. J. Holmes, “Flight evaluation of an insect contamination protection system for laminar flow wings,” *SAE Transactions*, pp. 486–494, 1985.

[36] C. Wohl, J. Smith, J. Connell, E. Siochi, R. Penner, and J. Gardner, “Engineered surfaces for mitigation of insect residue adhesion,” in *51st AIAA Aerospace Sciences Meeting including the New Horizons Forum and Aerospace Exposition*, 2013, p. 413.

[37] R. D. Joslin, “Overview of laminar flow control,” 1998.

[38] M. Kok and T. M. Young, “Evaluation of insect residue resistant coatings–Correlation of a screening method with a conventional assessment technique,” *Prog Org Coat*, vol. 77, no. 9, pp. 1382–1390, 2014.

[39] M. Kok, E. F. Tobin, P. Zikmund, D. Raps, and T. M. Young, “Laboratory investigation into anti-contamination coatings for mitigating insect contamination with application to laminar flow technologies,” *Contamination Mitigating Polymeric Coatings for Extreme Environments*, pp. 291–313, 2017.

[40] T. M. Young, E. F. Tobin, and M. Kok, “Laboratory testing of insect contamination for laminar flow applications using an insect-impact test facility,” in *28th International Congress of the Aeronautical Sciences, Brisbane, Australia*, 2012, pp. 23–28.

[41] J. Smith, T. Lorenzi, C. Wohl, R. Penner, and E. Siochi, “Influence of surface energy on insect residue adhesion,” in *Proceeding of the 35th annual meeting of the adhesion society, New Orleans, USA*, 2012, pp. 26–29.

[42] M. Kok, D. Raps, and T. M. Young, “Effects of surface roughness and energy on insect residue adhesion to aircraft leading edge surfaces,” in *Proceeding of the 36th annual meeting of the adhesion society, Daytona Beach, USA*, 2013, pp. 3–6.

[43] F. X. Wortmann, “A method for avoiding insect roughness on aircraft(installation of highly elastic rubber coverings on leading edges),” 1974.

[44] J. B. Barlow, W. H. Rae Jr, and A. Pope, “Low speed wind tunnel testing,” *INCAS Bulletin*, vol. 7, no. 1, p. 133, 2015.

[45] A. Hyvärinen, “Investigation of blockage correction methods forfull-scale wind tunnel testing of trucks.” 2015.

[46] O. Yi, “Investigation of factors affecting the sticking of insects on aircraft wing surfaces,” Virginia Polytechnic Institute and State University, 1988.

[47] N. S. Eiss Jr, J. P. Wightman, D. R. Gilliam, and E. J. Siochi, “A fundamental approach to the sticking of insect residues to aircraft wings,” 1984.

[48] E. J. Siochi, N. S. Eiss, D. R. Gilliam, and J. P. Wightman, “A fundamental study of the sticking of insect residues to aircraft wings,” *J Colloid Interface Sci*, vol. 115, no. 2, pp. 346–356, 1987.

[49] D. Carter and E. Loth, “Insect Residue Height for Different Coatings and Conditions,” in *2018 AIAA Aerospace Sciences Meeting*, 2018, p. 313.

[50] M. Kok and T. M. Young, “The evaluation of hierarchical structured superhydrophobic coatings for the alleviation of insect residue to aircraft laminar flow surfaces,” *Appl Surf Sci*, vol. 314, pp. 1053–1062, 2014.

[51] F. X. Wortmann, “A possibility of avoiding surface roughness due to insects,” 1984.

[52] D. Neuhart, L. Jenkins, M. Choudhari, and M. Khorrami, “Measurements of the flowfield interaction between tandem cylinders,” in *15th AIAA/CEAS Aeroacoustics Conference (30th AIAA Aeroacoustics Conference)*, 2009, p. 3275.

[53] W. Sellers and S. Kjelgaard, “The Basic Aerodynamics Research Tunnel-A Facility Dedicated to Code Validation,” in *15th Aerodynamic Testing Conference*, 1988, p. 1997.

[54] I. S. Bayer *et al.*, “Thermal alternating polymer nanocomposite (TAPNC) coating designed to prevent aerodynamic insect fouling,” *Sci Rep*, vol. 6, no. 1, pp. 1–13, 2016.

[55] D. v Maddalon and A. L. Braslow, “Simulated-airline-service flight tests of laminar-flow control with perforated-surface suction system,” 1990.

[56] D. J. Marsden and M. DJ, “WIND TUNNEL TESTS OF A SLOTTED FLAPPED WING SECTION.,” 1978.

[57] A. Elsenaar and H. N. Haasnoot, “A SURVEY ON SCHIPHOL AIRPORT OF THE CONTAMINATION OF WING LEADING EDGES OF THREE DIFFERENT AIRCRAFT TYPES UNDER OPERATING CONDITIONS.,” 1992.

[58] C. J. Wohl, F. L. Palmieri, and J. W. Connell, “The physics of insect impact and residue expansion,” *Contamination Mitigating Polymeric Coatings for Extreme Environments*, pp. 235–290, 2018.

[59] A. Milionis, K. G. Krishnan, and E. Loth, “Hemolymph drop impact outcomes on surfaces with varying wettability,” *Appl Surf Sci*, vol. 345, pp. 36–43, 2015.

[60] “Roughness (surface roughness) | KRÜSS Scientific.” https://www.kruss-scientific.com/en/know-how/glossary/surface-roughness (accessed Aug. 25, 2022).

[61] C. J. Wohl, B. M. Atkins, and J. W. Connell, “Method and apparatus for the quantification of particulate adhesion forces on various substrates,” 2011.

[62] “Takeoff - Wikipedia.” https://en.wikipedia.org/wiki/Takeoff (accessed Jun. 28, 2022).

[63] D. v Maddalon, D. F. Fisher, L. A. Jennett, and M. C. Fischer, “Simulated airline service experience with laminar-flow control leading-edge systems,” *Research in Natural Laminar Flow and Laminar-Flow Control, Part 1*, 1987.

[64] N. Zhao, N. Li, Y. Sun, and Z. Gao, “4D Trajectory Planning of Aircraft Taxiing considering Time and Fuel,” *Math Probl Eng*, vol. 2020, 2020, doi: 10.1155/2020/9603968.

[65] “Sessile drop technique - Wikipedia.” https://en.wikipedia.org/wiki/Sessile_drop_technique (accessed Aug. 25, 2022).

[66] “Young-Laplace fit | KRÜSS Scientific.” https://www.kruss-scientific.com/en/know-how/glossary/young-laplace-fit (accessed Aug. 25, 2022).

[67] “Understanding Boxplots. The image above is a boxplot. A boxplot… | by Michael Galarnyk | Towards Data Science.” https://towardsdatascience.com/understanding-boxplots-5e2df7bcbd51 (accessed Aug. 25, 2022).

Appendices

Appendix A – Past coatings list from literature

		Young	Wohl	Krishnan	Notes
Aluminum	SE (mN/m)	37.18	84 degrees	79 degrees	
	Ra (µm)	0.2	0.31		
Nusil	SE (mN/m)	10.57		117 degrees	
	Ra (µm)	0.56			
Urethane acrylate	SE (mN/m)	22.3	85 - 108 degrees		
	Ra (µm)	0.07	0.32 - 1.84		
PU clear coat	SE (mN/m)	37.18			Default on aircraft
	Ra (µm)	0.02			
HCS	SE (mN/m)	42.02			
	Ra (µm)	0.13			
PU Silane	SE (mN/m)	45.97			
	Ra (µm)	0.2			
TiO2	SE (mN/m)	0.39			
	Ra (µm)	0.24			
SH Epoxy	SE (mN/m)	0.7			
	Ra (µm)	5.26			
SH	SE (mN/m)	2.04			
	Ra (µm)	4.91			
Hydrophobic	SE (mN/m)	10.57			
	Ra (µm)	0.85			
PU Polish	SE (mN/m)	16.1			

	Ra (µm)	0.23			
Teflon	SE (mN/m)	19.4		124 degrees	
	Ra (µm)	2.5			
FPD	SE (mN/m)	20.21			
	Ra (µm)	8.38			
Sol-gel	SE (mN/m)	28.42			
	Ra (µm)	0.18			
PU Topcoat	SE (mN/m)	39.04			
	Ra (µm)	0.99			
Fluorinated Topcoat	SE (mN/m)	14.1			
	Ra (µm)	0.72			
Acrylic clear-coat	SE (mN/m)	34.77			
	Ra (µm)	0.04			
Electropolished specimens	SE (mN/m)	51.06, 75.48, 80.69			
	Ra (µm)	0.06, 0.06, 0.15			
Sandblasted specimens	SE (mN/m)	39.01, 63.96, 40.19			
	Ra (µm)	0.8, 2.4, 10,7			
Hybrid Sol-gel1,2,3	SE (mN/m)	17.26, 20.04, 39.52			
	Ra (µm)	1.65, 1.3, 0.05			
Sandblasted and commercial specimens	SE (mN/m)	0.04 - 33.9			
	Ra (µm)	0.55 - 23.08			
Solgel, electropolish, and polyurethane specimens	SE (mN/m)	0.13 - 79.7			
	Ra (µm)	0.02 - 23.08			

Commercial specimens	SE (mN/m)		9.2 - 46.3		
	Ra (µm)				
NyeBar	SE (mN/m)		9.1		
	Ra (µm)		0.43		
PIO/40% SiO2	SE (mN/m)		14.5		
	Ra (µm)				
PIO/60% SiO2	SE (mN/m)		36.9		
	Ra (µm)				
PIO/50% MoS2	SE (mN/m)		24.5		
	Ra (µm)				
Si Mix	SE (mN/m)		20.9		
	Ra (µm)				
pHEMA	SE (mN/m)		54.7		
	Ra (µm)		0.38		
Commercial specimens	SE (mN/m)		11.5 - 54.9		
	Ra (µm)		0.37 - 0.61		
Epoxy with MoS2 or SiO2 filler specimens	SE (mN/m)		0.7 - 25.6		
	Ra (µm)				
Epoxy and urethan specimens	SE (mN/m)		84 - 107 degree		
	Ra (µm)		0.31 - 8.19		
ABS	SE (mN/m)			163 degrees	
	Ra (µm)				
Silprocoat	SE (mN/m)			111 degrees	
	Ra (µm)				
Capstone	SE (mN/m)			113 degrees	

	Ra (µm)				
Hydrobead	SE (mN/m)			168 degrees	
	Ra (µm)				
TAPNC	SE (mN/m)			No data	
	Ra (µm)				
FAE Epoxy	SE (mN/m)			No data	
	Ra (µm)				

Appendix B – Arduino code

```
#include <math.h>
#include <stdint.h>

const int IR_OUTPUT = A1; //IR output pin
const int IR_VOLTAGE = 13; //IR power pin
int IR_MAX = 100; //initial values
int IR_MIN = 500; //initial values
int IR_CUTOFF = 300; //initial values

const int IR_time = 300; //rpm range ={100, 4000}
const int IR_iter = 1000; //initial samples number for estimating the rpm
int list_IR[IR_iter];

float RPM = 0; //RPM is a "float" variable
const long time_calibration_1 = 110; //initial values, automated
const long time_calibration_2 = 110; //initial values, automated

const long time_calibration_3 = 0; //find it each time // uS
const int ShootTime = 51; //time that particle hits the wing or pass the destinated point
const float loc = 0.2; //location of impact in a quarter of circular path 0.2 or 18deg

const int relay = 8; //the number of the relay pin
const int relay_power = 9; //relay power pin
const int camera = 10; //camera pin

//Launcher
#define stp 2
#define dir 3
#define MS1 4
#define MS2 5
#define EN  6
int steps = 160; //used for controlling the motor
```

```
//Define pin connections & motor's steps per revolution //Shooter
const int volPin = 7;
const int dirPin = 11;
const int stepPin = 12;
const int stepsPerRevolution = 4200;

//----------------------------initial setup----------------------------// //one time execution code for doing the initial setups of the components
void setup()
{

  Serial.begin(9600);

  //////Relay & camera////// //relay and camera initial setups
  pinMode (relay, OUTPUT);
  digitalWrite(relay, HIGH);

  pinMode (camera, OUTPUT);
  digitalWrite(camera, LOW);

  pinMode (relay_power, OUTPUT);
  digitalWrite(relay_power, HIGH);
  //////END Relay & camera//////

  //////Stepper-Shooter////// //launchers initial setups
  pinMode(stepPin, OUTPUT);
  pinMode(dirPin, OUTPUT);
  pinMode (volPin, OUTPUT);
  digitalWrite(volPin, HIGH);
  //////END Stepper-Shooter//////

  //////Stepper////// //particle dropper initial setups
  pinMode(stp, OUTPUT);
```

```
  pinMode(dir, OUTPUT);
  pinMode(MS1, OUTPUT);
  pinMode(MS2, OUTPUT);
  pinMode(EN, OUTPUT);
  resetEDPins(); //Set step, direction, microstep and enable pins to default states
  //////END Stepper//////

  //////Finding IR max & min & cutoff////// //finding the max and min values of IR diodes affected by
lightning of the room
  pinMode (IR_OUTPUT, INPUT);
  pinMode (IR_VOLTAGE, OUTPUT);
  digitalWrite (IR_VOLTAGE, HIGH);

  for (int i = 0; i < IR_iter; i++)
  {
    list_IR[i] = analogRead(IR_OUTPUT);
    delayMicroseconds(IR_time);
  }

  for (int i = 0; i < IR_iter; i++)
  {
    if (IR_MAX < list_IR[i])
    {
      IR_MAX = list_IR[i];
    }
  }
  Serial.print (IR_MAX);
  Serial.print ("\n");

  for (int i = 0; i < IR_iter; i++)
  {
    if (IR_MIN > list_IR[i])
    {
      IR_MIN = list_IR[i];
```

```
    }
  }
  Serial.print (IR_MIN);
  Serial.print ("\n");

  IR_CUTOFF = (IR_MAX + IR_MIN) / 2;
  //////END Finding IR max & min & cutoff//////

  //////Menu////// //creating the menu for user
  Serial.println( "1) Shoot" );
  Serial.println( "2) Fill" );
  //////END Menu//////

}
//----------------------------END Setup----------------------------//



//----------------------------Loop----------------------------// //repetitive execution code for particle
launching and dropping
void loop()
{

  byte key; //get the next character from the serial port or in the other words user decide an
option from the menu
  while (!Serial.available())
    ;
  key = Serial.read(); //execute the menu option based on the character received


  switch (key)
  {
    //////Fill////// //filling the particle launcher is selected. Particle dropper starts to work.
    case '2':
```

```
    Serial.println( "Fill" );

    digitalWrite(EN, LOW);
    stepMode(8);
    rotate(1, steps); //rotate step number of steps(with 160 steps at step mode 8, the rotation =
30 degrees)
    resetEDPins();
    Serial.println( "5" ); //5s waiting time for particle to be placed in the particle launcher
    delay(1000);
    Serial.println( "4" );
    delay(1000);
    Serial.println( "3" );
    delay(1000);
    Serial.println( "2" );
    delay(1000);
    Serial.println( "1" );
    delay(1000);
    Serial.println( "preparing 0/2" );

    digitalWrite(relay, LOW); //particle launcher starts to compact the spring and initiating the
camera and relay setups for launching
    digitalWrite(camera, HIGH);
    digitalWrite(dirPin, LOW);
    for (int x = 0; x < stepsPerRevolution; x++)
    {
      digitalWrite(stepPin, HIGH);
      delayMicroseconds(1000);
      digitalWrite(stepPin, LOW);
      delayMicroseconds(1000);
    }
    delay(1000);

    Serial.println( "preparing 1/2" );
```

```
      digitalWrite(relay, HIGH);
      digitalWrite(camera, LOW);
      delay(1000);
      digitalWrite(dirPin, HIGH);
      for (int x = 0; x < stepsPerRevolution; x++)
      {
        digitalWrite(stepPin, HIGH);
        delayMicroseconds(1000);
        digitalWrite(stepPin, LOW);
        delayMicroseconds(1000);
      }
      delay(1000);

      Serial.println( "preparing 2/2" );
      Serial.println( "Go!" ); //particle launcher is ready for launching the insect

      break;
    //////END Fill//////

    //////Shoot////// //launching the particle launcher is selected. Particle launcher starts to work.
    case '1':
      Serial.println( "Shoot" );

repeat:
      float sign = 0;
      long a = 0, b = 0;

      float Rot_Time = RotationDuration (IR_CUTOFF); //finding the exact time of a full rotation
      int n = ((ShootTime + int (time_calibration_3 / 1000)) / (long)(Rot_Time / 2000)) + 1;
//calculating the least number of half rotations which is needed in Equation 2-2
      Serial.print ("Rotation time: ");
      Serial.print ((long)Rot_Time);
      Serial.print ("\n");
      Serial.print ("# of half rotations: ");
```

```
    Serial.print (n);
    Serial.print ("\n");

    int first = 0;
    int previous = 0;
    int current = 0;

    first = analogRead(IR_OUTPUT);
    if (IR_CUTOFF < first)
    {
      Serial.print ("Repeat!\n");
      goto repeat;
    }

    while (sign == 0) //determining the location of the airfoil
    {
      current = analogRead(IR_OUTPUT);
      if (current > IR_CUTOFF and IR_CUTOFF > previous and IR_CUTOFF > first)
      {
        a = micros();
        sign = 1;
      }
      previous = current;
    }

    b = micros();
    while ( ((b - a)) < (n * (long)(Rot_Time/2) + (long)(Rot_Time/4*loc) - (long)ShootTime * 1000
- (long)time_calibration_3) ) //waiting before launching the particle
    {
      b = micros();
    }
    shoot(); //launching the particle

    break;
```

```
      //////END Shoot//////
  }

}
//----------------------------END Loop----------------------------//



//----------------------------Rotation duration----------------------------// //this function returns one full rotation time in microseconds as a float
float RotationDuration (int IR_CUTOFF)
{
  //---guessing rpm---//
  long iter = 1000;
  int list[iter];
  long delay_time = 300;

here:
  float sign = 0, first = 0 , second = 0, rot_time;
  long a = 0, b = 0, c = 0, d = 0;

  long time_cal = time_calibration_2;
  do
  {
    time_cal += 1;
    a = micros();

//To obtain time intervals of about microseconds, instead of using the “delay”, the “micros” command was used. “Micros” returns the exact time of the system; however, “delay” ceases the process for a period of time. The time period of ceasing the code in addition to the execution time of the “delay” command, leads to a false value for the passed time. However, using “micros”, both ceasing time and execution time could be considered.//

    int i = 0;
```

```
  d = micros();

  while (i < (long)iter)
  {
    c = micros();
    if ((c - d) >= ((long) delay_time - time_cal))
    {
      list[i] = analogRead(IR_OUTPUT);
      i++;
      d = micros();
    }
  }

  b = micros();

  Serial.print ("Calibration 2: ");
  Serial.print (b - a); //for time calibration
  Serial.print (" --> ");
  Serial.print (delay_time * iter);
  Serial.print ("\n");
} while ((b - a) > (delay_time * iter));

for (int i = 1; i < iter; i++)
{
  if (list[i] > IR_CUTOFF and IR_CUTOFF > list[i - 1] and sign == 1)
  {
    second = i;
    sign = 2;
  }

  if (list[i] > IR_CUTOFF and IR_CUTOFF > list[i - 1] and IR_CUTOFF > list[0] and sign == 0)
  {
    first = i;
    sign = 1;
```

```
  }
}

if (first > 0 and second > 0)
{
  float cons = ((float) b - (float) a) / ((float) delay_time * (float) iter);
  rot_time = (second - first) * 2.0 * delay_time * cons;
}
else
{
  Serial.print ("here!\n");
  goto here;
}

if ((long)rot_time >= 50000)
{
  iter = 400;
  long delay_time_float = rot_time / 400;
  delay_time = (long)delay_time_float;
  Serial.print ("First 0.4 cm! 400 Samples!\n");
}
else if ((long)rot_time >= 24000)
{
  iter = 200;
  float delay_time_float = rot_time / 200;
  delay_time = (long)delay_time_float;
  Serial.print ("First 0.8 cm! 200 Samples!\n");
}
else
{
  iter = 135;
  float delay_time_float = rot_time / 135;
  delay_time = (long)delay_time_float;
  Serial.print ("First 1.2 cm! 135 Samples!\n");
```

```
  }
  //---End guessing rpm---//

again:
  sign = 0, first = 0 , second = 0;
  a = 0, b = 0, c = 0, d = 0;

  time_cal = time_calibration_1;
  do
  {
    time_cal += 1;
    a = micros();
    int i = 0;
    d = micros();

    while (i < (long)iter)
    {
      c = micros();
      if ((c - d) >= ((long) delay_time - time_cal))
      {
        list[i] = analogRead(IR_OUTPUT);
        i++;
        d = micros();
      }
    }

    b = micros();

    Serial.print ("Calibration 1: ");
    Serial.print (b - a); //for time calibration
    Serial.print (" --> ");
    Serial.print (delay_time * iter);
    Serial.print ("\n");
  } while ((b - a) > (delay_time * iter));
```

```
for (int i = 1; i < iter; i++)
{
  if (list[i] > IR_CUTOFF and IR_CUTOFF > list[i - 1] and sign == 1)
  {
    second = i;
    sign = 2;
  }

  if (list[i] > IR_CUTOFF and IR_CUTOFF > list[i - 1] and IR_CUTOFF > list[0] and sign == 0)
  {
    first = i;
    sign = 1;
  }
}

if (first > 0 and second > 0)
{
  float cons = ((float) b - (float) a) / ((float) delay_time * (float) iter);
  Serial.print ("Accuracy = ");
  Serial.print (cons * 100);
  Serial.print (" %\n");
  float RPM = 60000000 / ((second - first) * 2.0 * delay_time * cons);
  Serial.print ("RPM: ");
  Serial.print (RPM);
  Serial.print ("\n");
  return (second - first) * 2.0 * delay_time * cons; //exact full rotation time
}
else
{
  Serial.print ("Again!\n");
  goto again;
}
```

```
}
//----------------------------END Rotation duration----------------------------//



//----------------------------Relay & camera----------------------------// //this function triggers the particle launcher and camera at the same time
void shoot()
{

  digitalWrite(relay, LOW); //shoot
  digitalWrite(camera, HIGH); //trigger

  delay(1000);

  digitalWrite(relay, HIGH);
  digitalWrite(camera, LOW);



}
//----------------------------END Relay & camera----------------------------//



//----------------------------Stepper rotation----------------------------// //this function rotates the particle dropper top disk
void rotate(byte motDir, int numSteps)
{

  //Serial.println(motDir, numSteps);
  switch (motDir)
  {
    case 1:
      digitalWrite(dir, LOW); //Pull direction pin low to move "forward"
```

```
      //rotate 36 degrees forward
      for (int x = 1; x <= numSteps; x++)
      {
        forwardStep();
        //Serial.println(x);
      }
      break;

    case 2:
      digitalWrite(dir, HIGH); //Pull direction pin high to move in "reverse"
      //rotate 36 degrees backward
      for (int x = 1; x <= numSteps; x++)
      {
        reverseStep();
      }
      break;
  }
}



void forwardStep()
{
  digitalWrite(stp, HIGH); //Trigger one step forward
  delay(1);
  digitalWrite(stp, LOW); //Pull step pin low so it can be triggered again
  delay(1);

}



void reverseStep()
{
```

```
  digitalWrite(stp, HIGH); //Trigger one step
  delay(1);
  digitalWrite(stp, LOW); //Pull step pin low so it can be triggered again

}



void stepMode(int stepDivisor)
{

  if (stepDivisor == 1) //Full step
  {
    digitalWrite(MS1, LOW);
    digitalWrite(MS2, LOW);
  }
  else if (stepDivisor == 2) //Half step
  {
    digitalWrite(MS1, HIGH);
    digitalWrite(MS2, LOW);
  }
  else if (stepDivisor == 4) //Quarter step
  {
    digitalWrite(MS1, LOW);
    digitalWrite(MS2, HIGH);
  }
  else if (stepDivisor == 8) //Eighth step
  {
    digitalWrite(MS1, HIGH);
    digitalWrite(MS2, HIGH);
  }

}
```

```
void resetEDPins()
{

  digitalWrite(stp, LOW);
  digitalWrite(dir, LOW);
  digitalWrite(MS1, LOW);
  digitalWrite(MS2, LOW);
  digitalWrite(EN, HIGH);

}
//----------------------------END Stepper rotation----------------------------//
```

Appendix C – Mechanical drawings

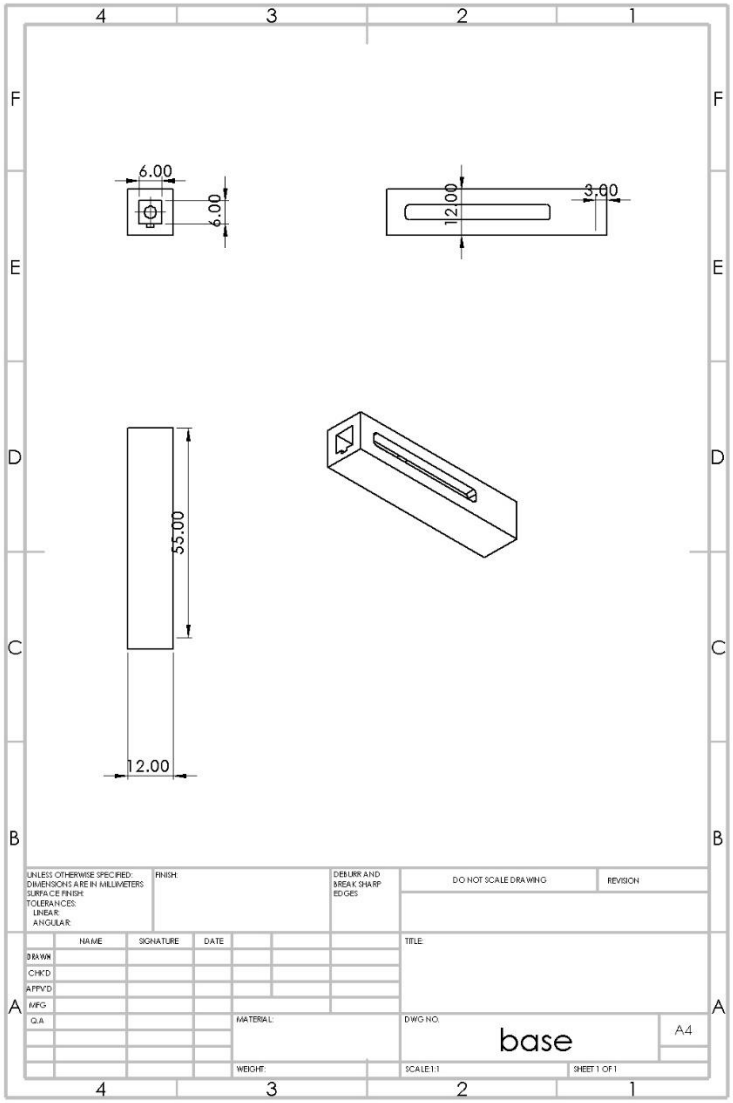

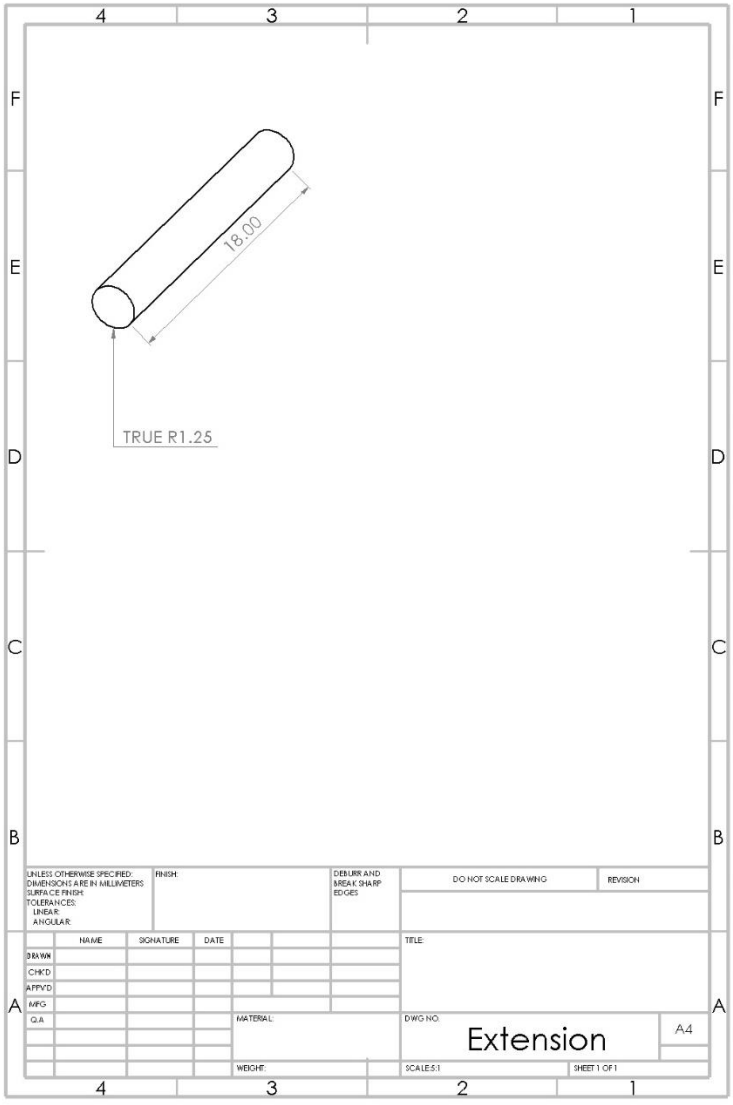
4
3
2
1
F
E
D
C
B
A
18.00
TRUE R1.25
UNLESS OTHERWISE SPECIFIED:
DIMENSIONS ARE IN MILLIMETERS
SURFACE FINISH:
TOLERANCES:
LINEAR:
ANGULAR:
FINISH:
DEBURR AND BREAK SHARP EDGES
DO NOT SCALE DRAWING
REVISION
NAME
SIGNATURE
DATE
DRAWN
CHK'D
APPV'D
MFG
Q.A
TITLE:
MATERIAL:
DWG NO.
Extension
A4
WEIGHT:
SCALE:5:1
SHEET 1 OF 1

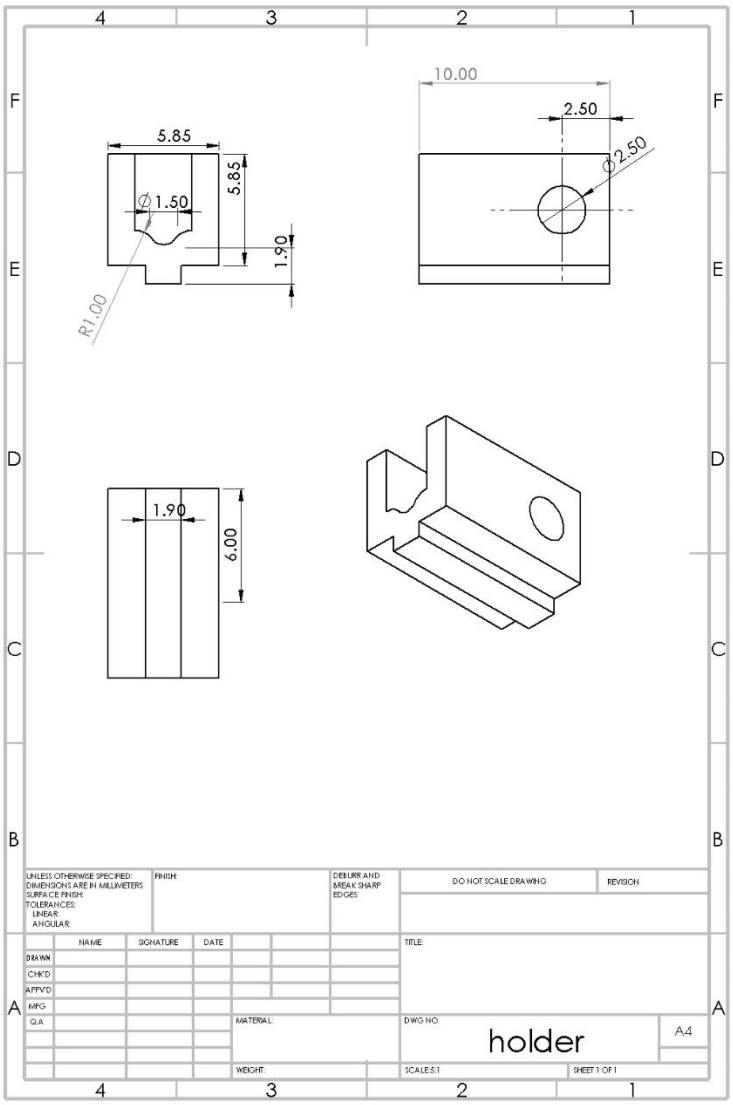
10.00
2.50
Ø2.50
5.85
5.85
Ø1.50
1.90
R1.00
1.90
6.00
holder
A4

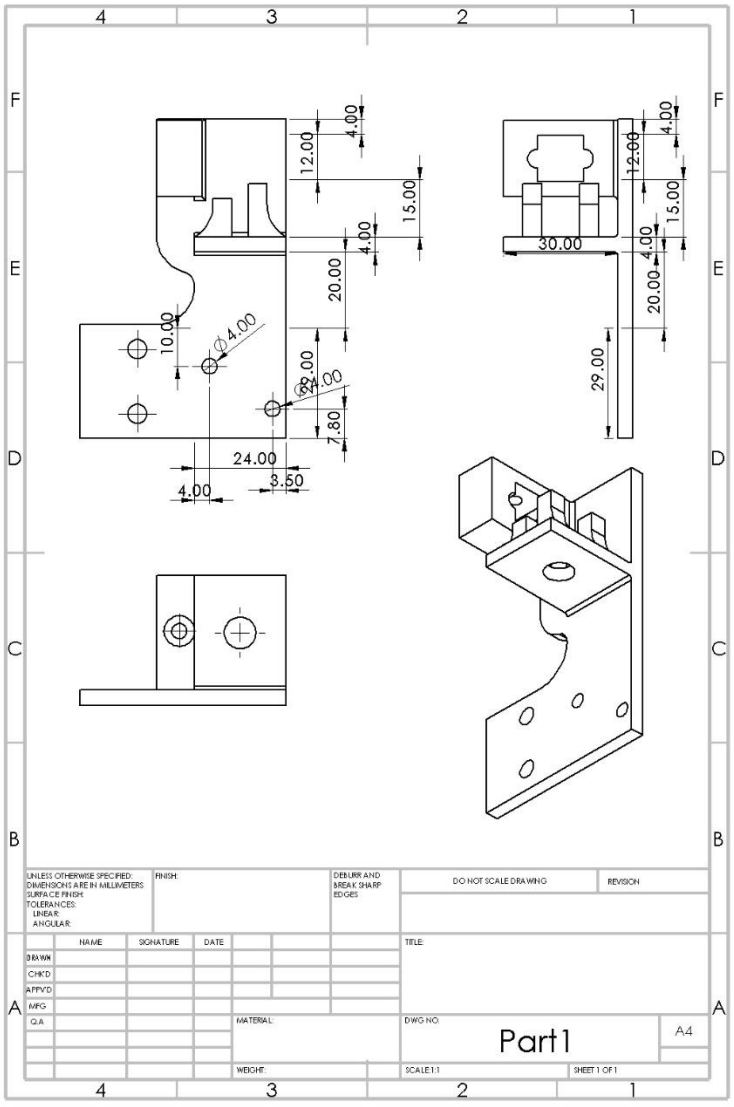
4.00
12.00
15.00
4.00
20.00
10.00
Ø4.00
Ø4.00
8.00
7.80
24.00
4.00
3.50
30.00
29.00
UNLESS OTHERWISE SPECIFIED:
DIMENSIONS ARE IN MILLIMETERS
SURFACE FINISH:
TOLERANCES:
LINEAR:
ANGULAR:
FINISH:
DEBURR AND BREAK SHARP EDGES
DO NOT SCALE DRAWING
REVISION
NAME
SIGNATURE
DATE
DRAWN
CHK'D
APP'VD
MFG
Q.A
TITLE:
MATERIAL:
DWG NO.
Part1
A4
WEIGHT:
SCALE:1:1
SHEET 1 OF 1

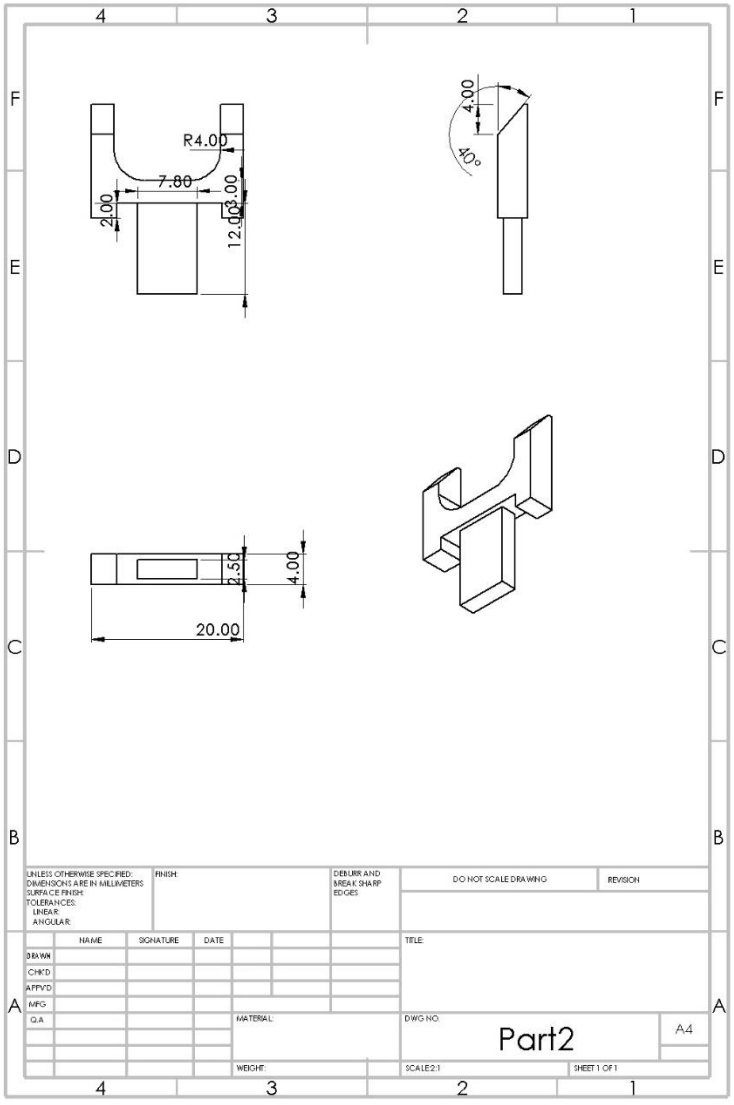
R4.00
7.80
2.00
3.00
12.00
4.00
40°
2.50
4.00
20.00
UNLESS OTHERWISE SPECIFIED:
DIMENSIONS ARE IN MILLIMETERS
SURFACE FINISH:
TOLERANCES:
LINEAR:
ANGULAR:
FINISH:
DEBURR AND BREAK SHARP EDGES
DO NOT SCALE DRAWING
REVISION
NAME
SIGNATURE
DATE
DRAWN
CHKD
APPVD
MFG
Q.A
TITLE:
MATERIAL:
DWG NO.
Part2
A4
WEIGHT:
SCALE:2:1
SHEET 1 OF 1

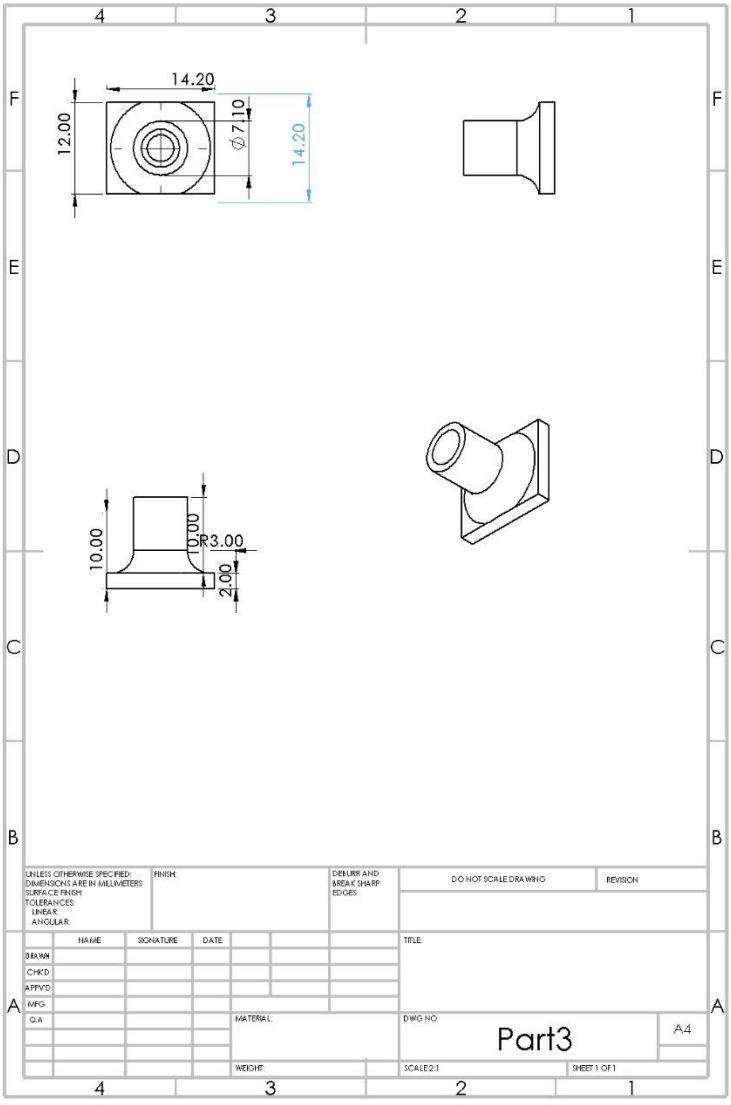
14.20
12.00
Ø7.10
14.20
10.00
10.00
R3.00
2.00
UNLESS OTHERWISE SPECIFIED:
DIMENSIONS ARE IN MILLIMETERS
SURFACE FINISH:
TOLERANCES:
LINEAR:
ANGULAR:
FINISH:
DEBURR AND BREAK SHARP EDGES
DO NOT SCALE DRAWING
REVISION
NAME
SIGNATURE
DATE
DRAWN
CHKD
APPV'D
MFG
Q.A
TITLE:
MATERIAL:
DWG NO.
Part3
A4
WEIGHT:
SCALE:2:1
SHEET 1 OF 1

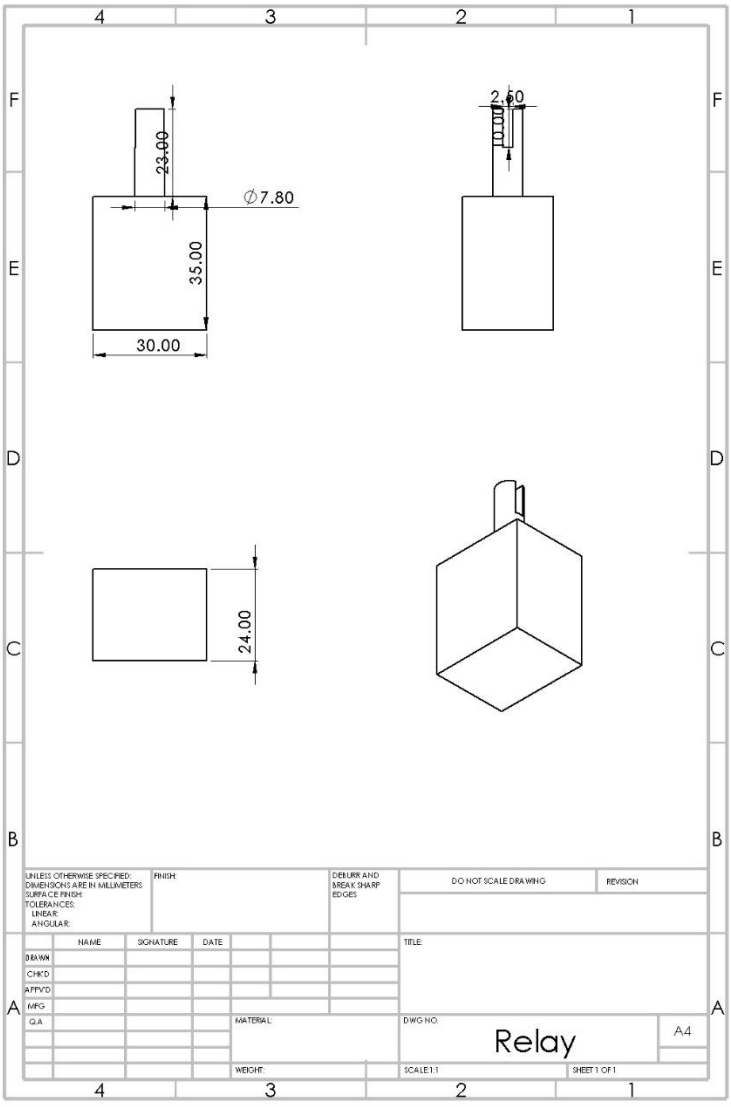
4
3
2
1
F
E
D
C
B
A
23.00
∅7.80
35.00
30.00
2.50
10.00
24.00
UNLESS OTHERWISE SPECIFIED:
DIMENSIONS ARE IN MILLIMETERS
SURFACE FINISH:
TOLERANCES:
LINEAR:
ANGULAR:
FINISH:
DEBURR AND BREAK SHARP EDGES
DO NOT SCALE DRAWING
REVISION
NAME
SIGNATURE
DATE
DRAWN
CHK'D
APPV'D
MFG
Q.A
TITLE:
MATERIAL:
DWG NO.
Relay
A4
WEIGHT:
SCALE:1:1
SHEET 1 OF 1

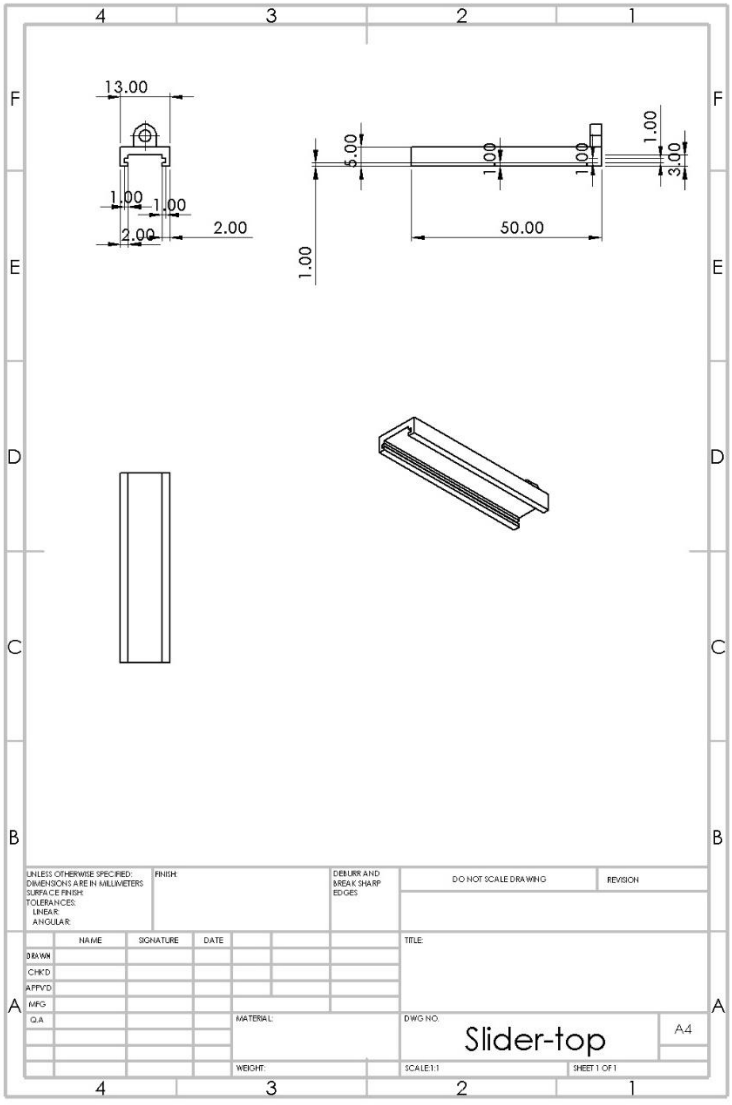
13.00
1.00
1.00
2.00
2.00
5.00
1.00
1.00
1.00
3.00
50.00
1.00
UNLESS OTHERWISE SPECIFIED:
DIMENSIONS ARE IN MILLIMETERS
SURFACE FINISH:
TOLERANCES:
LINEAR:
ANGULAR:
FINISH:
DEBURR AND BREAK SHARP EDGES
DO NOT SCALE DRAWING
REVISION
NAME
SIGNATURE
DATE
DRAWN
CHK'D
APP'VD
MFG
Q.A
MATERIAL:
WEIGHT:
TITLE:
DWG NO.
Slider-top
A4
SCALE:1:1
SHEET 1 OF 1

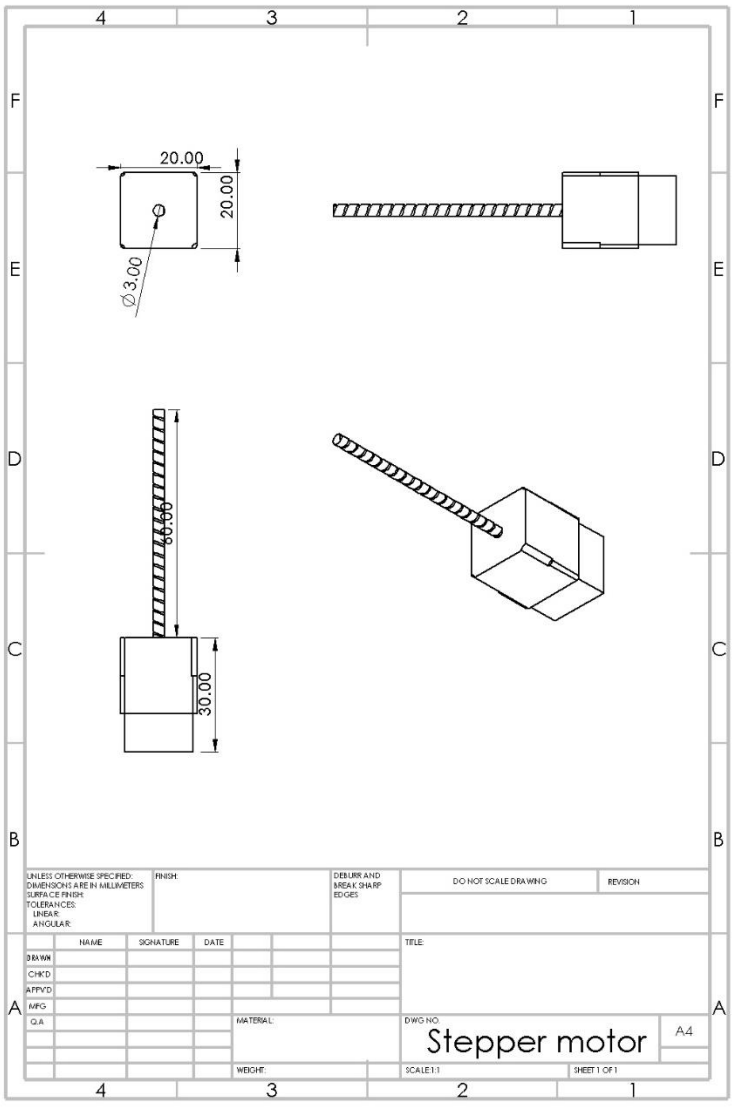
20.00
20.00
Ø3.00
60.00
30.00
UNLESS OTHERWISE SPECIFIED:
DIMENSIONS ARE IN MILLIMETERS
SURFACE FINISH:
TOLERANCES:
LINEAR:
ANGULAR:
FINISH:
DEBURR AND BREAK SHARP EDGES
DO NOT SCALE DRAWING
REVISION
NAME
SIGNATURE
DATE
DRAWN
CHK'D
APPV'D
MFG
Q.A
TITLE:
MATERIAL:
DWG NO.
Stepper motor
A4
WEIGHT:
SCALE:1:1
SHEET 1 OF 1

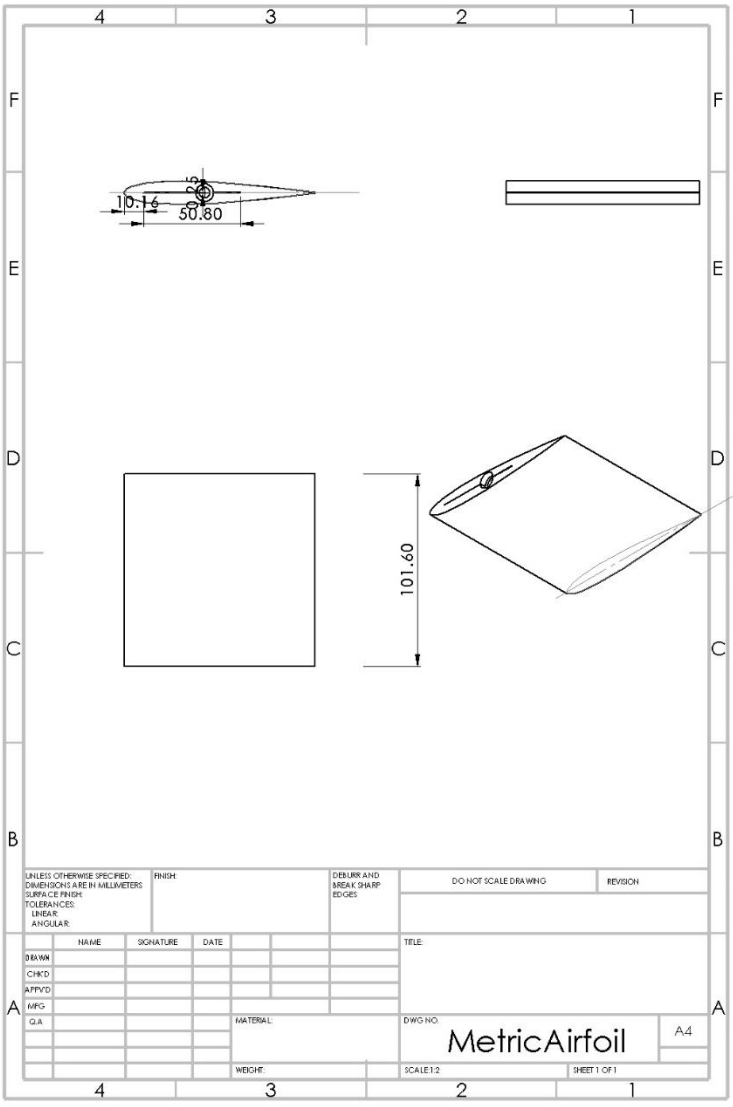
4
3
2
1
F
E
D
C
B
A
10.16
50.80
101.60
UNLESS OTHERWISE SPECIFIED:
DIMENSIONS ARE IN MILLIMETERS
SURFACE FINISH:
TOLERANCES:
LINEAR:
ANGULAR:
FINISH:
DEBURR AND BREAK SHARP EDGES
DO NOT SCALE DRAWING
REVISION
NAME
SIGNATURE
DATE
DRAWN
CHK'D
APPV'D
MFG
Q.A
TITLE:
MATERIAL:
DWG NO.
MetricAirfoil
A4
WEIGHT:
SCALE:1:2
SHEET 1 OF 1

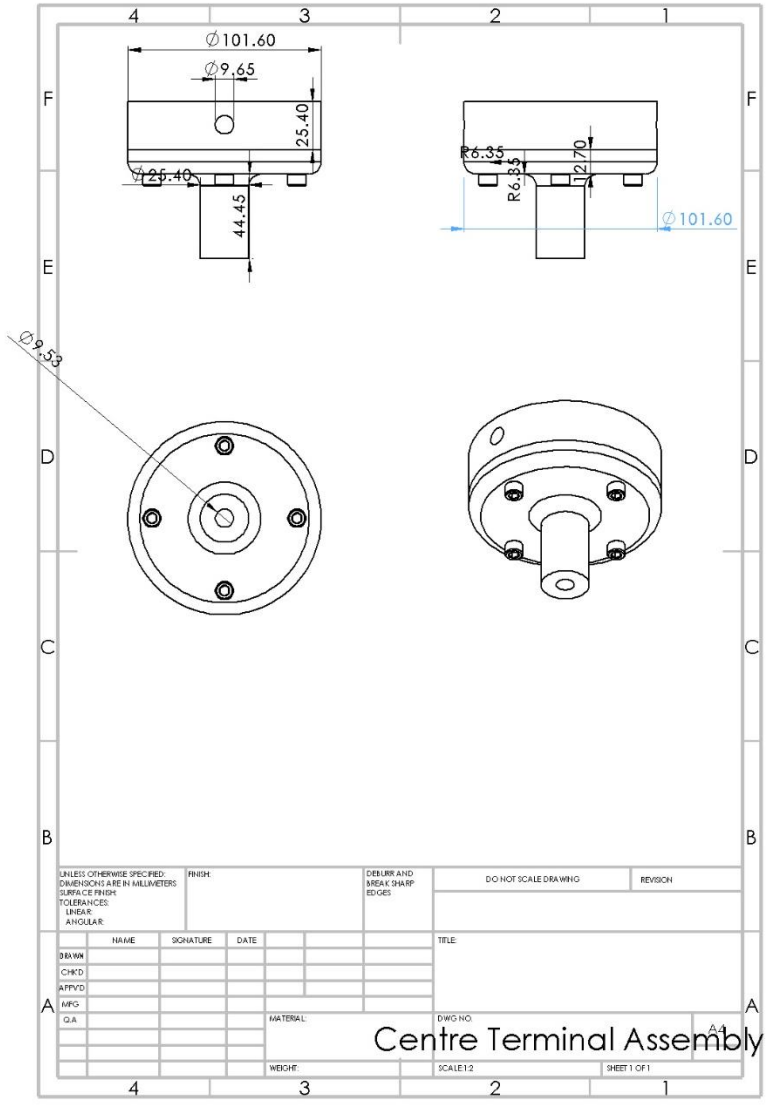
∅101.60
∅9.65
25.40
∅25.40
44.45
R6.35
R6.35
12.70
∅101.60
∅9.53
UNLESS OTHERWISE SPECIFIED:
DIMENSIONS ARE IN MILLIMETERS
SURFACE FINISH:
TOLERANCES:
LINEAR:
ANGULAR:
FINISH:
DEBURR AND BREAK SHARP EDGES
DO NOT SCALE DRAWING
REVISION
NAME
SIGNATURE
DATE
DRAWN
CHK'D
APPV'D
MFG
Q.A
TITLE:
MATERIAL:
DWG NO.
A4
Centre Terminal Assembly
WEIGHT:
SCALE:1:2
SHEET 1 OF 1

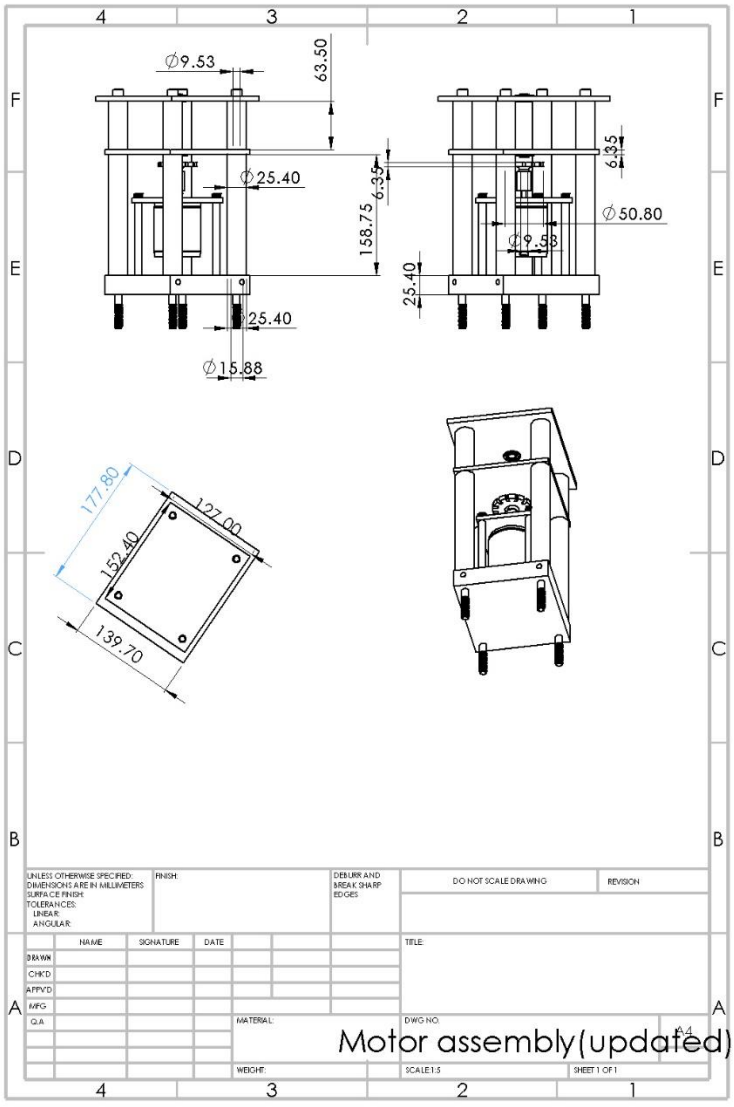
Ø9.53
63.50
Ø25.40
158.75
6.35
25.40
Ø15.88
Ø50.80
Ø9.53
177.80
127.00
152.40
139.70
UNLESS OTHERWISE SPECIFIED:
DIMENSIONS ARE IN MILLIMETERS
SURFACE FINISH:
TOLERANCES:
LINEAR:
ANGULAR:
FINISH:
DEBURR AND BREAK SHARP EDGES
DO NOT SCALE DRAWING
REVISION
NAME
SIGNATURE
DATE
DRAWN
CHK'D
APP'VD
MFG
Q.A
TITLE:
MATERIAL:
DWG NO.
A4
WEIGHT:
SCALE:1:5
SHEET 1 OF 1
Motor assembly(updated)

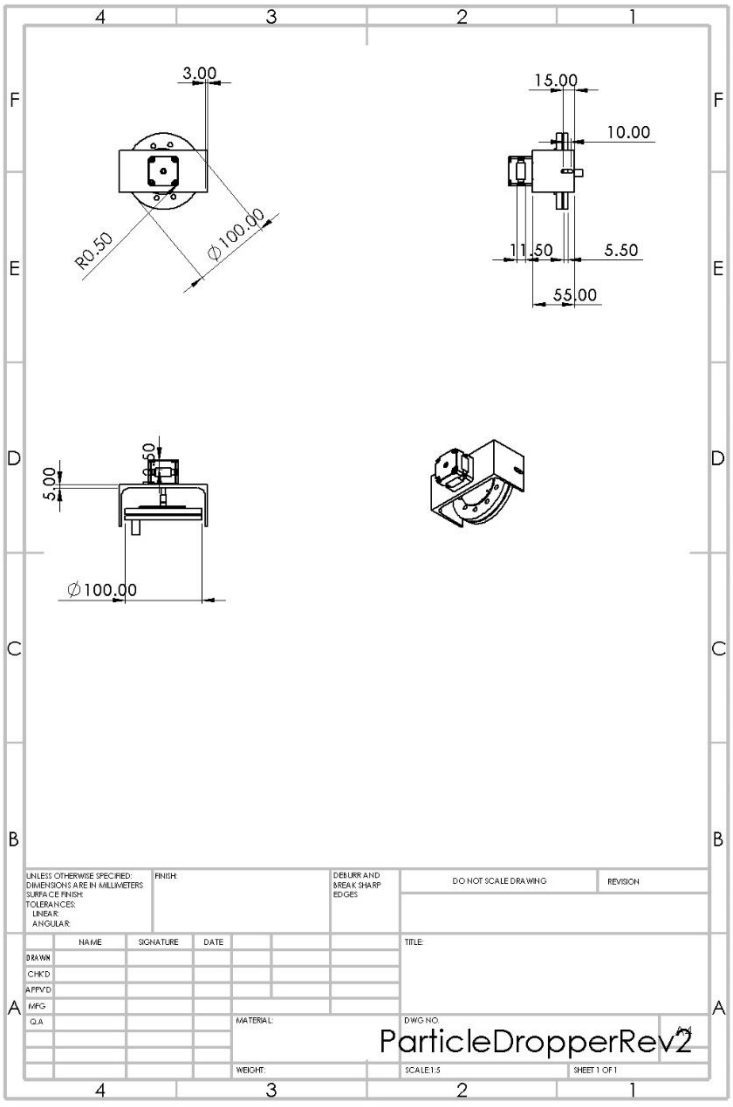
3.00
R0.50
Ø100.00
15.00
10.00
11.50
5.50
55.00
5.00
5.50
Ø100.00
ParticleDropperRev2